Available online at www.sciencedirect.com
SCIENCE DIRECT®
Progress in Oceanography 61 (2004) 277–348
Progress in Oceanography
www.elsevier.com/locate/pocean

Atlas of Japan (East) Sea hydrographic properties in summer, 1999

Lynne D. Talley [a,*], Pavel Tishchenko [b], Vladimir Luchin [c], Alexander Nedashkovskiy [b], Sergey Sagalaev [b], Dong-Jin Kang [d], Mark Warner [e], Dong-Ha Min [f]

[a] *Scripps Institution of Oceanography, UCSD, La Jolla, CA 92093, USA*
[b] *V. Il'ichev Pacific Oceanological Institute, Far Eastern Branch Russian National Academy of Sciences, Vladivostok, Russia*
[c] *Far Eastern Regional Hydrometeorological Research Institute, Vladivostok, Russia*
[d] *Seoul National University, Seoul, Republic of Korea*
[e] *University of Washington, Seattle, WA, USA*
[f] *Pennsylvania State University, University Park, PA 16802, USA*

Received 31 December 2003

Abstract

Hydrographic properties from CTD and discrete bottle sample profiles covering the Japan (East) Sea in summer, 1999, are presented in vertical sections, maps at standard depths, maps on isopycnal surfaces, and as property–property distributions. This data set covers most of the Sea with the exception of the western boundary region and northern Tatar Strait, and includes nutrients, pH, alkalinity, and chlorofluorocarbons, as well as the usual temperature, salinity, and oxygen observations.

Keywords: Japan sea; Ocean chemistry; Ocean atlas; Marginal seas; Water masses

1. Introduction

The Japan or East Sea is a nearly completely enclosed marginal sea of the western North Pacific (Fig. 1(a)). It has three relatively deep basins, the Ulleung, the Yamato, and the Japan. The basins are separated from each other by a major topographic feature, Yamato Rise. Continental shelves are narrow

* Corresponding author. Tel.: +1 8585346610; fax: +1 8585349820.
E-mail address: ltalley@ucsd.edu (L.D. Talley).

0079-6611/$ - see front matter © 2004 Elsevier Ltd. All rights reserved.
doi:10.1016/j.pocean.2004.06.011

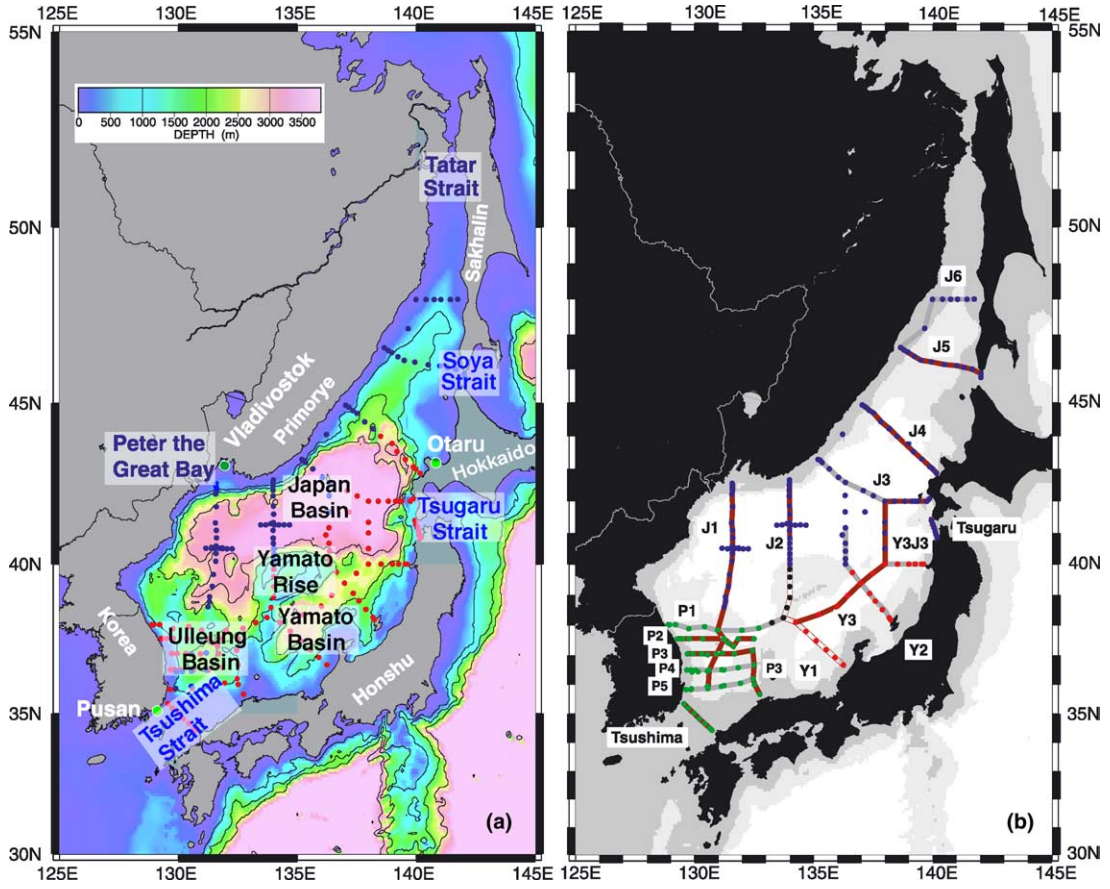

Fig. 1. (a) Stations from the *R/V Revelle* (24 June–17 July, 1999: red) and *Professor Khromov* (22 July–11 August, 1999: blue), superimposed on etopo5 bathymetry. (b) Sections in this publication (brown) and sections in the online atlas (gray and brown). Station color indicates use in property–property distributions: Ulleung Basin (green), Yamato Basin (red), Japan Basin (blue), Yamato Rise (black). (For interpretation of the references to color in this figure legend, the reader is referred to the web version of this article.)

except in the north in the region that is referred to generally as Tatar Strait. The Japan Sea is connected to the Pacific through two relatively shallow straits – Tsushima in the south and Tsugaru between Honshu and Hokkaido. It is connected to the Okhotsk Sea by two even shallower straits – Soya (La Perouse) between Hokkaido and Sakhalin, and Tatar, between Sakhalin and the continent.

In June through August, 1999, a hydrographic survey of the Japan (East) Sea was carried out on two research vessels (*R/V Roger Revelle* and *R/V Professor Khromov*), with the objective of obtaining coverage of properties and circulation of the sea from top to bottom and in almost all regions (Fig. 1(a) and Table 1). The only regions not covered were the North Korean zone and the northern Tatar Strait. The property distributions and circulation are described in a companion article (Talley et al., 2004a). Here we present a comprehensive atlas of the methods and property distributions. Because of prohibitive printing costs, only subsets of the vertical sections and horizontal maps are included in this print version, and most of the figures are in black and white. A digital version of the complete set of color graphics, including all figures shown here as well as properties along all sections shown in Fig. 1(b), and on all standard depth and

Table 1
Hydrographic measurements and principal investigators for the summer, 1999 survey

Measurement	Principal investigator	Institution
CTD temperature, salinity, oxygen	Lynne Talley	SIO (ODF)
Discrete salinity	Lynne Talley	SIO (ODF)
Discrete oxygen	Lynne Talley	SIO (ODF)
Discrete nutrients (nitrate, nitrite, dissolved silica, phosphate)	Lynne Talley	SIO (ODF)
pH, alkalinity	Pavel Tishchenko	POI
pH, alkalinity	Kyung-Ryul Kim	SNU
Chlorofluorocarbons	Mark Warner	University of Washington
Tritium, δ^3He, neon, argon, krypton	William Jenkins	SOC (now at WHOI)
δ^{18}O	William Jenkins	SOC (now at WHOI)
δ^{18}O	Kyung-Ryul Kim	SNU
Δ^{14}C	Kyung-Ryul Kim	SNU
Bio-optical profiling	B. Greg Mitchell	SIO
Ship-mounted ADCP*	Lynne Talley	SIO
Lowered ADCP	Lynne Talley and Peter Hacker	SIO and University of Hawaii
Thermosalinograph and underway atmospheric gases	Kyung-Ryul Kim	SNU
Shipbased meteorological measurements	Clive Dorman and Robert Beardsley	SIO and WHOI
PALACE floats	Stephen Riser	University of Washington
Minimet surface drifters	Dong-Kyu Lee and Pearn Niiler	Pusan National University and SIO
Towed video plankton recorder	Carin Ashjian and Cabell Davis	WHOI

Acronyms. FERHRHI, Far-Eastern Regional Hydrometeorological Research Institute, Vladivostok, Russia; POI, Pacific Oceanological Institute, Far Eastern Branch Russian Academy of Sciences, Vladivostok, Russia; SIO, Scripps Institution of Oceanography, University of California San Diego, La Jolla, CA, USA; SIO/ODF, SIO Oceanographic Data Facility; SNU, Seoul National University, Seoul, Republic of Korea; UW, University of Washington, School of Oceanography, Box 357940, Seattle, WA, USA; WHOI, Woods Hole Oceanographic Institution, Woods Hole, MA, USA.

Table 2
Mean and standard deviation of CTD properties at specified pressures

Pressure (dbar)	Number of stations	Mean potential temperature (°C)	Standard deviation potential temperature (°C)	Mean salinity	Standard deviation salinity	Mean Brunt-Vaisala frequency (cph)	Standard deviation Brunt-Vaisala frequency (cph)	Mean sound speed (m/s)	Standard deviation sound speed (m/s)
0.0	194	19.545	2.866	33.723	0.430	NA	NA	1518.5	8.3
50.0	192	8.958	5.812	34.193	0.196	6.460	2.954	1484.3	21.7
100.0	185	5.820	4.456	34.113	0.120	3.541	2.348	1473.6	17.4
200.0	165	2.427	2.009	34.064	0.031	2.218	1.693	1461.8	8.4
300.0	158	1.157	0.550	34.067	0.019	1.129	0.721	1458.1	2.4
400.0	153	0.782	0.237	34.070	0.010	0.717	0.328	1458.1	1.1
500.0	150	0.587	0.160	34.070	0.006	0.556	0.203	1458.8	0.7
750.0	144	0.336	0.108	34.068	0.003	0.359	0.137	1461.8	0.5
1000.0	133	0.219	0.053	34.067	0.002	0.268	0.153	1465.5	0.2
1500.0	106	0.124	0.016	34.066	0.002	0.188	0.208	1473.5	0.1
2000.0	90	0.086	0.007	34.067	0.001	0.104	0.203	1481.9	0.03
2500.0	65	0.070	0.005	34.067	0.001	0.198	0.162	1490.4	0.03
3000.0	51	0.065	0.002	34.068	0.001	0.245	0.130	1499.1	0.01
3400.0	20	0.063	0.001	34.068	0.001	0.259	0.004	1507.9	0.00

Maps are presented at these depths and also at: 10, 20, 30, 40, 60, 70, 80, 90, 120, 150, and 170 dbar (Figs. 12–29 and D22–D71).

Table 3
Mean and standard deviation of bottle properties interpolated to specified pressures

Pressure (dbar)	Number of stations	Mean and standard oxygen (μmol/kg)	Mean and standard nitrate (μmol/kg)	Mean and standard phosphate (μmol/kg)	Mean and standard dissolved silica (μmol/kg)	Mean and standard pH	Mean and standard alkalinity (mmol/kg)	Mean and standard CFC-11 (pmol/kg)	Mean and standard CFC-12 (pmol/kg)
0.0	194	238.1 ± 13.6	0.1 ± 0.2	0.06 ± 0.04	3.2 ± 1.2	7.974 ± 0.090	2.266 ± 0.013	3.478 ± 1. 473	1.867 ± 0.679
50.0	192	267.6 ± 40.2	6.2 ± 4.5	0.56 ± 0.32	10.8 ± 5.8	7.857 ± 0.125	2.273 ± 0.007	4.042 ± 1.119	2.117 ± 0.504
100.0	185	268.5 ± 29.6	10.6 ± 4.4	0.83 ± 0.34	15.5 ± 7.1	7.771 ± 0.125	2.271 ± 0.007	4.491 ± 0.878	2.320 ± 0.389
200.0	165	270.2 ± 24.1	15.7 ± 4.1	1.23 ± 0.32	24.5 ± 7.4	7.643 ± 0.092	2.268 ± 0.004	4.838 ± 0.504	2.435 ± 0.257
300.0	158	258.0 ± 24.5	19.5 ± 3.3	1.53 ± 0.26	32.7 ± 7.0	7.556 ± 0.060	2.267 ± 0.004	4.590 ± 0.597	2.269 ± 0.321
400.0	153	247.3 ± 24.9	21.5 ± 2.9	1.70 ± 0.23	38.8 ± 7.8	7.541 ± 0.055	2.268 ± 0.004	4.043 ± 0.746	1.972 ± 0.394
500.0	150	237.2 ± 22.2	22.8 ± 2.4	1.80 ± 0.19	44.5 ± 7.9	7.486 ± 0.047	2.269 ± 0.004	3.422 ± 0.798	1.649 ± 0.405
750.0	144	225.1 ± 13.5	24.2 ± 1.3	1.91 ± 0.11	55.2 ± 7.3	7.458 ± 0.025	2.272 ± 0.004	2.318 ± 0.710	1.113 ± 0.353
1000.0	133	219.9 ± 4.7	24.7 ± 0.3	1.95 ± 0.04	63.0 ± 5.6	7.449 ± 0.011	2.275 ± 0.005	1.570 ± 0.382	0.756 ± 0.174
1500.0	106	213.3 ± 2.8	25.3 ± 0.2	2.00 ± 0.03	74.2 ± 3.0	7.444 ± 0.008	2.281 ± 0.004	0.778 ± 0.191	0.392 ± 0.092
2000.0	90	209.5 ± 2.1	25.7 ± 0.1	2.03 ± 0.02	81.7 ± 3.3	7.443 ± 0.008	2.285 ± 0.004	0.370 ± 0.085	0.198 ± 0.043
2500.0	65	211.1 ± 1.5	25.7 ± 0.1	2.03 ± 0.01	84.6 ± 1.2	7.448 ± 0.010	2.287 ± 0.003	0.237 ± 0.053	0.134 ± 0.028
3000.0	51	211.4 ± 0.9	25.7 ± 0.1	2.03 ± 0.02	85.2 ± 0.6	7.452 ± 0.008	2.288 ± 0.002	0.202 ± 0.029	0.117 ± 0.023
3400.0	20	212.3 ± 0.6	25.7 ± 0.0	2.02 ± 0.00	85.3 ± 0.8	7.453 ± 0.007	2.288 ± 0.003	0.186 ± 0.028	0.111 ± 0.022

Maps are presented at these depths and also at: 10, 20, 30, 40, 60, 70, 80, 90, 120, 150, and 170 dbar (Figs. 12–29 and D22–D71).

Table 4
Isopycnal surfaces used in Figs. 21–26 and D72–D101

Isopycnal referenced to 0 dbar (σ_θ) or 2000 dbar (σ_2)	Number of stations	Pressure (dbar)	Potential temperature (°C)	Salinity	Notes
$24.50\sigma_\theta$	150	18.640 ± 9.151	17.864 ± 1.196	33.988 ± 0.333	
$25.00\sigma_\theta$	187	23.118 ± 12.293	15.805 ± 1.327	34.022 ± 0.339	
$25.20\sigma_\theta$	187	26.610 ± 15.139	14.968 ± 1.419	34.049 ± 0.344	
$25.40\sigma_\theta$	187	31.011 ± 19.537	14.104 ± 1.500	34.075 ± 0.346	Shallow salinity maximum (Tsushima water)
$26.00\sigma_\theta$	186	43.930 ± 28.490	11.069 ± 1.400	34.077 ± 0.263	
$26.50\sigma_\theta$	181	69.221 ± 53.749	7.942 ± 1.050	34.036 ± 0.157	
$27.00\sigma_\theta$	173	107.387 ± 77.043	4.141 ± 0.605	34.037 ± 0.068	
$27.10\sigma_\theta$	172	122.291 ± 84.148	3.215 ± 0.447	34.044 ± 0.046	
$27.20\sigma_\theta$	170	152.347 ± 89.517	2.157 ± 0.270	34.053 ± 0.025	
$27.25\sigma_\theta$	166	190.819 ± 93.822	1.585 ± 0.168	34.061 ± 0.015	Main salinity minimum (East Sea Intermediate Water)
$27.30\sigma_\theta$	162	300.574 ± 104.163	0.971 ± 0.082	34.071 ± 0.007	
$27.32\sigma_\theta$	152	438.553 ± 111.682	0.672 ± 0.055	34.072±0.004	Main salinity maximum (UJSPW)
$27.33\sigma_\theta$	150	582.073 ± 114.966	0.466 ± 0.033	34.070 ± 0.002	
$27.34\sigma_\theta$	143	884.133 ± 140.000	0.252 ± 0.027	34.067 ± 0.002	
$36.665\sigma_2$	113	1452.982 ± 175.147	0.126 ± 0.010	34.066 ± 0.001	Deep salinity minimum (East Sea Deep Intermediate Water)
$36.670\sigma_2$	93	1975.516 ± 185.748	0.086 ± 0.006	34.067 ± 0.001	Oxygen minimum
$36.675\sigma_2$	5	2875.200 ± 415.502	0.064 ± 0.002	34.070 ± 0.000	

isopycnal surfaces listed in Tables 2–4, is published together with this print version. All files are also available at http://japansea_atlas.ucsd.edu (Talley et al., 2004b). The latter site also includes the original data and cruise reports.

This survey followed earlier basin-wide surveys carried out as part of the CREAMS program (Kim et al., 1996; Kim & Kim, 1996), and which included top-to-bottom coverage with nutrients as well as the standard observations.

Advances in the summer 1999 observations were the small station separation in boundary regions, the high quality of salinity and nutrient observations with greater coverage than in previous surveys, and the addition of the chlorofluorocarbon, pH, alkalinity, helium-3, and turbidity observations. Lowered acoustic Doppler current profiling (ADCP) observations were also made at all stations (Shcherbina, Talley, Firing, & Hacker, 2003). Underway ADCP measurements were made from the *R/V Revelle* (Helium-3, turbidity and ADCP measurements are not presented here.) Principal investigators for the measurements are listed in Table 1. Specifics of the two ship's programs are given in the following sections.

2. Cruise information

Two ships were used for this survey: the *R/V Roger Revelle* from the US (Scripps Institution of Oceanography or SIO) and *R/V Professor Khromov* from Russia (Far Eastern Regional Hydrometeorological Research Institute or FERHRI). The same sampling equipment, acquisition software, chemistry equipment, standards and methods were used on both ships. A large overlap of 17 scientific personnel between the two cruises also facilitated uniformity. A somewhat larger suite of measurements was carried out on the *Revelle* than on the *Khromov*. A total of 203 CTD/rosette stations were completed.

The *R/V Revelle*, with Captain D. Muirline and chief scientist L. Talley, departed Busan, Korea on June 24, 1999 and returned to Busan on July 17, 1999, completing 113 CTD stations with a rosette sampler with 24 10-l Niskin bottles, a lowered acoustic Doppler current profiler (ADCP), two transmissometers, and an altimeter to measure bottom approach. Most stations were separated by 10–30 nautical miles, and from the surface to within 5–10 m of the bottom. The station pattern covered most of the southern and eastern Japan Sea. Ship-mounted ADCP, thermosalinograph, GPS navigation, acoustic depth recording, and specialized meteorological measurements were collected underway. Separate bio-optical and video plankton recorder programs were also aboard, and surface drifters were also deployed.

The *R/V Professor Khromov* joined the *Revelle* in Busan for equipment and personnel transfer, including SIO personnel, and departed July 22, 1999 for a test cruise of nine stations in the Ulleung Basin. The *Khromov* returned to Busan, disembarked non-Russian personnel, and then continued on July 28, 1999, with Captain I. Kiselev and chief scientist V. Luchin, occupying a further 82 stations in the northern sector of the Japan Sea. All stations were to the bottom except for a few in two short east-west sections sampling eddies, at 131° 30′ E and 134° E. The *Khromov* completed its work with a port stop in Vladivostok on August 11, 1999. A reduced underway program was carried out, with specialized meteorological measurements and GPS navigation. Subsurface floats for a separate program were also deployed.

3. Measurement methods

3.1. CTD measurements

Neil Brown Instrument Systems (NBIS) MKIIIB CTDs with Sensormedics oxygen sensors were used for all stations. The two CTDs used were SIO ODF's instruments 3 (stations 1–8, 113) and 5 (stations 9–112,

114–203). Instrument 5 had identical dual temperature and conductivity sensors; the ''second'' temperature and ''second'' conductivity sensor were judged to be best and were used for the calibrated values. An ODF rosette frame and 24 ODF-built 10 l Niskin bottles (''Bullister'' style, with O-ring assembly and maintenance adapted for chlorofluorocarbon sampling) were used. The 150-KHz LADCP was built by RDI. Two Wetlabs Cstar 25 cm transmissometers were used.

The time series CTD data (20 frames per second) were converted to engineering units, filtered, response-corrected, and averaged in 1-s time bins. Time-averaged data were then converted to a 2-dbar pressure series, including correction for ship roll. Initial processing of the CTD pressure, temperature, and salinity data has been completed, with calibration to the salinity samples and pre- and post-cruise calibration of the pressure and temperature sensors in the calibration facility at SIO. (Final processing was completed after this article, in mid-2004). CTD oxygen data will probably not be processed. Final calibration accuracy, presumably available before the end of 2004, will be that of the World Ocean Circulation Experiment (Joyce, Corry, & Stalcup, 1991): 0.002 °C, 0.002 psu. The present calibration, used herein, nearly meets these standards, but deep salinities are not yet adequate to map variations in salinity and density of the deep salinity mininum (East Sea Deep Intermediate Water; Kim et al., 1996). Hence caution is advised when examining details of the maps of these CTD quantities at depths greater than 1000 dbar.

3.2. Salinity, oxygen, and nutrient analyses

Salinity samples were analyzed on one of two SIO ODF Guildline 8400A autosalinometers, in temperature-controlled laboratories. Water samples were equilibrated to laboratory temperature after about 8 h and were run within 8–12 h of the cast. At least one fresh vial of IAPSO Standard Seawater Batch P-134 was used for processing each station. Accuracy of the measurements is 0.002 psu or better. Precision is better, on the order of 0.0005, which means that this internally consistent data set can be used to map relative variations in deep salinity.

Dissolved oxygen samples were drawn from the Niskins soon after chlorofluorocarbon and helium samples. They were analyzed on an SIO-designed automated oxygen titrator using a Brinkman Dosimat automatic burette and photometric end-point detection. Accuracy of the measurements is 0.5–1%.

Nutrients (phosphate, nitrate plus nitrite, nitrite, silicic acid) were analyzed using ODF's four-channel Technicon Autoanalyzer-II CFA system. Accuracy of the measurements is 1–2% or better.

The three systems performed well throughout the cruises. All three systems had SIO-built computer acquisition interfaces, minimizing transcription errors. Data values were merged with CTD data within a day or two of analysis, for examination to determine problems with samples or the rosette sampler and bottles.

3.3. Alkalinity and pH analyses

Samples were collected and analyzed for pH and alkalinity at every station and at almost every Niskin bottle, using the Pacific Oceanological Institute (POI) systems. Samples at 15 stations (~130 samples) on the *R/V Revelle* were collected for analysis with the Seoul National University systems for comparison. The POI methods are described here since these are the basis for the vertical sections and maps.

The POI pH analysis is a potentiometric measurement in a potential cell without a liquid junction, since it had been reported that the liquid junction can degrade accuracy and reproducibility (Tishchenko & Pavlova, 1999). This method has excellent reproducibility, with a precision of 0.004 pH units. Comparison with the SNU samples, which were analyzed using spectrophotometry (Clayton & Byrne, 1993), and which had similar precision, showed similar values at a pH of 7.8, with increasing differ-

ences with decreasing pH, up to 0.35 at a pH of 7.5, which is the typical pH value from 200m depth to the bottom in the Japan Sea. Thus the two systems yield a systematic offset, with the POI values lower.

The POI alkalinity analysis used Bruevich's method (Bruevich, 1944), using colorimetric titration by hydrochloric acid in an open system using a mixed indicator (methylene blue and methyl red), under flow of CO_2-free air, and visual endpoint detection. The acid was standardized daily with A. Dickson's (SIO) certified reference material. Precision is 4–5 μmol/kg. The POI values were systematically 5–10 μmol/kg lower than the SNU values, obtained using a closed cell potentiometric titration (Millero, Zhang, Lee, & Campbell, 1993).

3.4. Chlorofluorocarbon analyses

Chlorofluorocarbons, CFC-11, CFC-12 and CFC-113, were measured in seawater at 111 of the 112 R/V Revelle stations, at many of the 90 Professor Khromov stations, and in the overlying atmosphere (Min & Warner, 2004). The sampling strategy alternated casts with complete coverage of the water column (16–20 samples) and casts where only 6–10 samples were collected at target depths (usually the bottom or the East Sea Intermediate Water layer). The Revelle measurements were made using standard analytical techniques in the ship's laboratory. Of the 1220 *R/V Revelle* samples, approximately 40 were duplicates from the same Niskin to establish the measurement precision. The precision appears to meet or exceed WOCE standards (standard deviation of 1.5% or 0.005 pmol/kg, whichever is greater).

The *Professor Khromov* measurements were made from samples collected in glass ampoules and flame-sealed for later analysis at the University of Washington. Approximately 600 samples were collected during the *Khromov* trip, but only a few of the samples could actually be run. For comparison with shipboard laboratory analyses, ampoule samples were collected from 137 bottles on the *R/V Revelle* immediately after the syringe sample for shipboard analysis was drawn; the comparisons were favorable. Detailed discussion of the procedures for the ampoule samples is given by Min and Warner (2004).

Surface CFC concentrations were at or slightly above the expected values based on Warner and Weiss (1985) solubilities. Since there are CFCs throughout the entire water column, the typical method of using the measured CFC concentrations in waters which should be CFC-free to estimate the sampling blank could not be applied. Instead, CFC-free water, produced by bubbling nitrogen through the sample, was allowed to sit in a Niskin bottle. By measuring the change in CFC concentration with time, the amount of contamination due to desorption was estimated.

The analysis was based upon the purge-and-trap technique described by Bullister and Weiss (1988) with a few modifications. The same volume of water for every sample was purged through the use of a glass sample chamber with a calibrated volume. Ultra high purity nitrogen (99.999% pure) was used as the carrier gas. (An analysis of the CFC content found less than 1 part per trillion of both CFC-11 and CFC-12). A Hewlett–Packard 5890-II gas chromatograph with electron capture detector was used to detect the CFCs. The analog output (voltage) of the detector was converted to a digital signal by a Hewlett–Packard 35900E and the digital chromatograms analyzed on a Sun Sparcstation LX using software developed by Peter Salameh. The results are reported on the SIO 1993 scale using a calibrated standard gas cylinder (#39765).

Only minor analytical difficulties were encountered during the *R/V Revelle* cruise. The sensitivity of the detector to an injection of a calibrated volume of the standard gas was steady during the cruise with a standard deviation of ±0.90% for CFC-12 and ±1% for CFC-11. Calibration curves were prepared while in port in Busan and additional points were added to the curves during the course of the expedition. These additional points fitted the initial curve so that one calibration curve could be used for the entire 23 days.

The atmospheric concentrations of the CFCs were determined at 20 locations during the *R/V Revelle* cruise. Air samples were pumped from the bow through Decabon tubing to the analytical system. The measured atmospheric concentrations of CFC-11 and CFC-12 both decreased with increasing latitude.

The means and standard deviations (in ppt) are: CFC-11: 256.5 ± 5.3; CFC-12: 538.8 ± 8.3; CFC-113: 81.5 ± 2.4.

4. Property–property distributions (Figs. 2 and 3)

Properties in the Japan (East) Sea are first presented here as scatter plots for all stations as a function of depth and as a function of each other (Figs. 2 and 3). Properties plotted are: potential temperature, salinity, oxygen, silicate, nitrate, phosphate, chlorofluorocarbon-11, pH, alkalinity. The near-uniformity of the more conservative properties (especially salinity, potential temperature) in the waters below the pycnocline, which is not much deeper than the sill depth of the inflow at Tsushima Strait, is evident in the figures. The near-uniformity is also evident in the mean and standard deviation of properties at standard depths (Tables 2–4). Stations are color-coded by region (see Fig. 1(a)).

5. Vertical sections (digital Figs. D4–D21)

The CTD and bottle sample data, including chlorofluorocarbons (CFC-11 and CFC-12) (Min & Warner, 2004) are displayed in vertical cross-sections along 18 tracks shown in Fig. 1(b). All sections are available in the copyrighted accompanying digital version of this publication and can also be accessed through the informal website: http://japansea_atlas.ucsd.edu (Talley et al., 2004b). Because the total number of sections is large, only representative sections are included in the printed version. Black and white versions of sections at Tsushima Strait, Tsugaru Strait, "J1" (131° E), "P3" (37° N), "Y1–J2" (134° E), "J4" (44° N), and "J5" (46° N) are included in the print version (Figs. 4, 5 and 7–11). Only one set of color sections, "P1-Y3J3" (Ulleung, Yamato and Japan Basins), is presented in the printed version (Fig. 6). All 18 sets of color sections are available in the digital version.

CTD sections were produced by smoothing the 2 dbar pressure series to 10 dbar with a Gaussian filter with a 5 dbar half-width. These slightly smoothed data were objectively mapped (Roemmich, 1983) to a regular grid, with 3 km and 10 dbar horizontal and vertical spacing along the section. A minimum of six stations was required for mapping.

Bottle sample sections were produced by objectively mapping the water sample data directly to the 3 km and 10 dbar grid using the Roemmich (1983) method.

Bathymetry plotted on the sections is either from the R/V Revelle's Seabeam or Precision Depth Recorder (all Revelle portions), or from the Smith and Sandwell (1994) global bathymetric data set based on satellite altimetry.

6. Maps at standard depths (digital Figs. D22–D71)

Maps of CTD and bottle sample properties are presented at standard depths (Figs. 12–29 in print version; Figs. D22–D71 in digital version). The pycnocline, as well as the thermocline, halocline, oxycline and nutricline, are exceptionally shallow (Talley et al., 2004a) compared with the open Pacific, due to the shallowness of the straits connecting the Japan Sea to the Pacific, and due to the limited sources of deep water within the Japan Sea (Gamo, Nozaki, Sakai, Nakai, & Tsubota, 1986; Senjyu & Sudo, 1994; Talley et al., 2003). Maps were computed at 25 different levels plus the bottom: at 10 dbar intervals from the surface to 100 dbar, at 25 dbar intervals to 200 dbar, at 100 dbar intervals to 500 dbar, at 750 dbar, and at 500 dbar intervals from 1000 to 3000 dbar plus 3400 dbar (near bottom). All of the maps are included in the digital version of this manuscript and in the website http://japansea_atlas.ucsd.edu (Talley et al., 2004b). One set of

color maps, at 10 dbar (Figs. 12 and 13), is included in the print version. Black and white maps of all properties at the depths listed in Tables 2 and 3 are included in the print version (Figs. 14–29).

From the CTD temperature and salinity data, maps of potential temperature, salinity, potential density, potential density referenced to the sea surface, isopycnic potential vorticity, Brunt-Vaisala frequency, and sound speed are displayed. Isopycnic potential vorticity is calculated as $(f\rho^{-1}\partial\rho/\partial z)$, where the density ρ is computed relative to the mid-point of the depth interval for the derivative (based on a least squares fit to the slope over 30 dbar). Brunt-Vaisala frequency N ($N^2 = -g\rho^{-1}\partial\rho/\partial z$) is computed similarly.

Properties that were mapped from bottle data are: oxygen, silicate, nitrate, phosphate, chlorofluorocarbon-11, chlorofluorocarbon-12, pH, and alkalinity. The bottle data were interpolated to standard depths using an Akima cubic spline.

The horizontal maps were created from the station data at each depth, using the Generic Mapping Tools (GMT) software (Wessel & Smith, 1995), which interpolates using splines (Smith & Wessel, 1990). GMT was also used for plotting. Some peculiarities remain in the mapped products, including sometimes excessive "bowing" of contour intervals through undersampled regions, and overshoot resulting in extrema where none were measured. Many of these problems were corrected by hand but some remain, given the very large number of maps presented.

7. Maps on isopycnals (digital Figs. D72–D105)

Maps of the same CTD and bottle sample properties were produced on isopycnal surfaces (Table 4, Figs. 30–41, digital Figs. D72–D105), many selected to represent particular "water masses" or core layers of property extrema (Kim et al., 1996; Senjyu & Sudo, 1994; Talley et al., 2004a). As for the standard depths, many more maps have been computed for the upper ocean because of the very shallow pycnocline. Because of the near-homogeneity of the deep waters in terms of potential density, only a few deep isopycnals were chosen. All color versions of the maps and all listed isopycnals are included in the digital version and in the aforementioned web-based atlas. Only one set of color maps is included in the print version (Figs. 36 and 37), at $27.32\sigma_\theta$, which represents the salinity maximum of the Upper Japan Sea Proper Water (Senjyu & Sudo, 1994). This isopycnal is also featured in Min and Warner (2004).

Potential density referenced to the sea surface is used for isopycnals in the upper 1000 dbar, and referenced to 2000 dbar for the remaining water column. Neutral density (Jackett & Mcdougall, 1997) appears inappropriate for this nearly isolated marginal sea, although the Jackett and Mcdougall software does find neutral surfaces within the Japan Sea and is used in Min and Warner (2004). Horizontal mapping on the surfaces again used GMT, with the same cautionary statements as in Section 6.

The outer boundary of the contoured region was chosen simply as the isobath at the shallowest part of the mapped isopycnal surface (or the crude outer limit of the sampling region, for instance, west of 131° E).

Acknowledgements

The captains and crews of the Revelle and Khromov, and scientific personnel from SIO/ODF, FEHRHI, and POI were central to these expeditions. The Office of Naval Research supported the SIO work (L.D.T.), through Grant N00014-98-1-0220.

Appendix A. Supplementary material

Supplementary data associated with this article can be found, in the online version at doi:10.1016/j.pocean.2004.06.011.

References

Bruevich, C. V. (1944). Determination alkalinity of small volumes of seawater by direct titration. In: Instruction of chemical investigation of seawater. Glavsevmorput, M.-L., 83p.

Bullister, J. L., & Weiss, F. R. (1988). Determination of CCl_3F and CCl_2F_2 in seawater and air. *Deep-Sea Research, 35*, 839–853.

Clayton, T. D., & Byrne, H. R. (1993). Spectrophotometric seawater pH measurements: total hydrogen ion concentration scale calibration of *m*-cresol purple and at-sea results. *Deep-Sea Research, 40*, 2115–2129.

Gamo, T., Nozaki, Y., Sakai, H, Nakai, T., & Tsubota, H. (1986). Spatial and temporal variations of water characteristics in the Japan Sea bottom layer. *Journal of Marine Research, 44*, 781–793.

Jackett, D. R., & Mcdougall, J. T. (1997). A neutral density variable for the world's oceans. *Journal of Physical Oceanography, 27*, 237–263.

Joyce, T., Corry, C., & Stalcup, M. (1991). WOCE operations manual, *Vol. 3*. The observational programme, Section 3.1: WOCE Hydrographic Programme, Part 3.1.2: Requirements for WHP Data Reporting, Rev. 1, WHP Office Report WHPO 90-1, WOCE Report No. 67/91.

Kim, K.-R., & Kim, K. (1996). What is happening in the East Sea (Japan Sea)? Recent chemical observations during CREAMS 93–96. *Journal of the Korean Society of Oceanography, 31*, 164–172.

Kim, K., Kim, K.-R., Kim, Y.-G., Cho, Y.-K., Chung, J.-Y., Choi, B.-H., et al. (1996). New findings from CREAMS observations: water masses and eddies in the East Sea. *Journal of the Korean Society of Oceanography, 31*, 155–163.

Millero, F. J., Zhang, J.-Z., Lee, K., & Campbell, M. D. (1993). Titration alkalinity of seawater. *Marine Chemistry, 44*, 153–166.

Min, D. -H., & Warner, M. (2004). Basin-wide circulation and ventilation study in the East Sea (Sea of Japan) using chlorofluorocarbon tracers. *Deep-Sea Research II* (in revision).

Roemmich, D. (1983). Optimal estimation of hydrographic station data and derived fields. *Journal of Physical Oceanography, 13*, 1544–1549.

Senjyu, R., & Sudo, H. (1994). The upper portion of the Japan Sea Proper Water; its source and circulation as deduced from isopycnal analysis. *Journal of Oceanography, 50*, 663–690.

Shcherbina, A., Talley, D. L., Firing, E., & Hacker, P. (2003). Near surface frontal zone trapping and deep upward propagation of internal wave energy in the Japan/East Sea. *Journal of Physical Oceanography, 33*, 900–912.

Smith, W. H. F., & Sandwell, T. D. (1994). Bathymetric prediction from dense altimetry and sparse shipboard bathymetry. *Journal of Geophysical Research, 99*, 21803–21824.

Smith, W. H. F., & Wessel, P. (1990). Gridding with continuous curvature splines in tension. *Geophysics, 55*, 293–305.

Talley, L. D., Lobanov, V., Ponomarev, V., Salyuk, A., Tishchenko, P., Zhabin, I., et al. (2003). Deep convection and brine rejection in the Japan Sea. *Geophysical Research Letters, 30*(4), 1159.

Talley, L. D., Shcherbina, A., Tishchenko, P., Luchin, V., Ponomarev, V., Nedashkovskiy, A., et al. (2004a). Water properties and circulation of the Japan/East Sea based on hydrographic surveys in summer, 1999. *Progress in Oceanography*, submitted.

Talley, L. D., Tishchenko, P., Luchin, V., Nedashkovskiy, A., Sagalaev, S., Kang, D. -J., et al. (2004b). Online atlas of hydrographic properties of the Japan (East) Sea in summer, 1999. Available: http://japansea_atlas.ucsd.edu.

Tishchenko, P. Ya., Pavlova, & G. Yu. (1999). Standardization of pH measurements of seawater by Pitzer's method. In: CO_2 in the Oceans, Extended Abstracts, Tsukuba.

Warner, M. J., & Weiss, F. R. (1985). Solubility of chlorofluorocarbons 11 and 12 in water and seawater. *Deep-Sea Research, 32*, 1485–1497.

Wessel, P., & Smith, W. H. F. (1995). New version of the Generic Mapping Tools released. *EOS Transactions of the American Geophysical Union, 76*, 329.

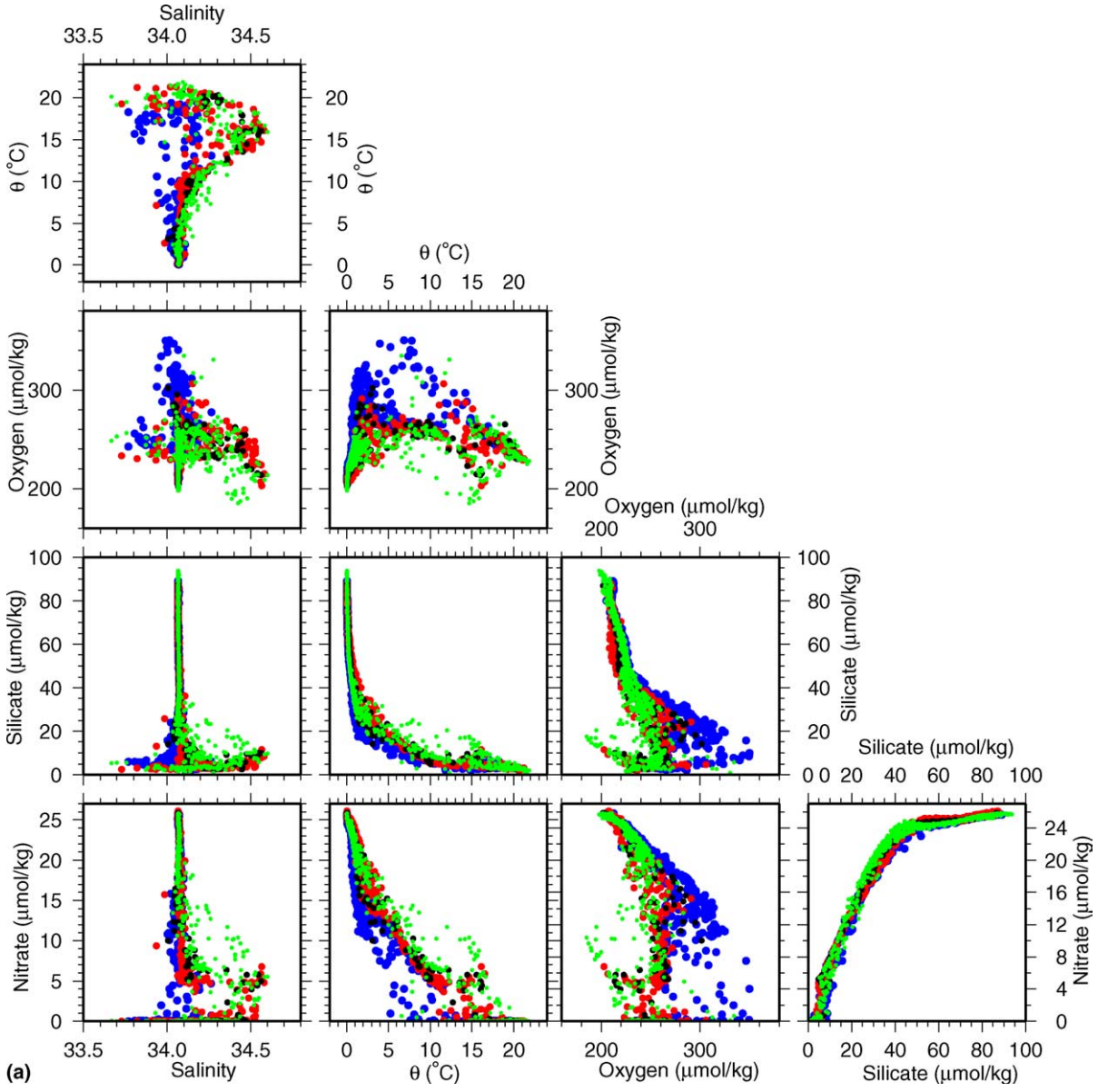

Fig. 2. (a) For the stations shown in Fig. 1(b) (Ulleung Basin – green, Yamato Basin – red, Japan Basin – blue, Yamato Rise – black): Salinity, potential temperature (°C), oxygen (µmol/kg), dissolved silicate (µmol/kg), nitrate (µmol/kg), phosphate (µmol/kg), pH, and alkalinity (mmol/kg). Property ranges were selected for full coverage, with the exception of a small number of very low salinity values. (b) For the stations shown in Fig. 1(b) (Ulleung Basin – green, Yamato Basin – red, Japan Basin – blue, Yamato Rise – black): Salinity, potential temperature (°C), oxygen (µmol/kg), dissolved silicate (µmol/kg), phosphate (µmol/kg), CFC-11 (pmol/kg), pH, alkalinity (mmol/kg), and depth (m). Property ranges were selected for full coverage, with the exception of a small number of very low salinity and alkalinity values. (c) For the stations shown in Fig. 1(b) (Ulleung Basin – green, Yamato Basin – red, Japan Basin – blue, Yamato Rise – black): Nitrate (µmol/kg), phosphate (µmol/kg), CFC-11 (pmol/kg), pH, alkalinity (mmol/kg), and depth (m). Property ranges were selected for full coverage, with the exception of a small number of very low alkalinity values.

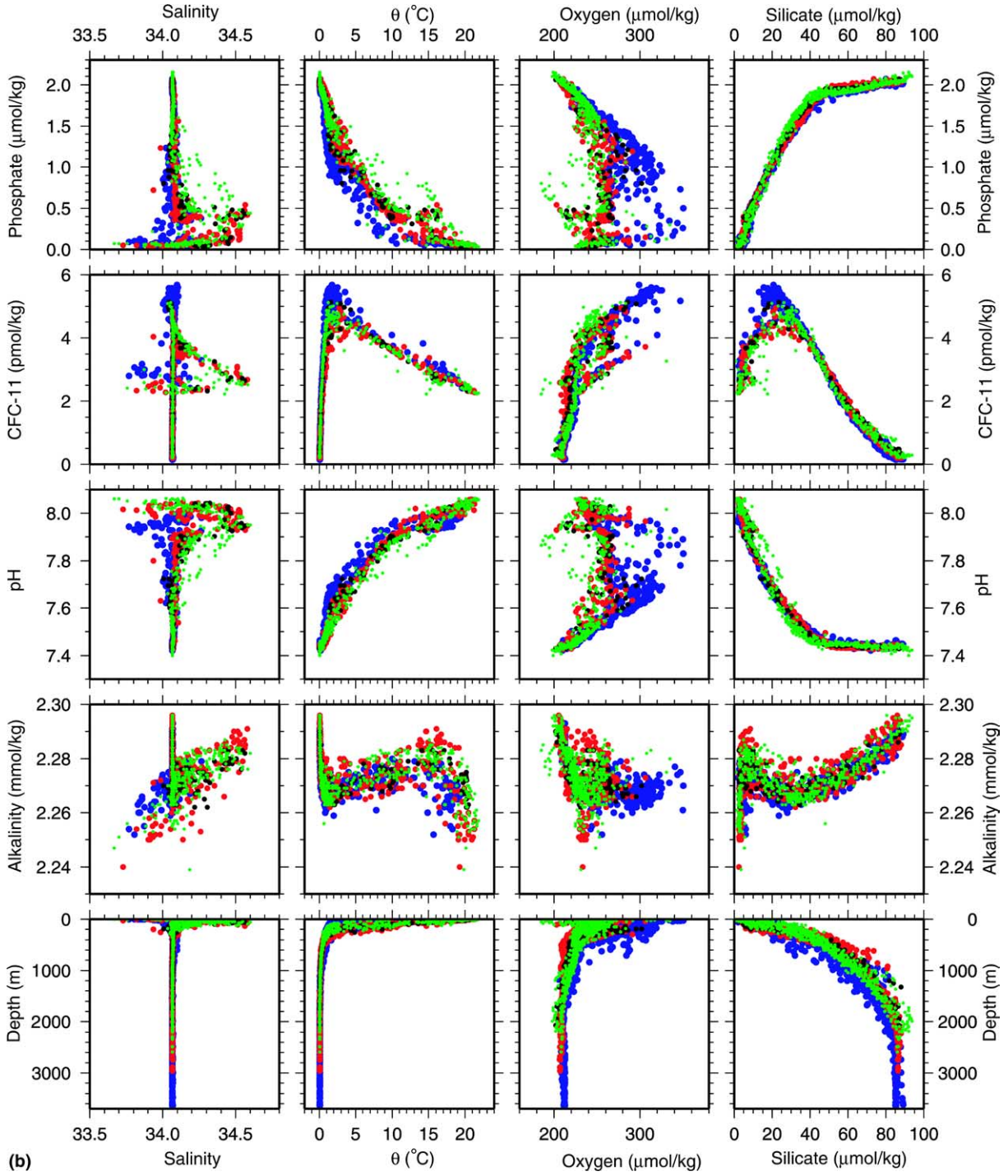

Fig. 2 (*continued*)

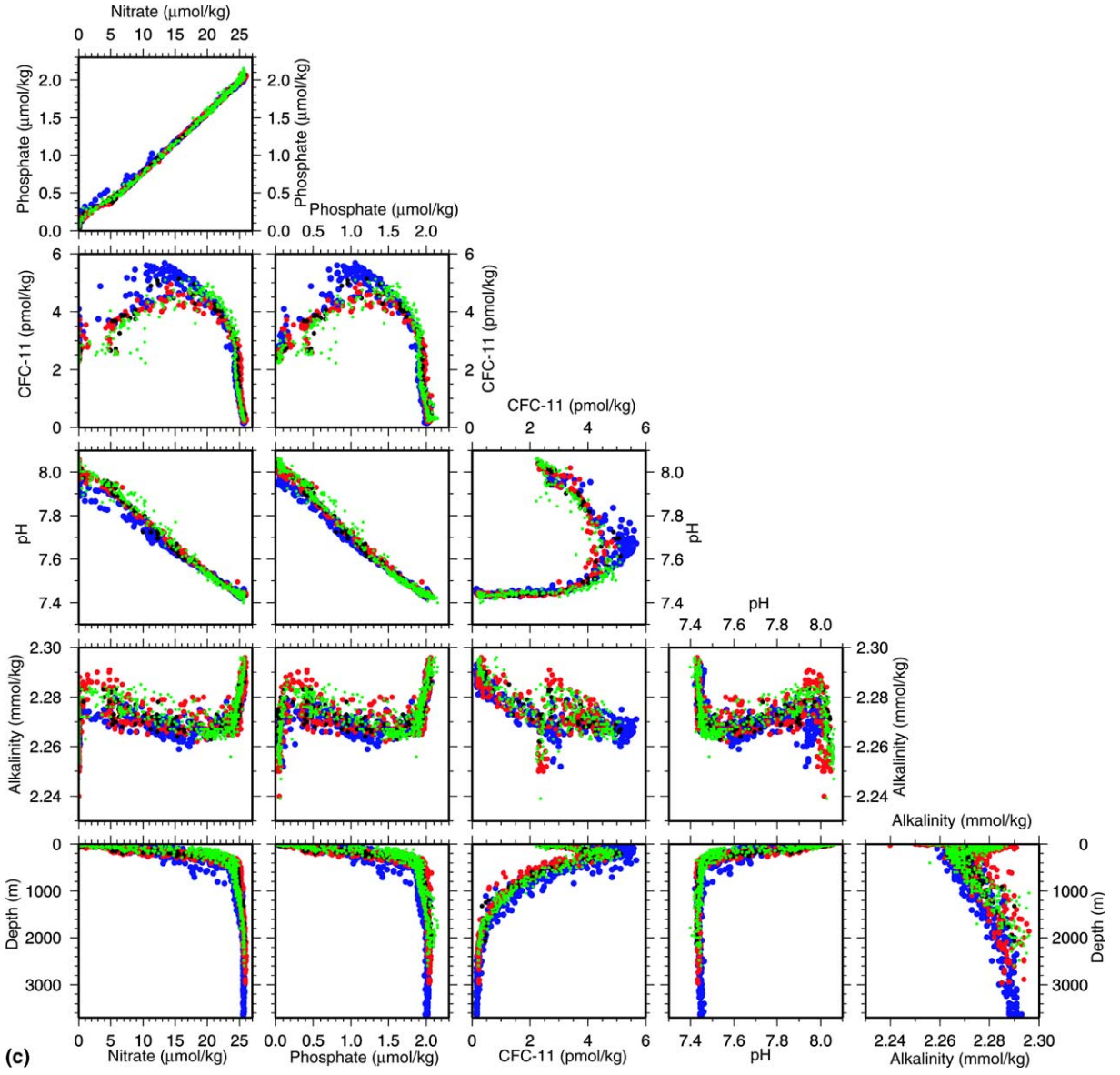

Fig. 2 (*continued*)

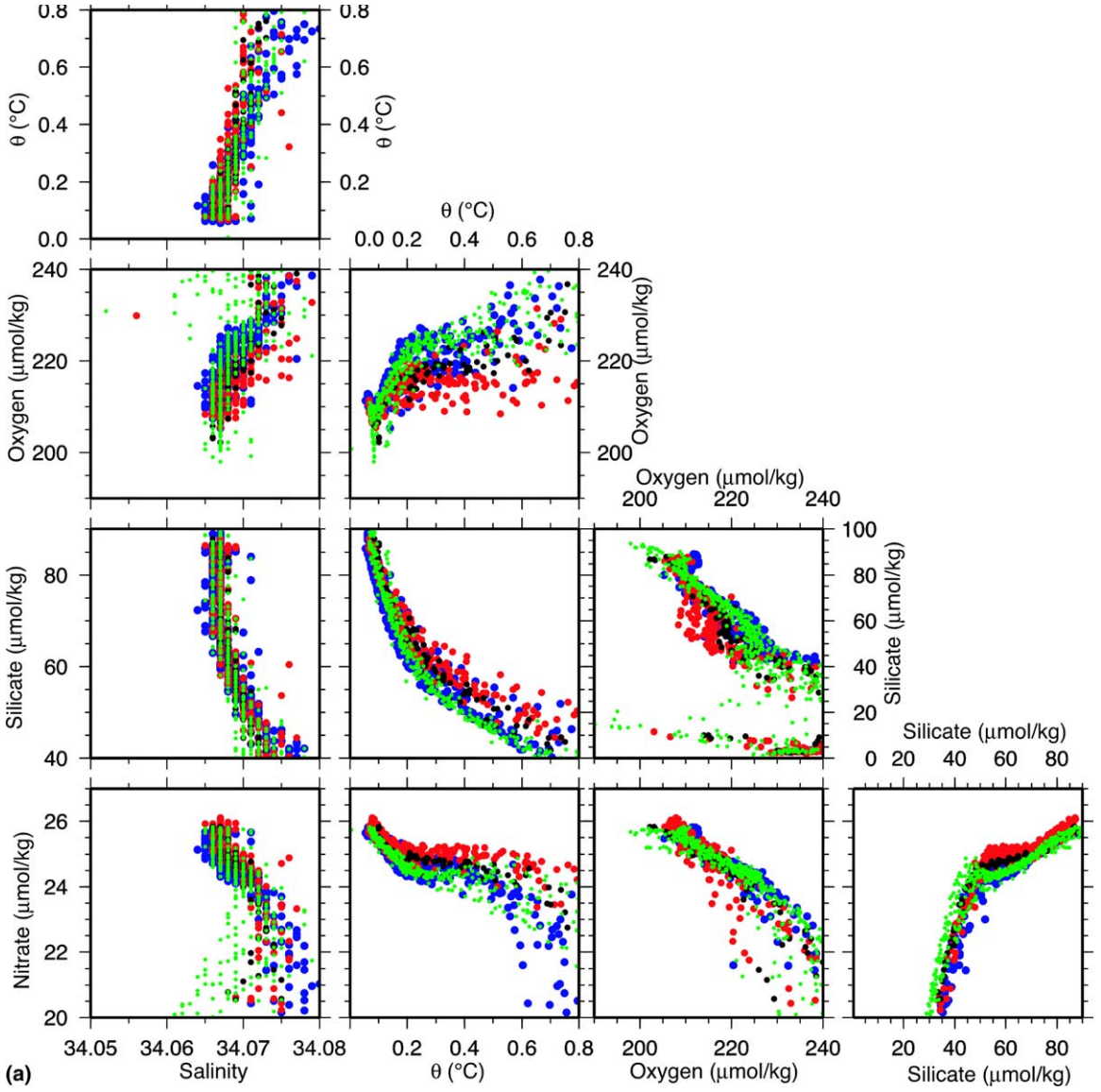

Fig. 3. (a) Property plots for the stations shown in Fig. 1(b) (Ulleung Basin – green, Yamato Basin – red, Japan Basin – blue, Yamato Rise – black) as in Fig. 2(a). (b) Property plots for the stations shown in Fig. 1(b) (Ulleung Basin – green, Yamato Basin – red, Japan Basin – blue, Yamato Rise – black) as in Fig. 2(b). (c) Property plots for the stations shown in Fig. 1(b) (Ulleung Basin – green, Yamato Basin – red, Japan Basin – blue, Yamato Rise – black) as in Fig. 2(c).

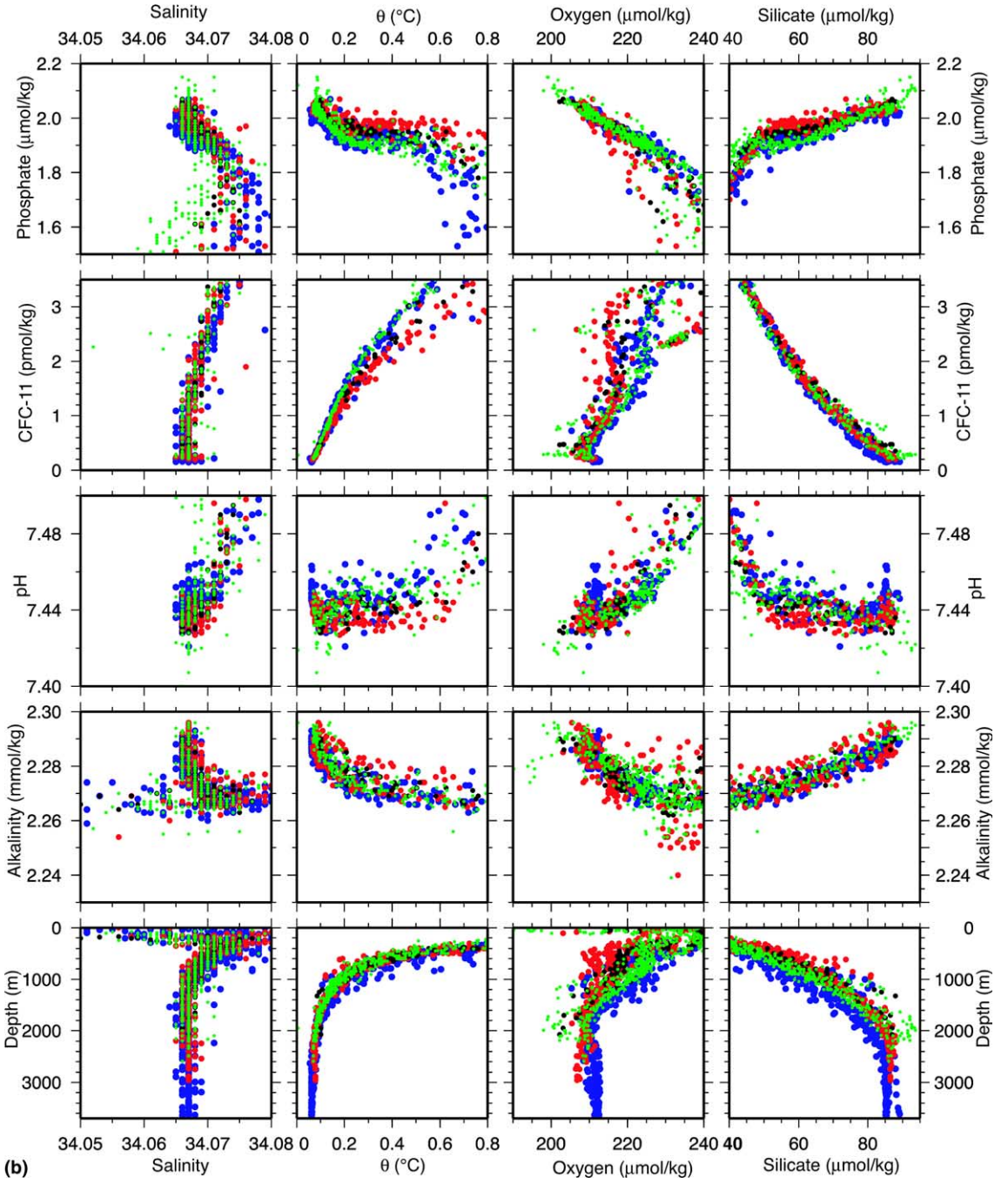

Fig. 3 (*continued*)

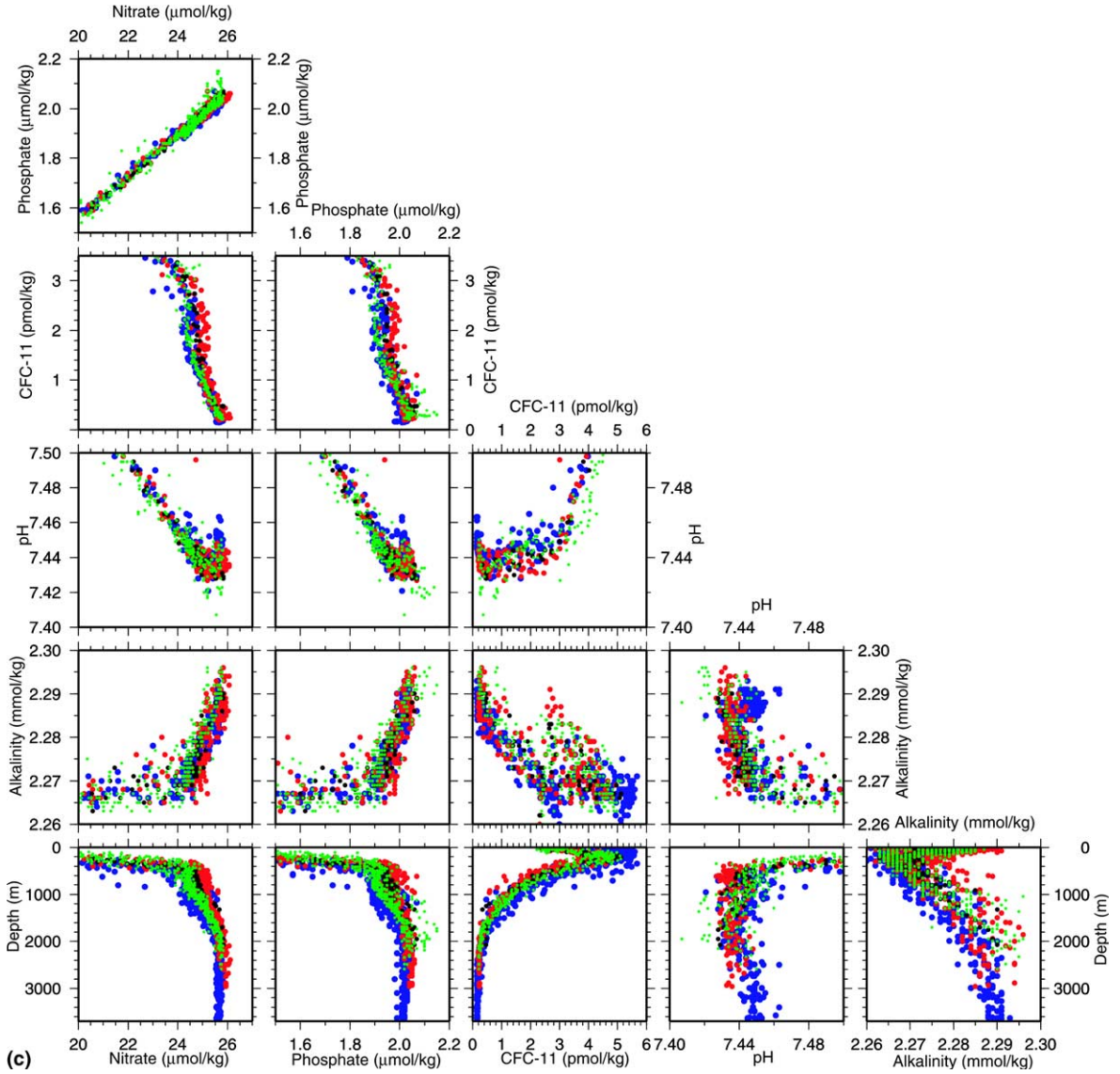

Fig. 3 (*continued*)

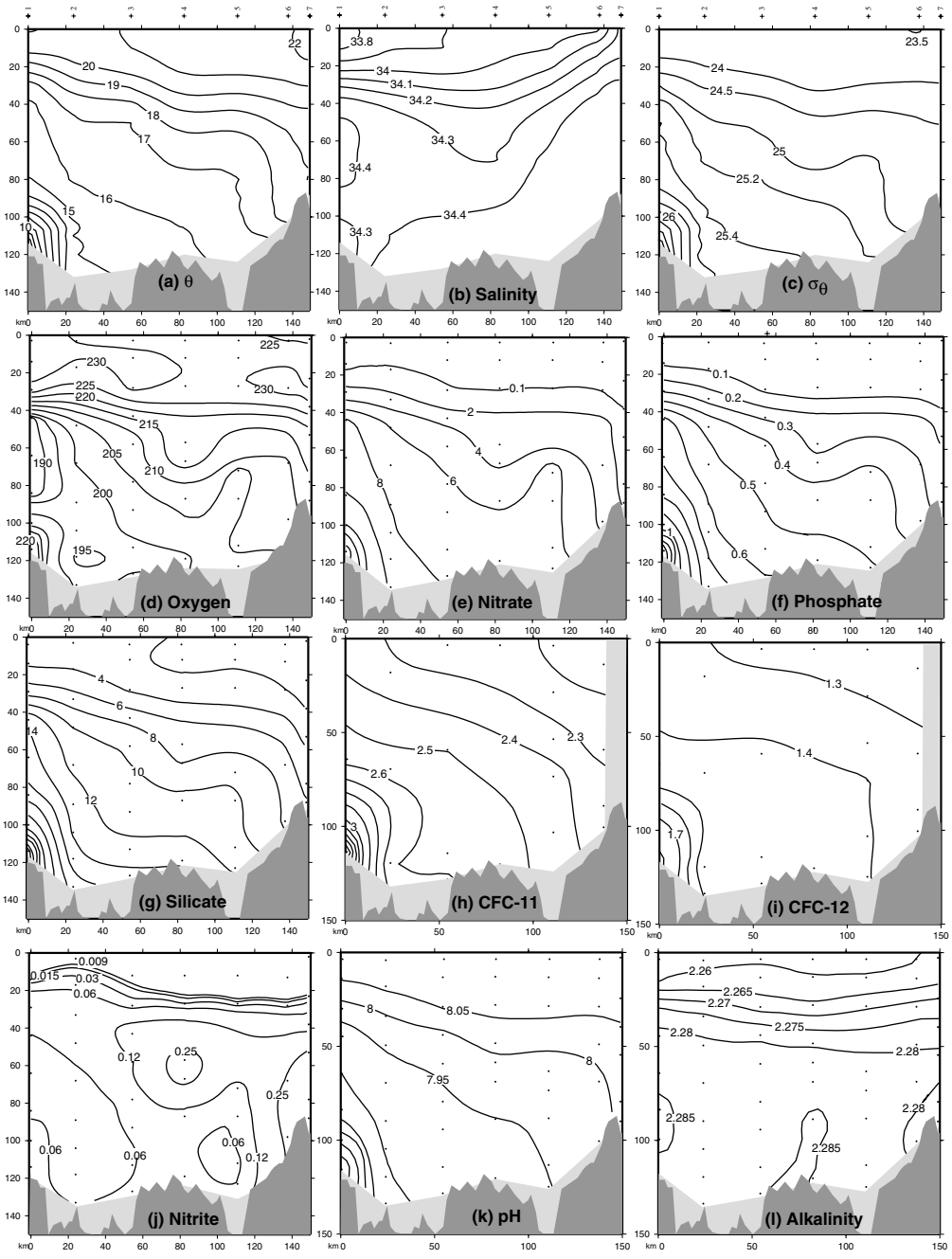

Fig. 4. Vertical sections at Tsushima Strait: (a) Potential temperature (°C), (b) salinity, (c) potential density σ_θ, (d) oxygen (μmol/kg), (e) nitrate (μmol/kg), (f) phosphate (μmol/kg), (g) dissolved silica (μmol/kg), (h) CFC-11 (pmol/kg), (i) CFC-12 (pmol/kg), (j) nitrite (μmol/kg), (k) pH, and (l) alkalinity (mmol/kg). Color versions are in the accompanying digital atlas.

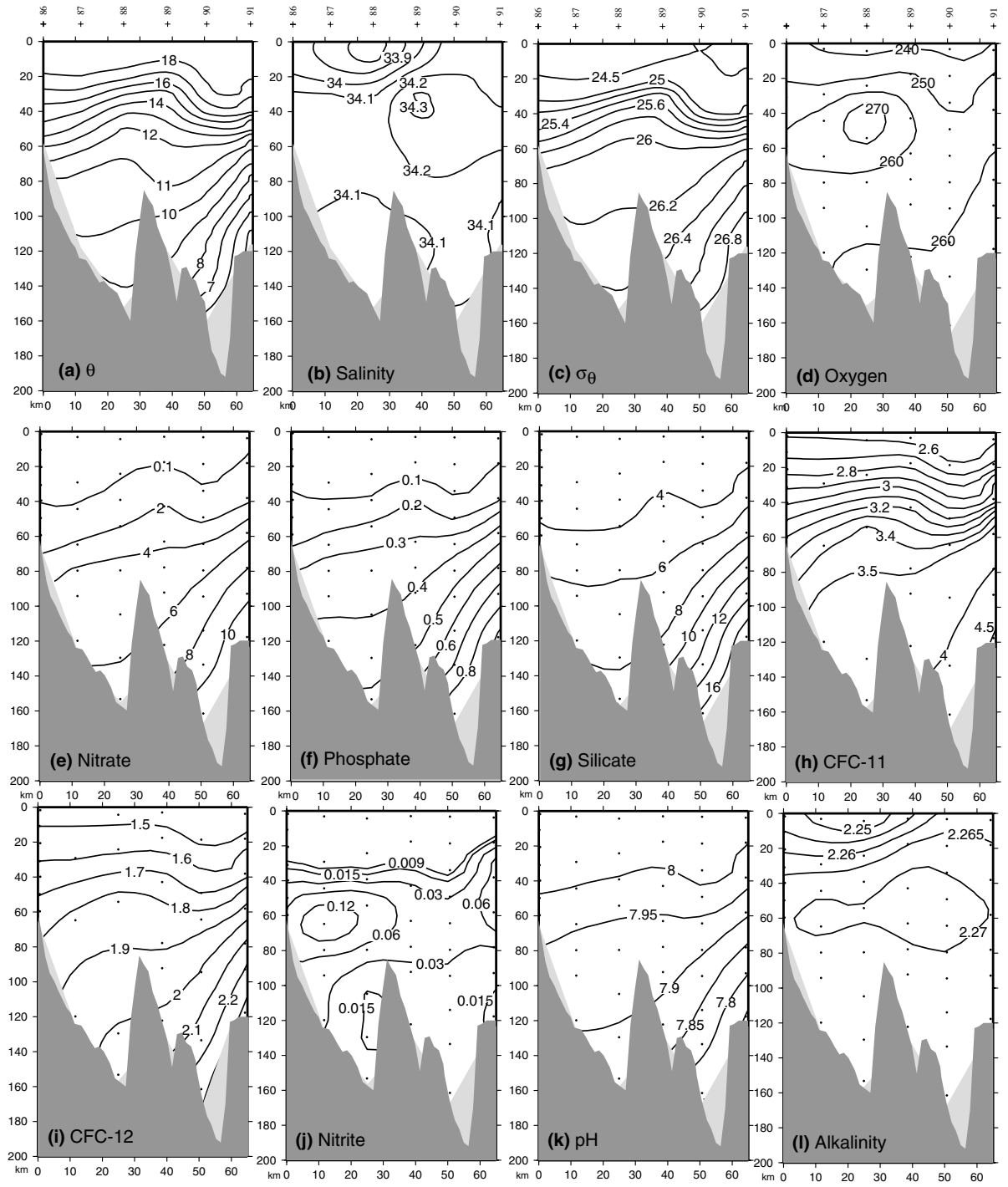

Fig. 5. Vertical sections at Tsugaru Strait: (a) Potential temperature (°C), (b) salinity, (c) potential density σ_θ, (d) oxygen (μmol/kg), (e) nitrate (μmol/kg), (f) phosphate (μmol/kg), (g) dissolved silica (μmol/kg), (h) CFC-11 (pmol/kg), (i) pH, and (j) alkalinity (mmol/kg). Color versions are in the accompanying digital atlas.

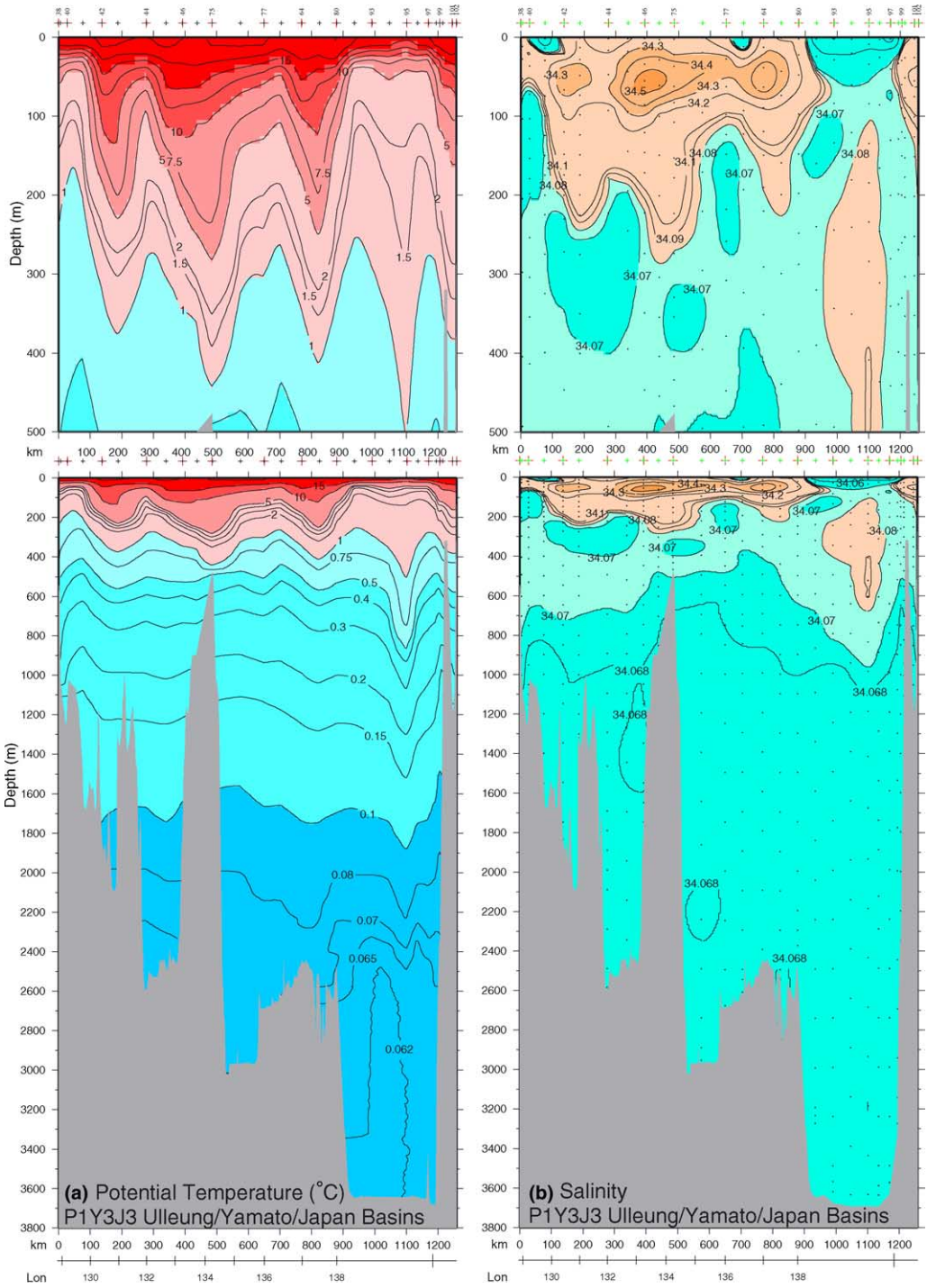

Fig. 6. Vertical sections through the Ulleung, Yamato, and Japan Basins (combined sections P1, Y3J3 in Fig. 1(b)): (a) Potential temperature (°C), (b) salinity, (c) potential density, (d) oxygen (μmol/kg), (e) nitrate (μmol/kg), (f) nitrite (μmol/kg), (g) phosphate (μmol/kg), (h) dissolved silica (μmol/kg), (i) CFC-11 (pmol/kg), (j) CFC-12 (pmol/kg), (k) pH, and (l) alkalinity (mmol/kg). The vertical axis is depth (m) and the horizontal axis is distance (km). Interpolated longitudes along the sections are also shown. Upper panel vertical exaggeration is 2500:1. Lower panel vertical exaggeration is 625:1. This set

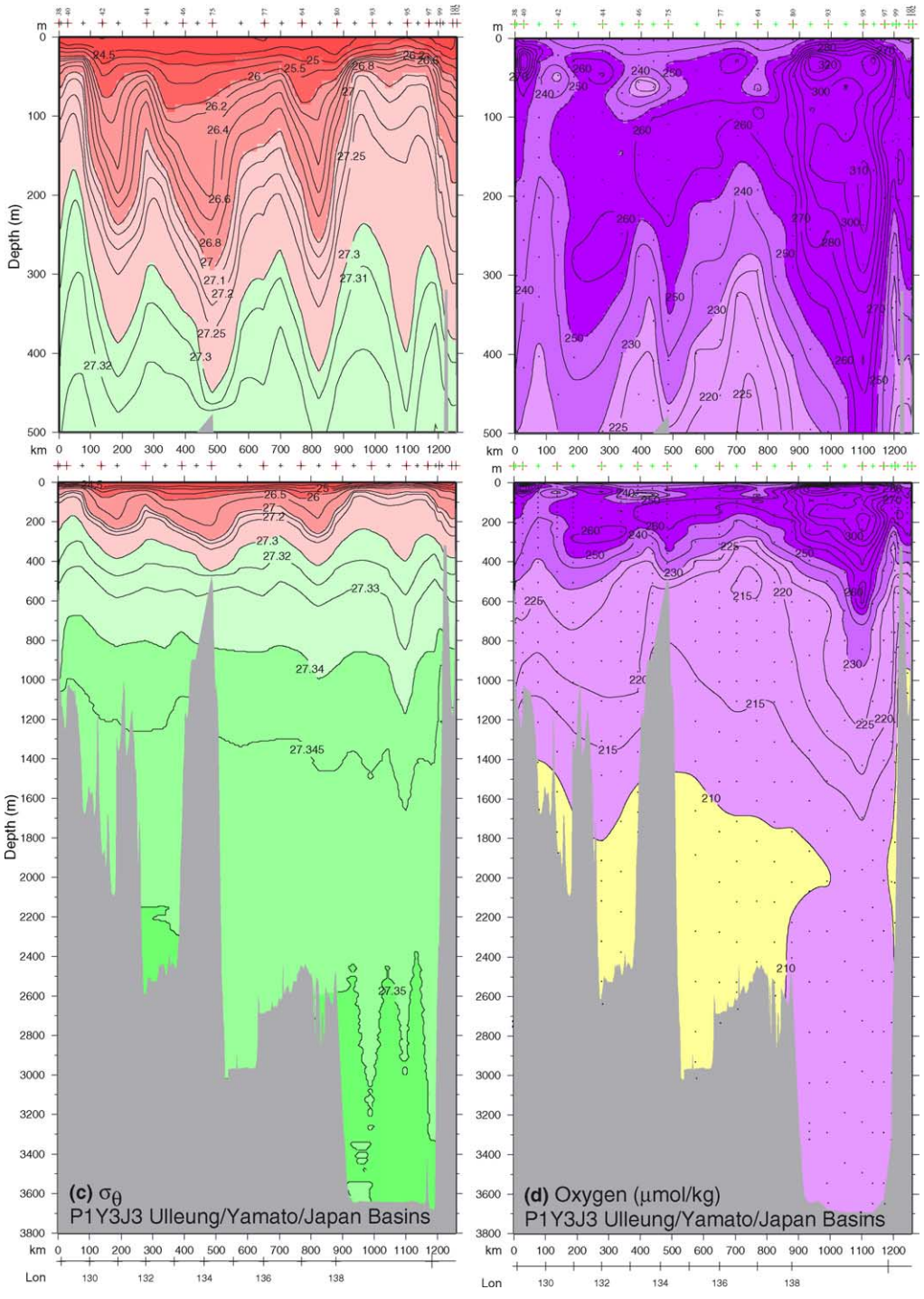

Fig. 6 (*continued*)

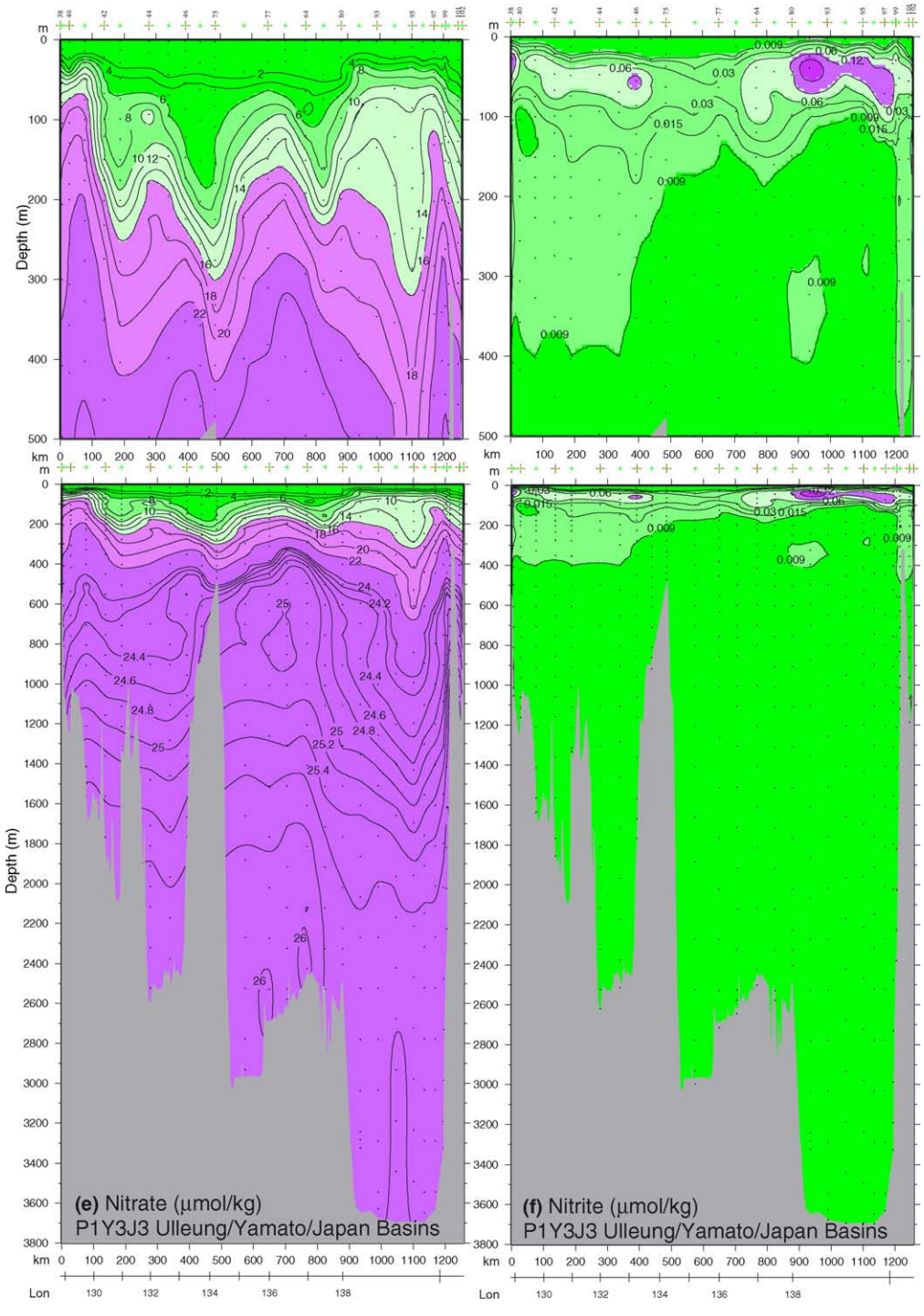

Fig. 6 (*continued*)

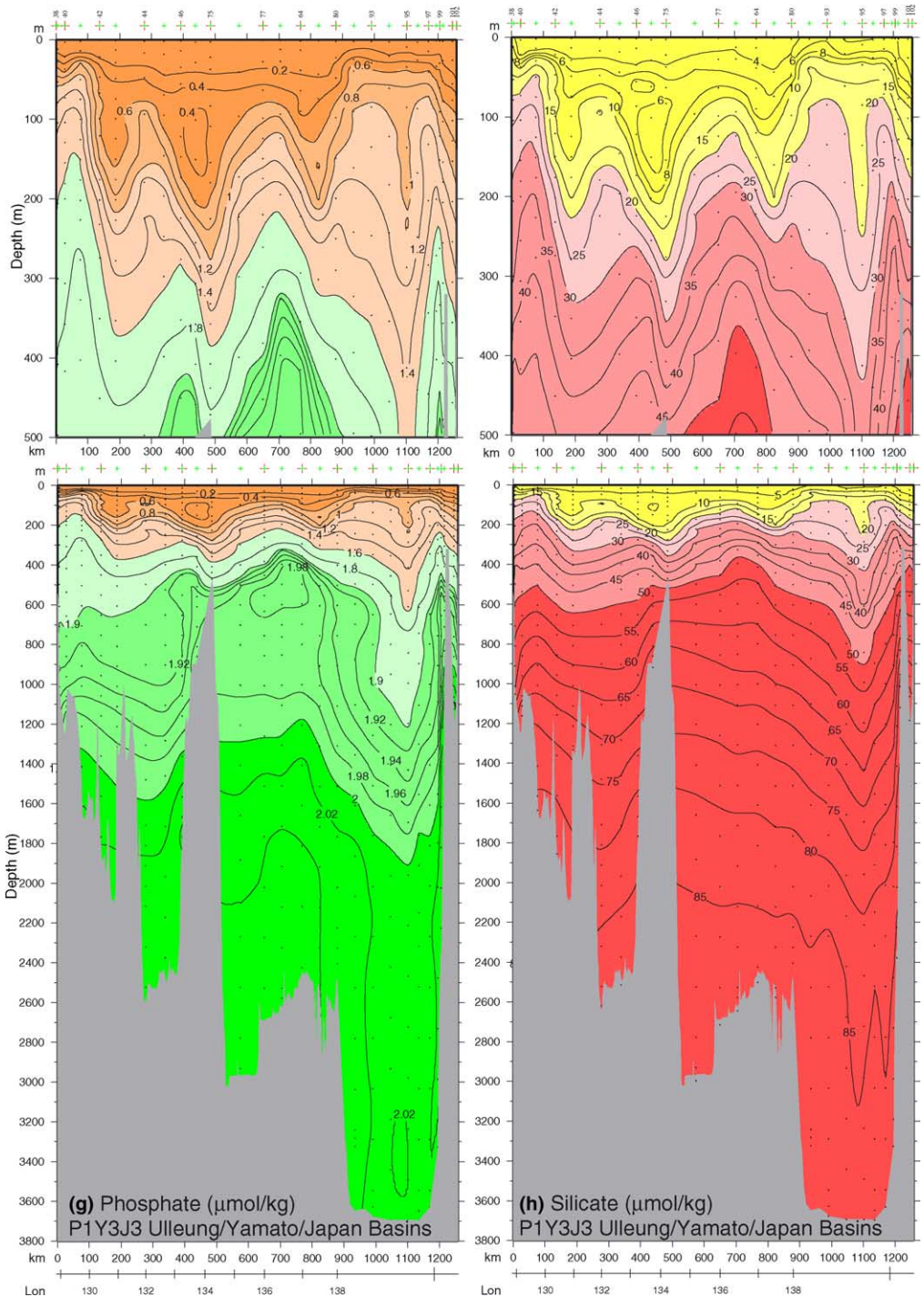

Fig. 6 (*continued*)

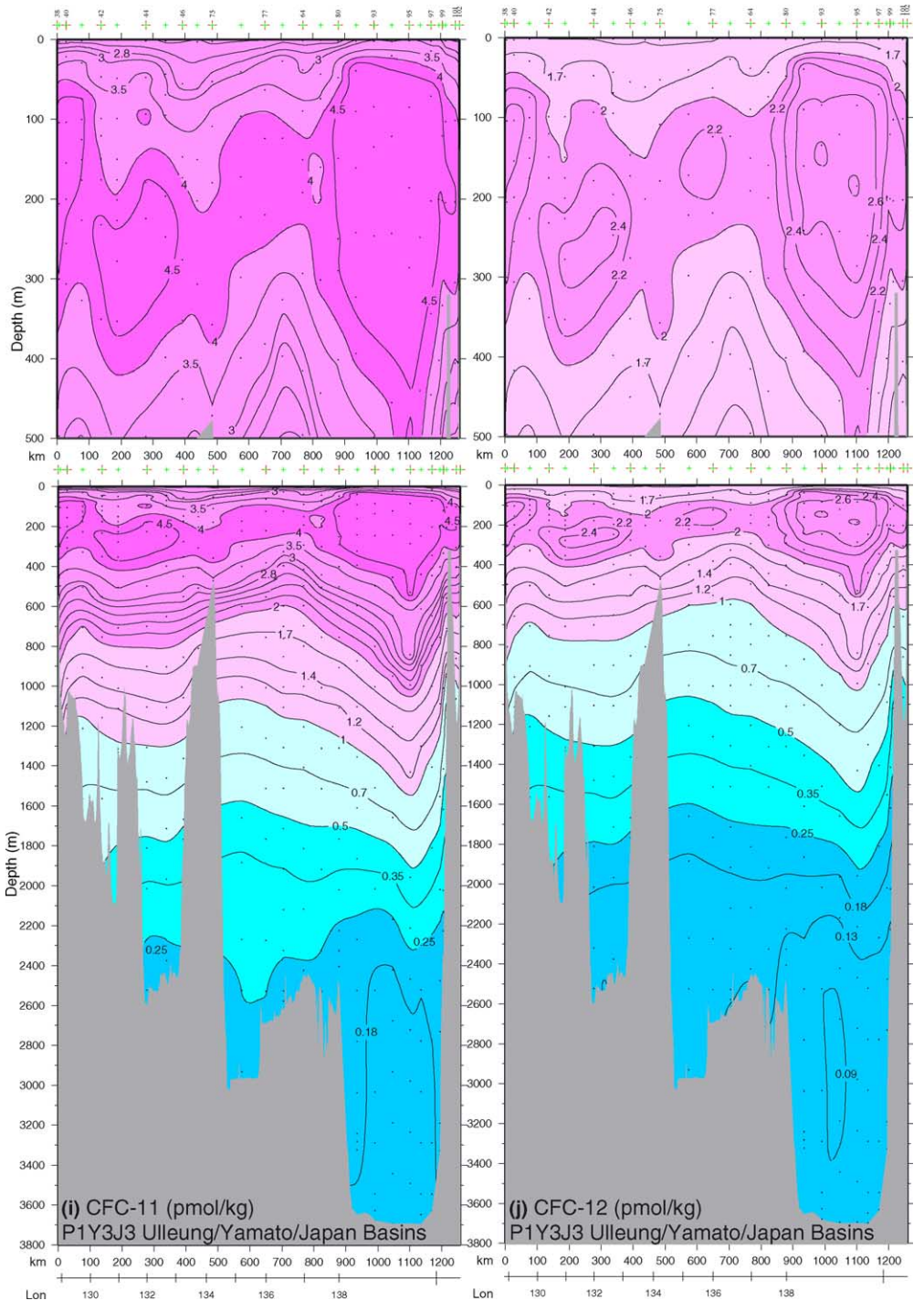

Fig. 6 (*continued*)

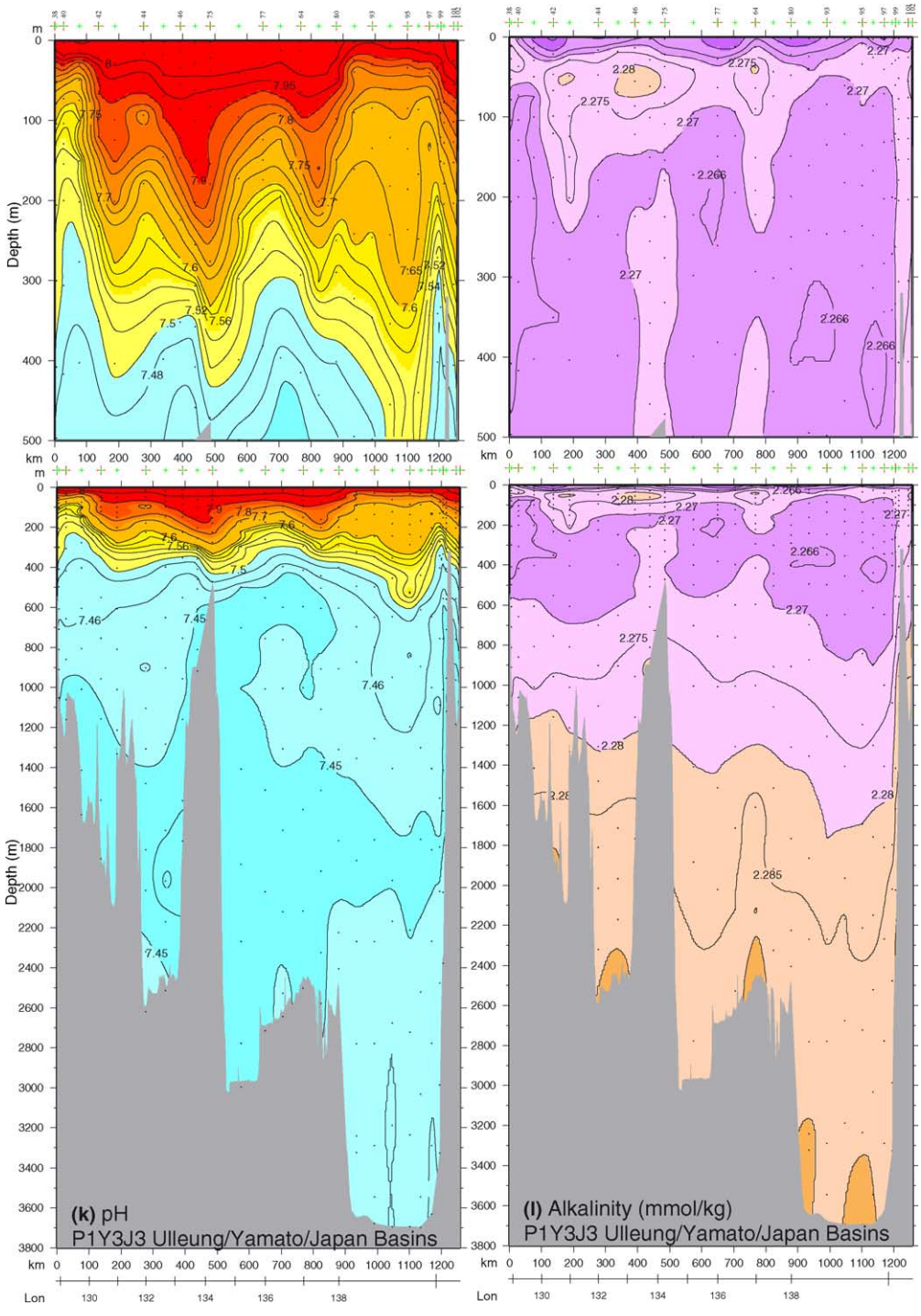

Fig. 6 (*continued*)

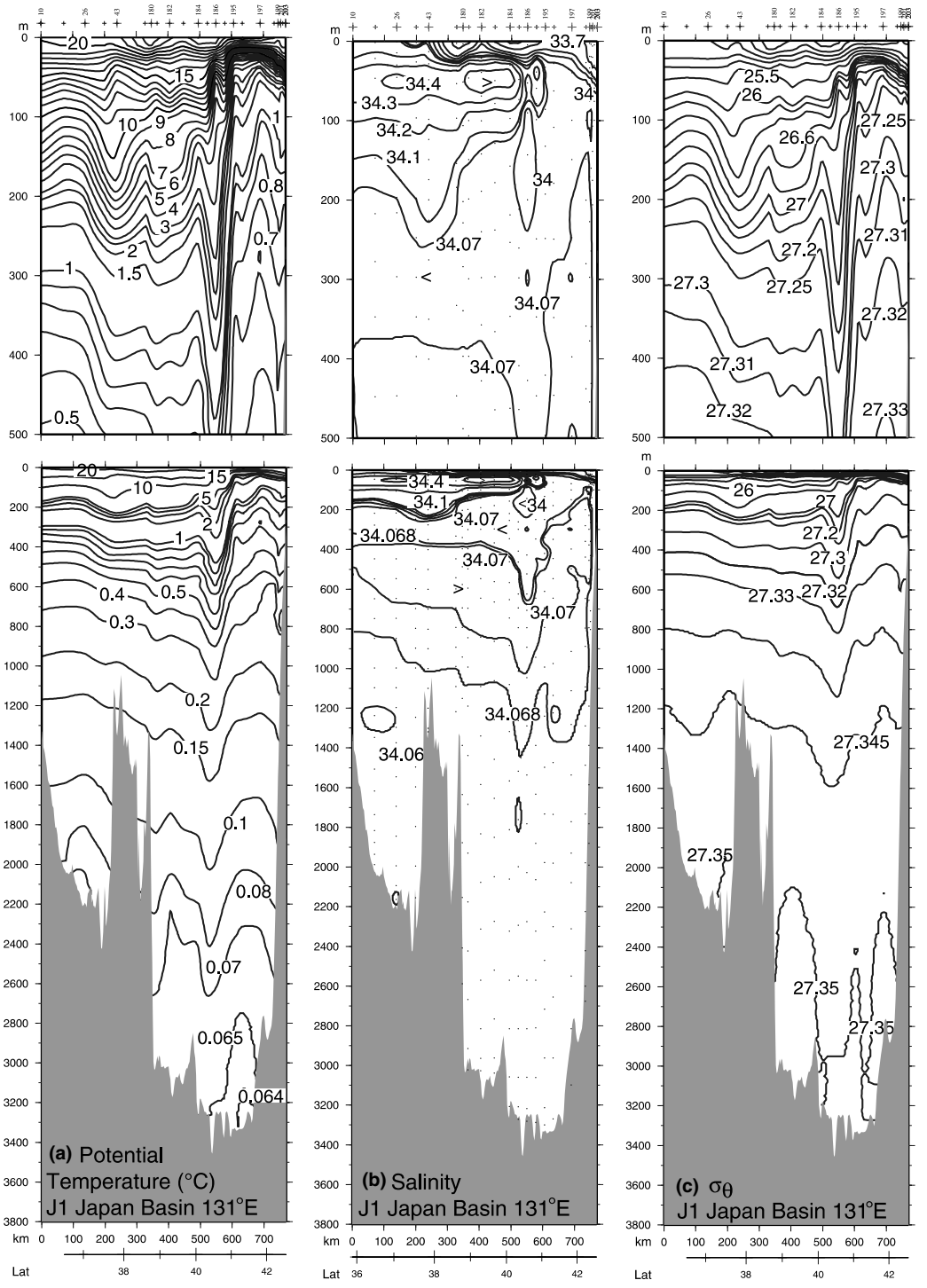

Fig. 7. Vertical sections (black and white versions) at approximately 131° E (Ulleung and Japan Basins) (J1 in Fig. 1(b)): (a) Potential temperature (°C), (b) salinity, (c) potential density, (d) oxygen (μmol/kg), (e) nitrate (μmol/kg), (f) nitrite (μmol/kg), (g) phosphate (μmol/kg), (h) dissolved silica (μmol/kg), (i) CFC-11 (pmol/kg), (j) CFC-12 (pmol/kg), (k) pH, and (l) alkalinity (mmol/kg). The vertical axis is depth (m) and the horizontal axis is distance (km). Interpolated longitudes along the sections are also shown. Upper panel vertical exaggeration is 2500:1. Lower panel vertical exaggeration is 625:1. Color

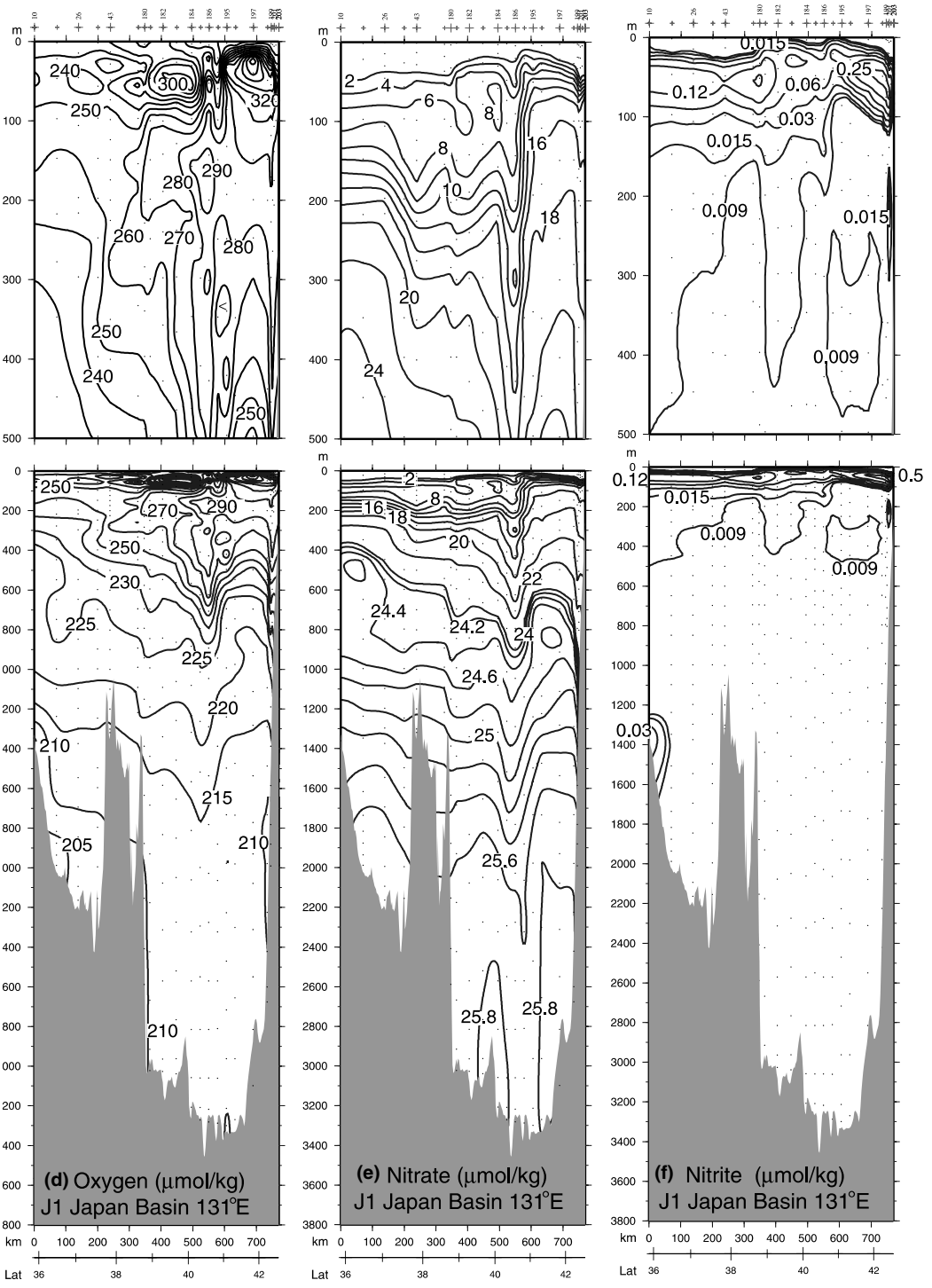

Fig. 7 (*continued*)

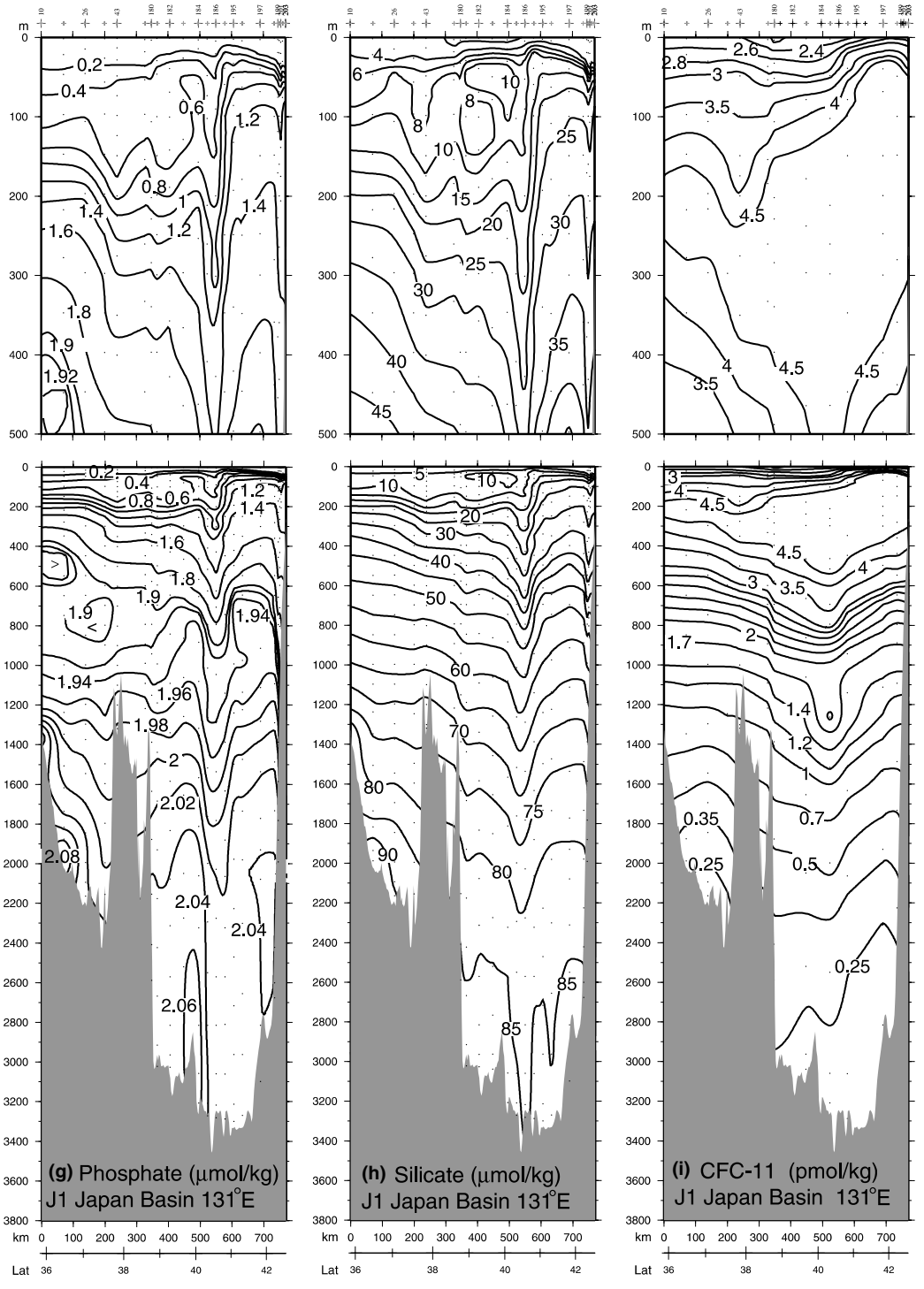

Fig. 7 (*continued*)

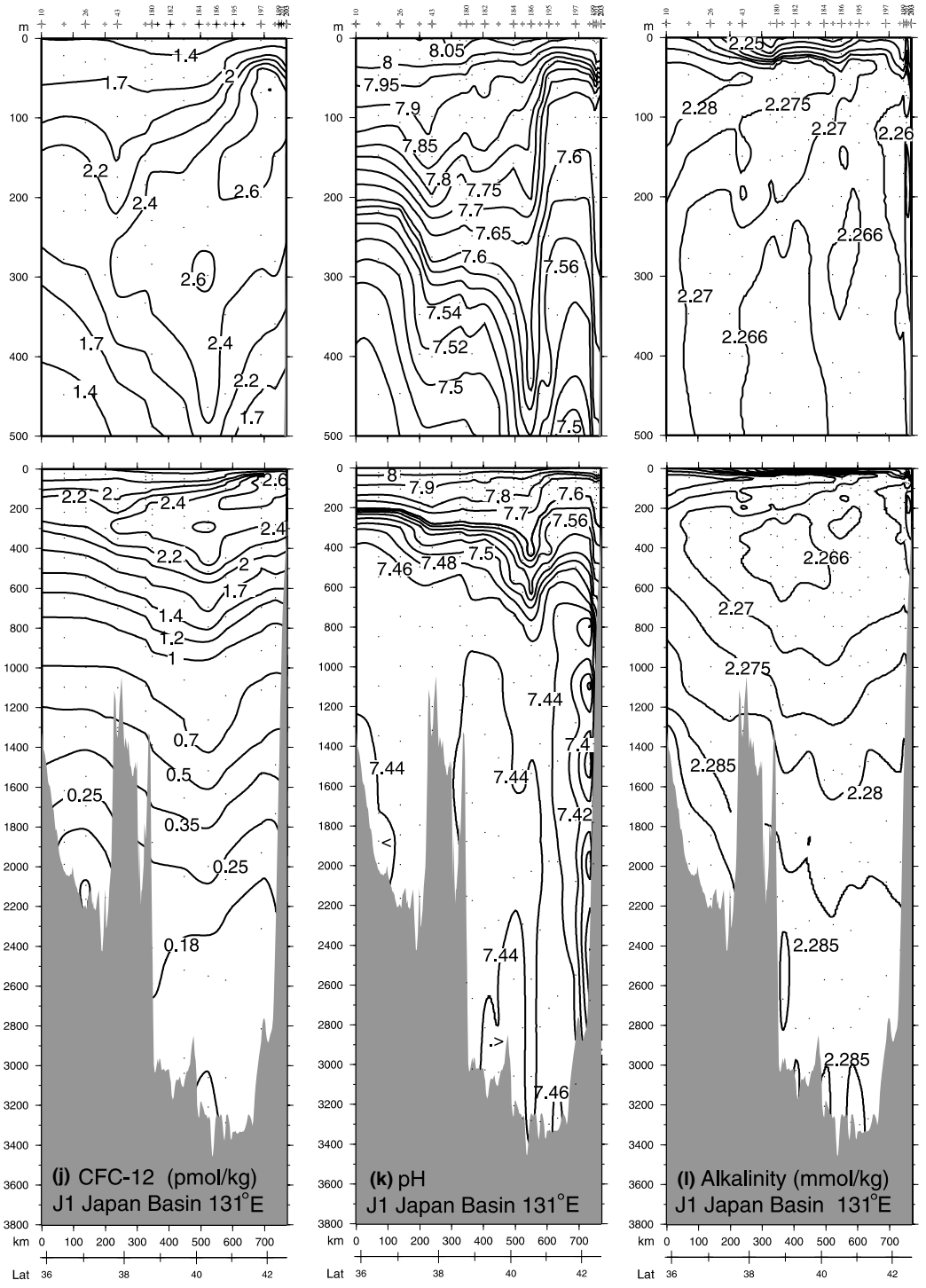

Fig. 7 (*continued*)

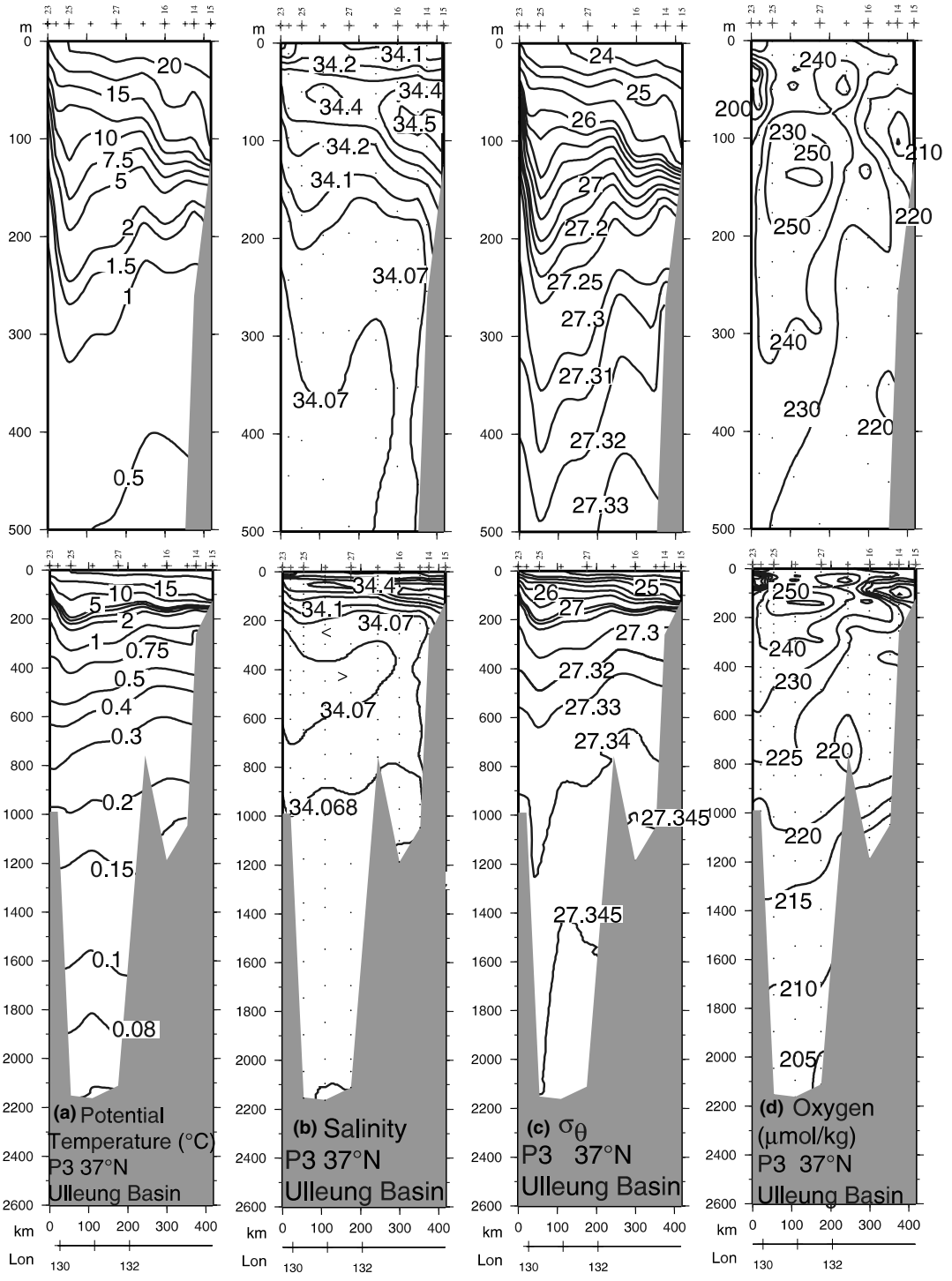

Fig. 8. Vertical sections at approximately 37° N (Ulleung Basin) (P3 in Fig. 1(b)): (a) Potential temperature (°C), (b) salinity, (c) potential density, (d) oxygen (μmol/kg), (e) nitrate (μmol/kg), (f) nitrite (μmol/kg), (g) phosphate (μmol/kg), (h) dissolved silica (μmol/kg), (i) CFC-11 (pmol/kg), (j) CFC-12 (pmol/kg), (k) pH, and (l) alkalinity (mmol/kg). The vertical axis is depth (m) and the horizontal axis is distance (km). Interpolated longitudes along the sections are also shown. Upper panel vertical exaggeration is 2500:1. Lower panel vertical exaggeration is 625:1. Color versions are in the accompanying

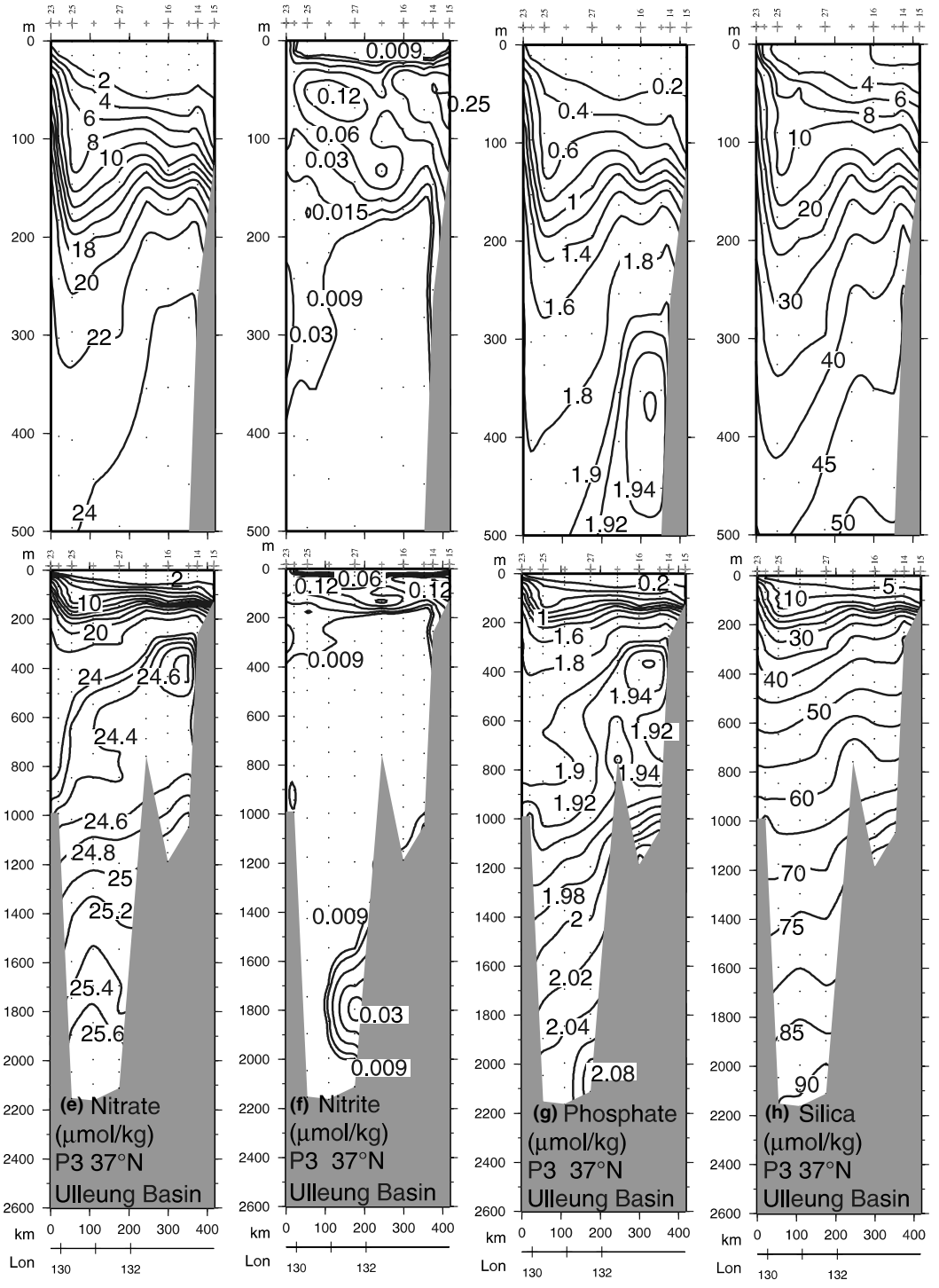

Fig. 8 (*continued*)

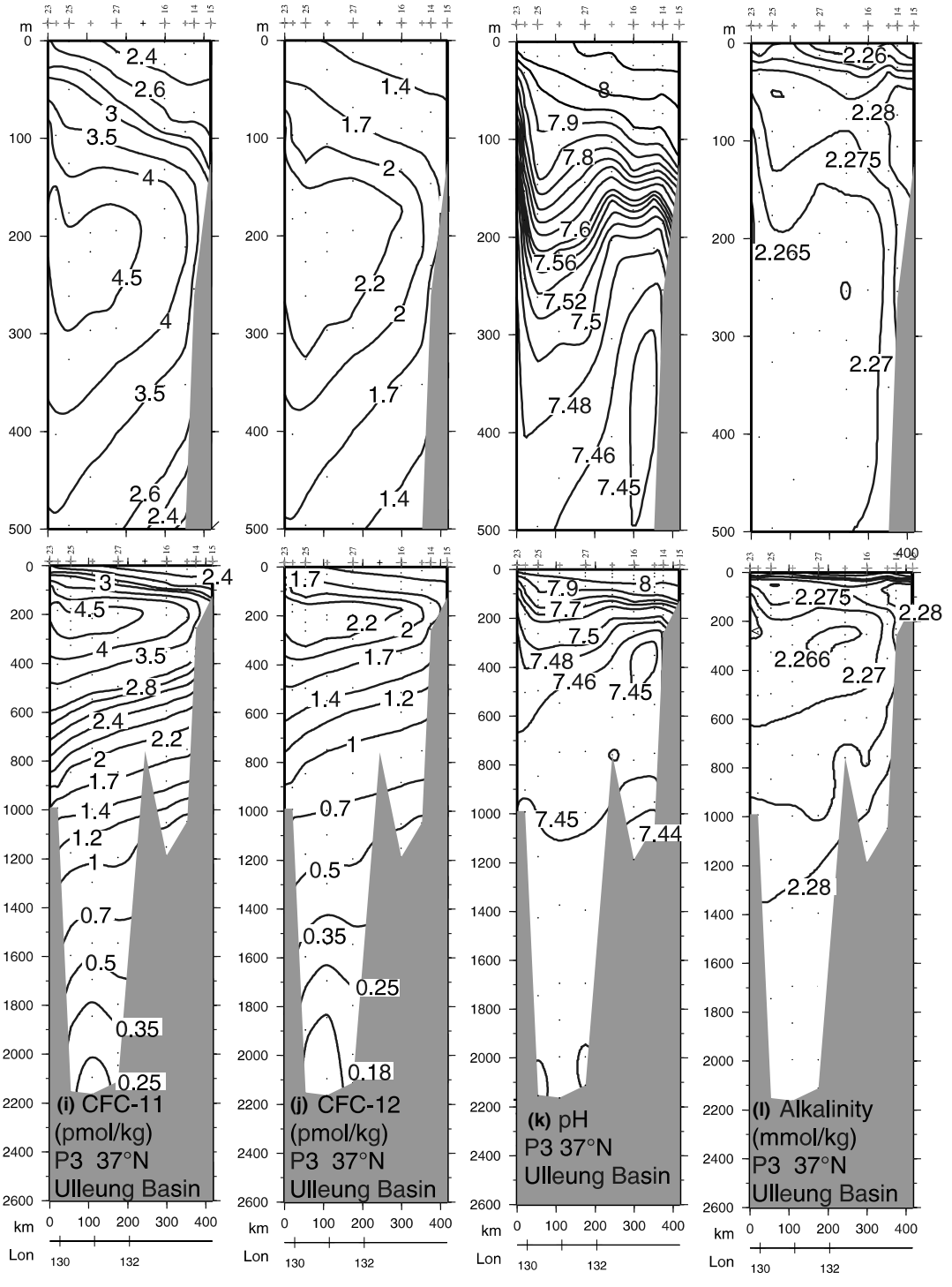

Fig. 8 (*continued*)

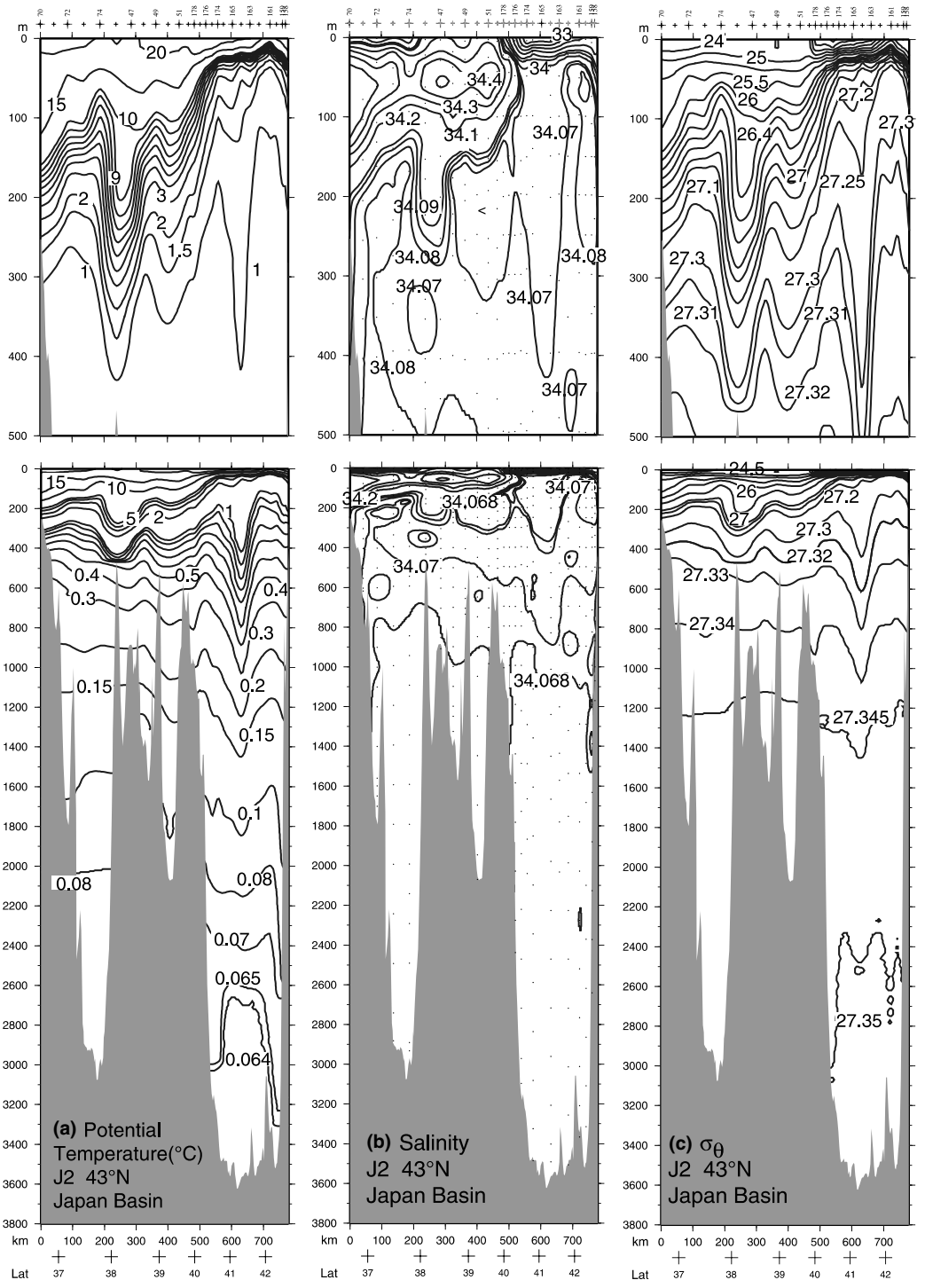

Fig. 9. Vertical sections at approximately 134° E (Yamato Basin, Yamato Rise, and Japan Basin) (Y1 and J2 in Fig. 1(b)): (a) Potential temperature (°C), (b) salinity, (c) potential density, (d) oxygen (μmol/kg), (e) nitrate (μmol/kg), (f) nitrite (μmol/kg), (g) phosphate (μmol/kg), (h) dissolved silica (μmol/kg), (i) CFC-11 (pmol/kg), (j) CFC-12 (pmol/kg), (k) pH, and (l) alkalinity (mmol/kg). The vertical axis is depth (m) and the horizontal axis is distance (km). Interpolated longitudes along the sections are also shown. Upper panel vertical exaggeration is 2500:1. Lower panel vertical exaggeration is 625:1. Color

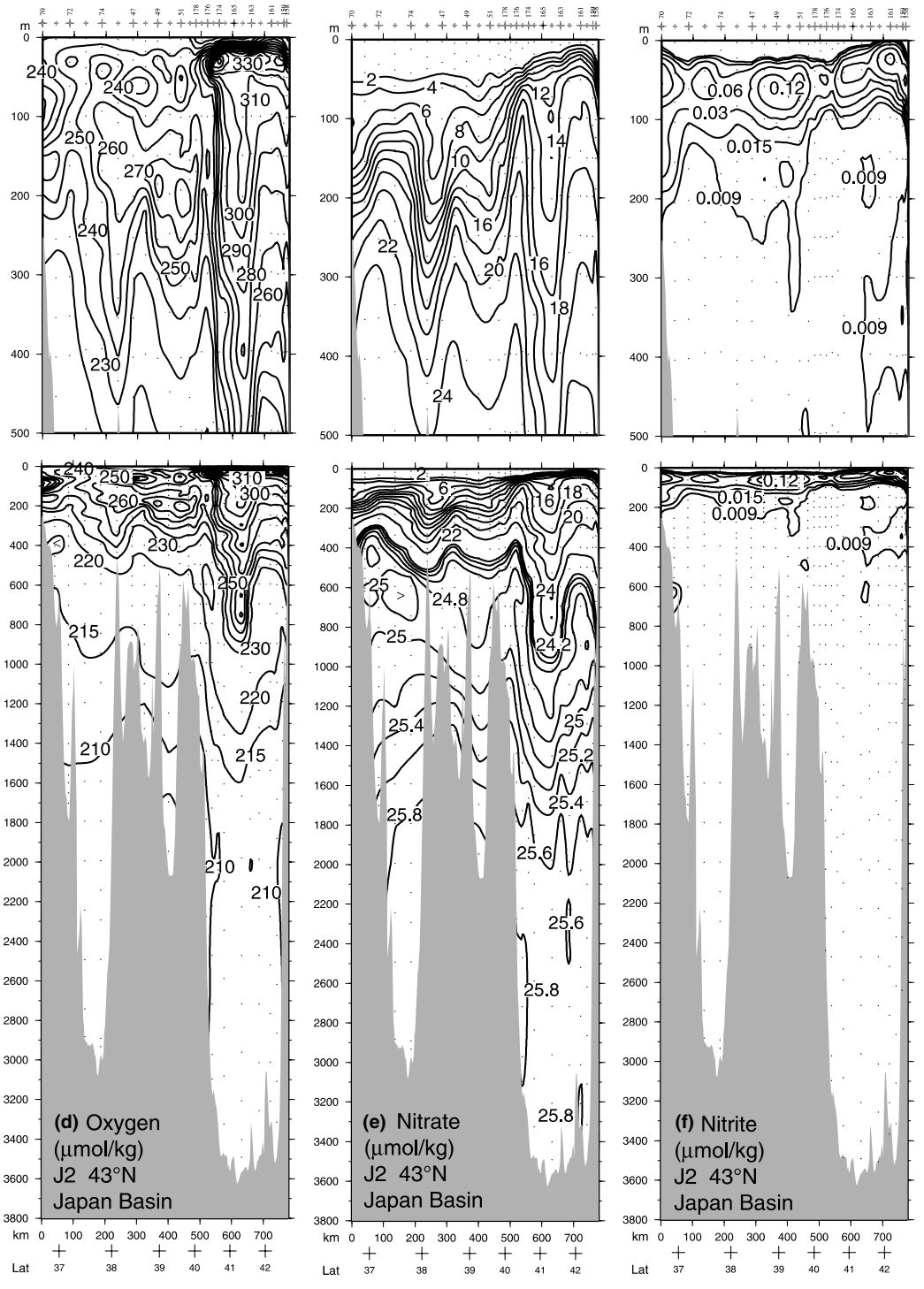

Fig. 9 (*continued*)

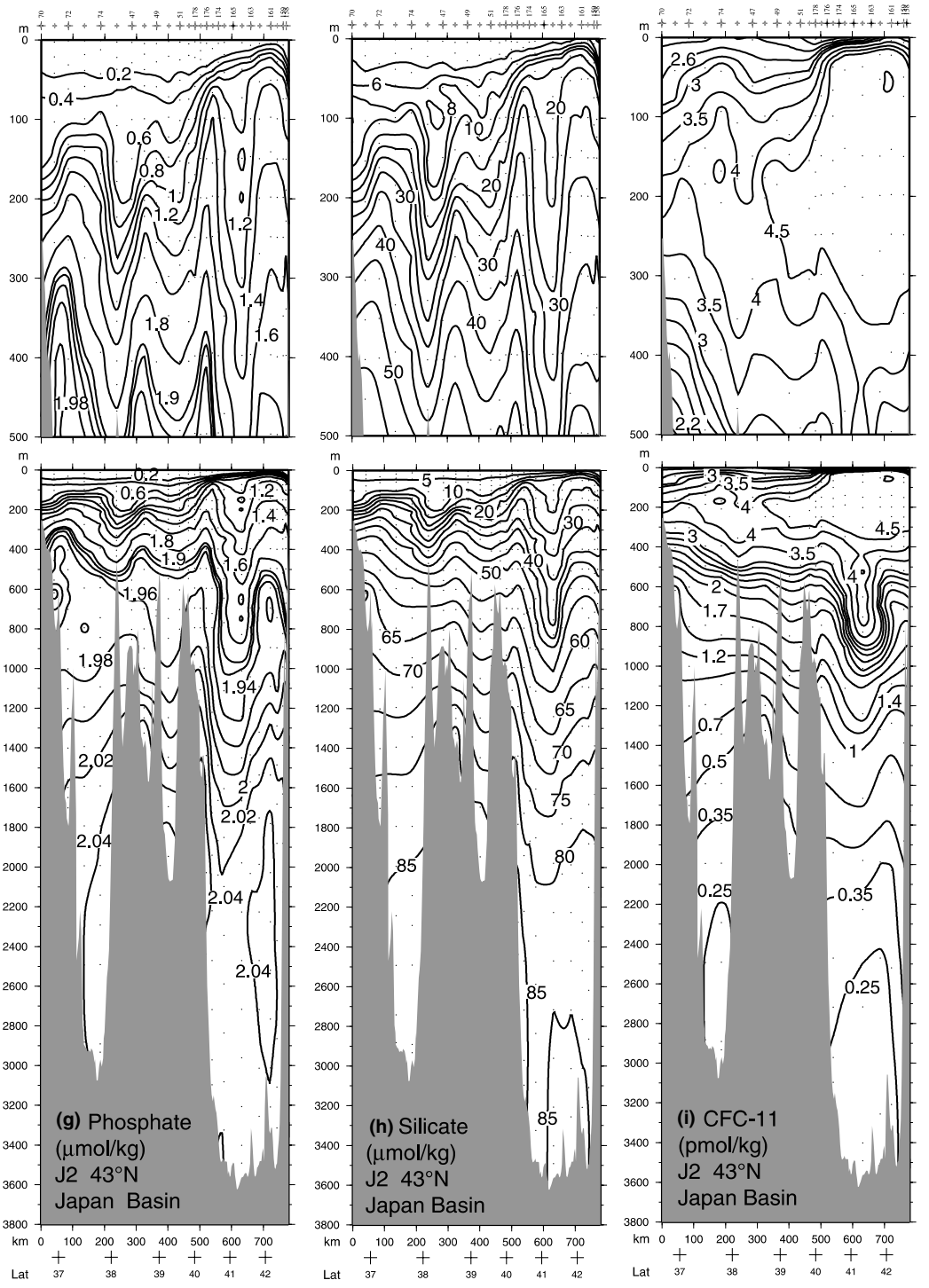

Fig. 9 (*continued*)

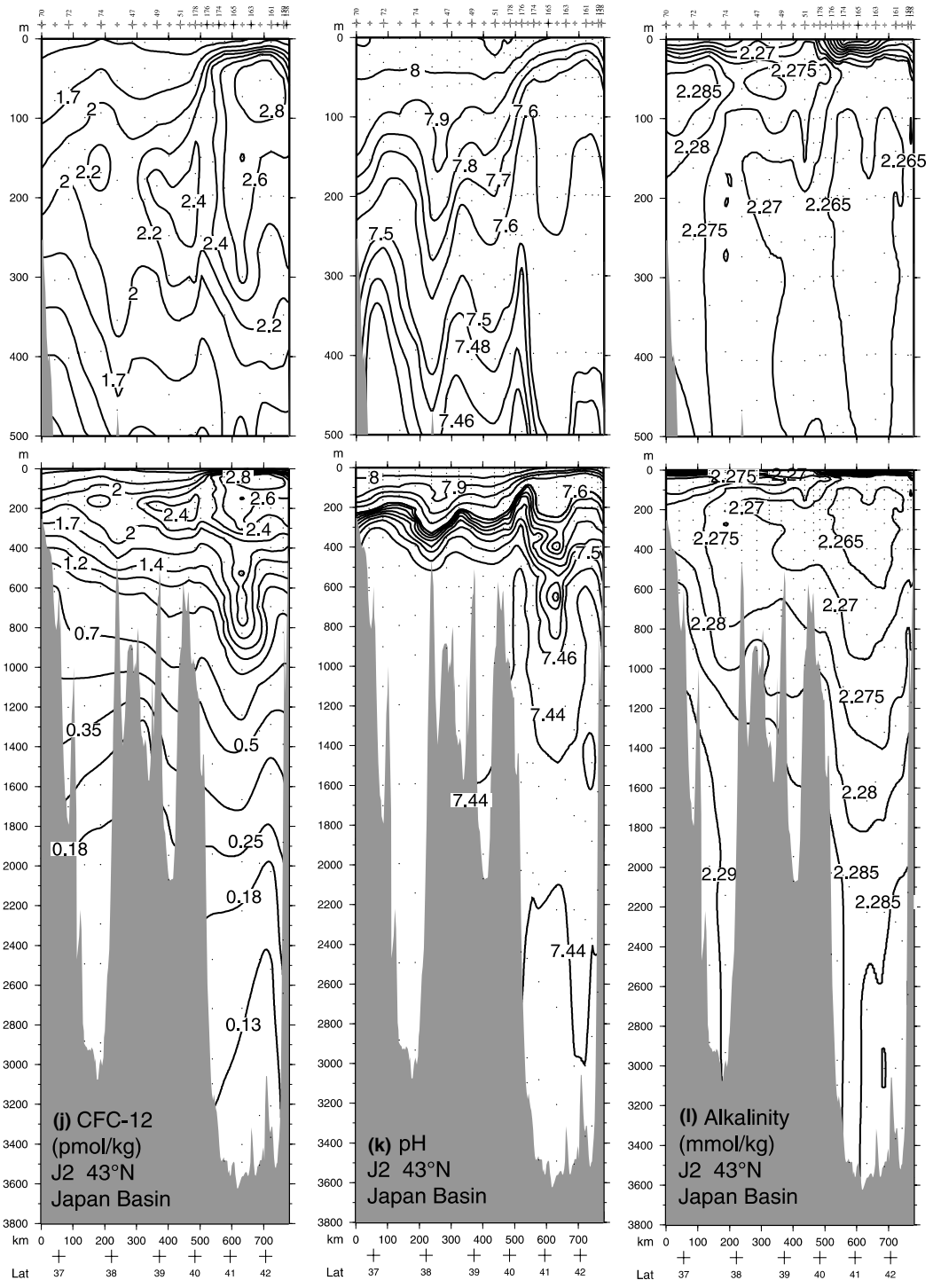

Fig. 9 (*continued*)

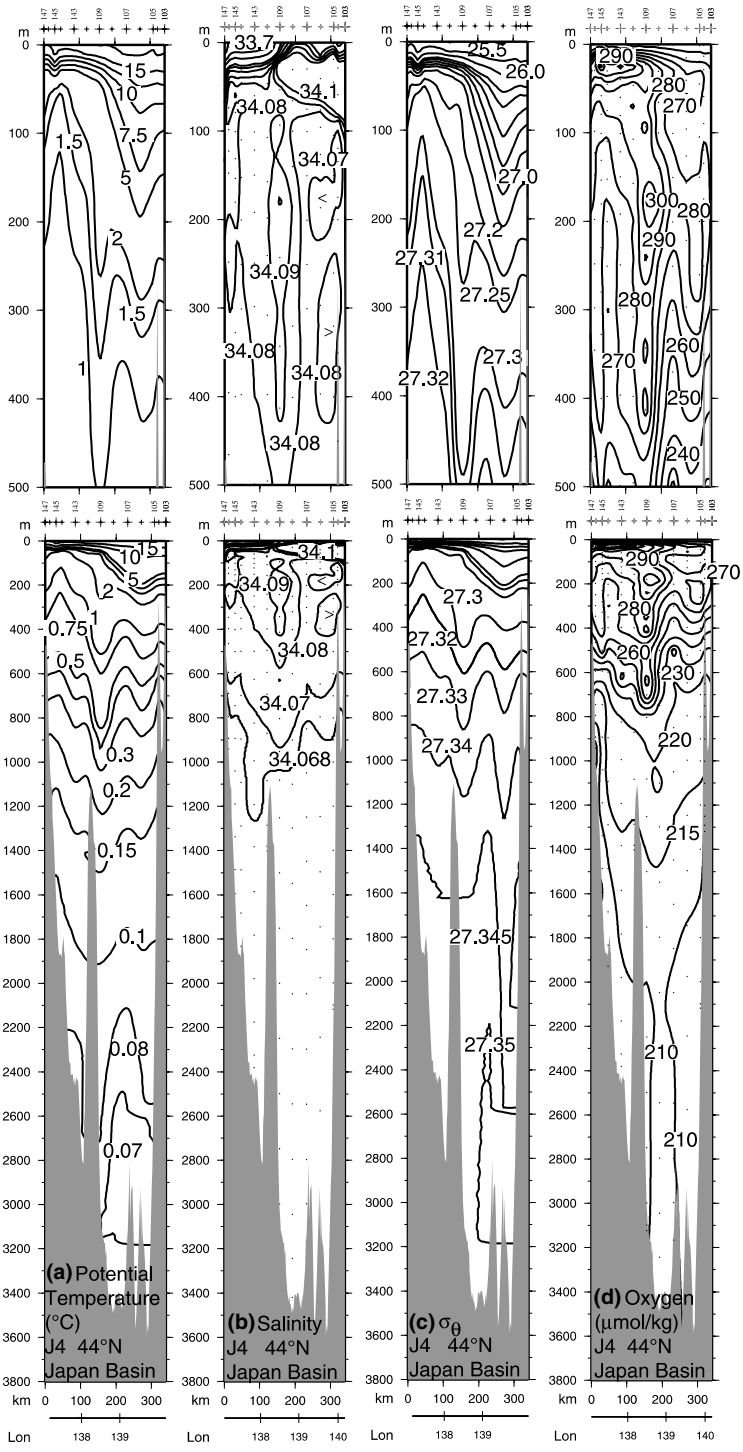

Fig. 10. Vertical sections at approximately 44° N (Japan Basin) (J4 in Fig. 1(b)): (a) Potential temperature (°C), (b) salinity, (c) potential density, (d) oxygen (μmol/kg), (e) nitrate (μmol/kg), (f) nitrite (μmol/kg), (g) phosphate (μmol/kg), (h) dissolved silica (μmol/kg), (i) CFC-11 (pmol/kg), (j) CFC-12 (pmol/kg), (k) pH, and (l) alkalinity (mmol/kg). The vertical axis is depth (m) and the horizontal axis is distance (km). Interpolated longitudes along the sections are also shown. Upper panel vertical exaggeration is 2500:1. Lower panel vertical exaggeration is 625:1. Color versions are in the accompanying

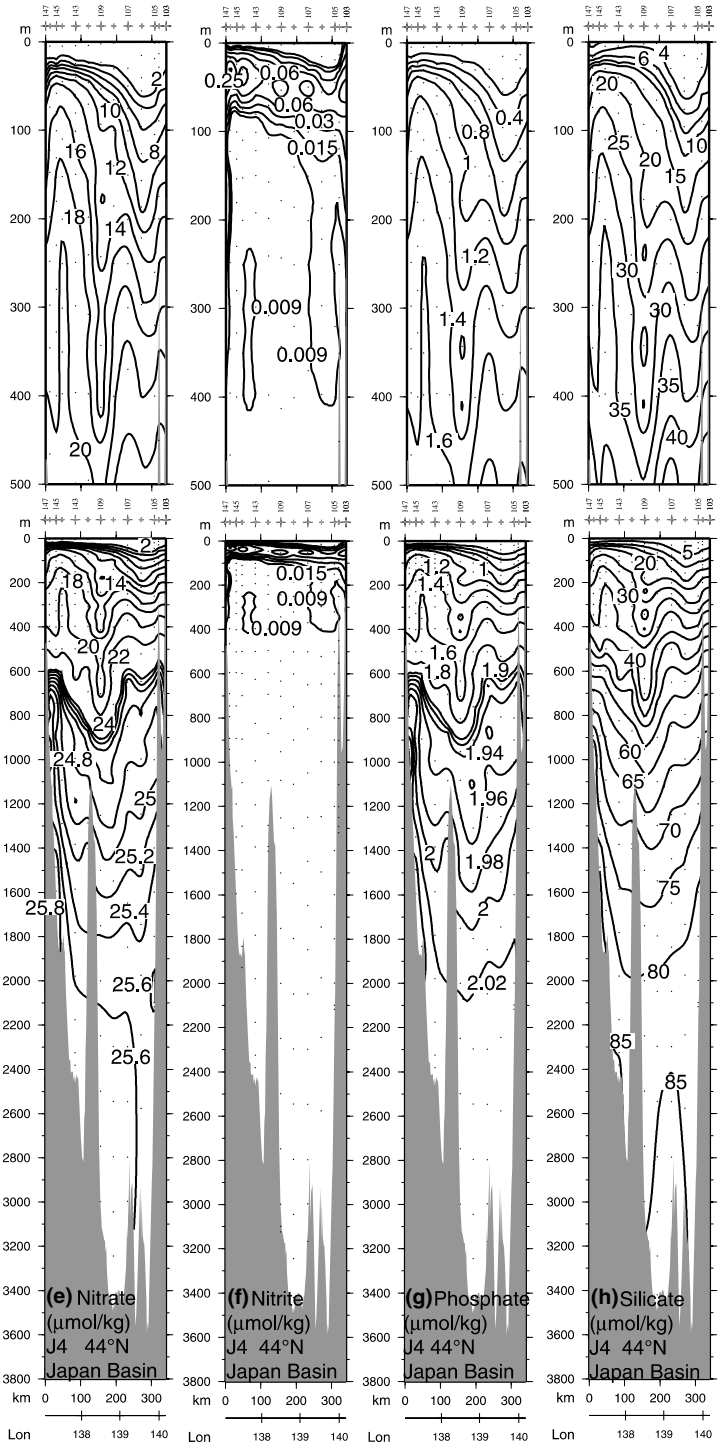

Fig. 10. (*continued*)

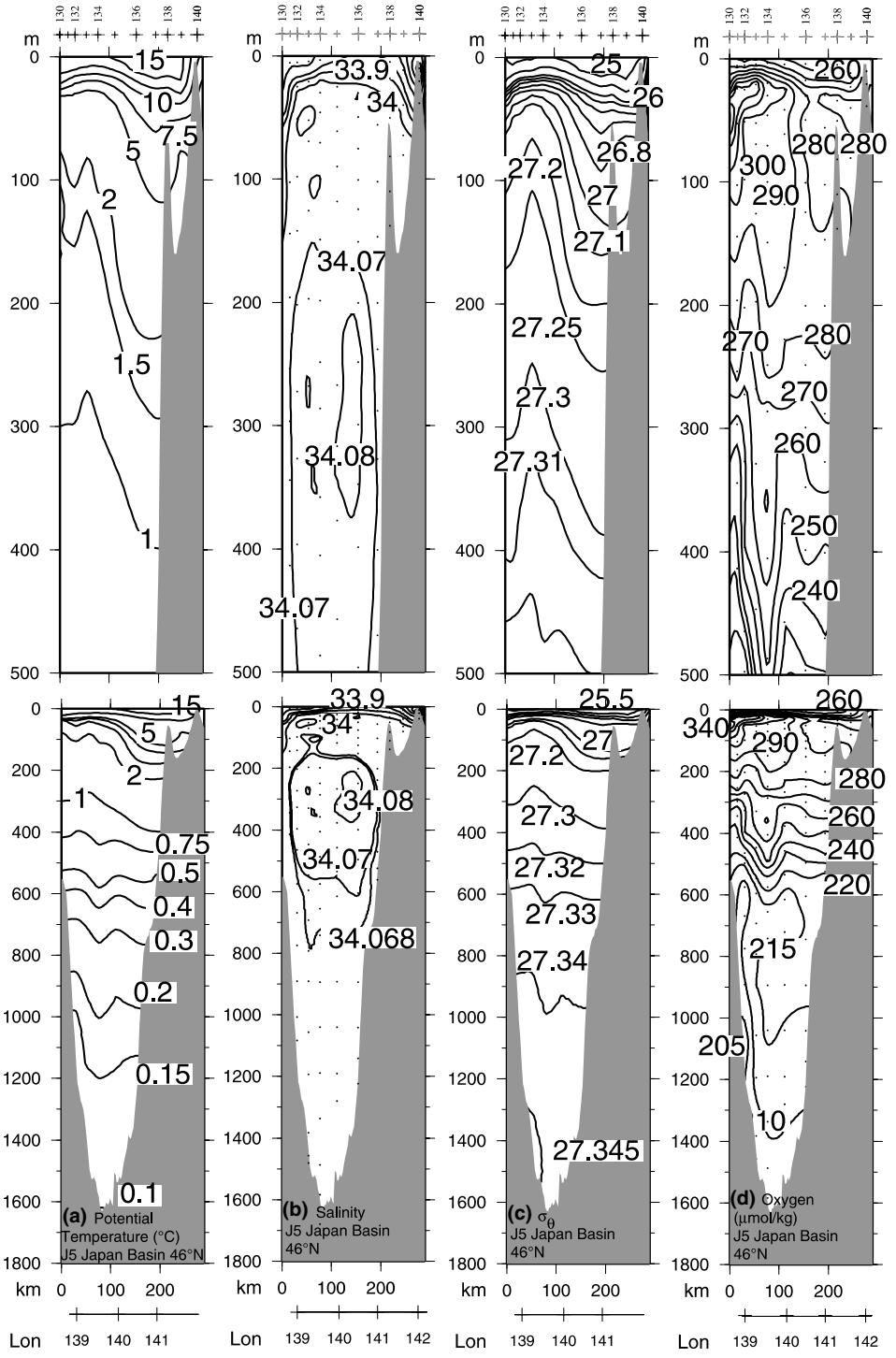

Fig. 11. Vertical sections at approximately 46° N (Japan Basin) (J5 in Fig. 1(b)): (a) Potential temperature (°C), (b) salinity, (c) potential density, (d) oxygen (μmol/kg), (e) nitrate (μmol/kg), (f) nitrite (μmol/kg), (g) phosphate (μmol/kg), (h) dissolved silica (μmol/kg), (i) CFC-11 (pmol/kg), (j) CFC-12 (pmol/kg), (k) pH, and (l) alkalinity (mmol/kg). The vertical axis is depth (m) and the horizontal axis is distance (km). Interpolated longitudes along the sections are also shown. Upper panel vertical exaggeration is 2500:1. Lower panel vertical exaggeration is 625:1. Color versions are in the accompanying

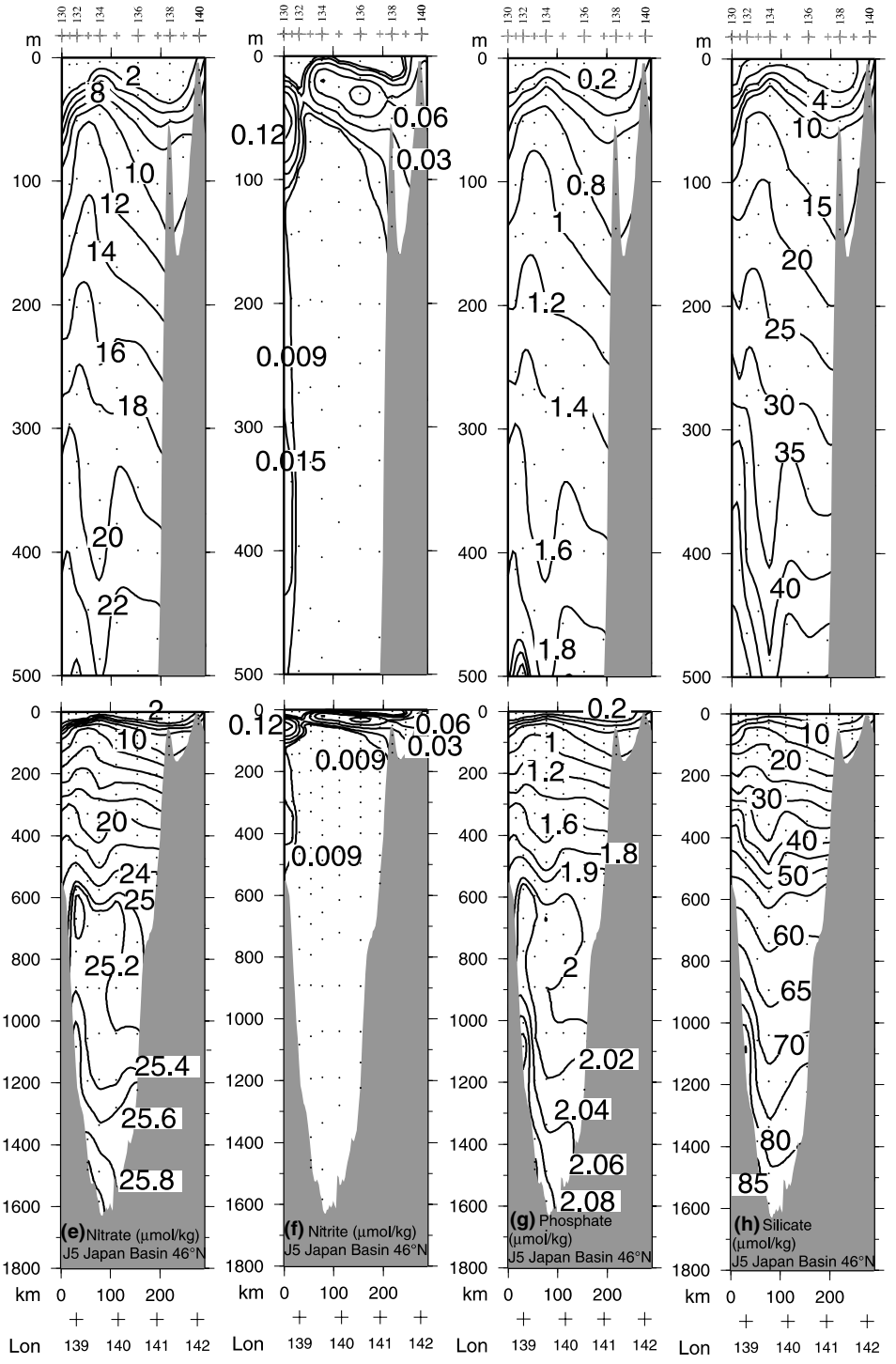

Fig. 11 (*continued*)

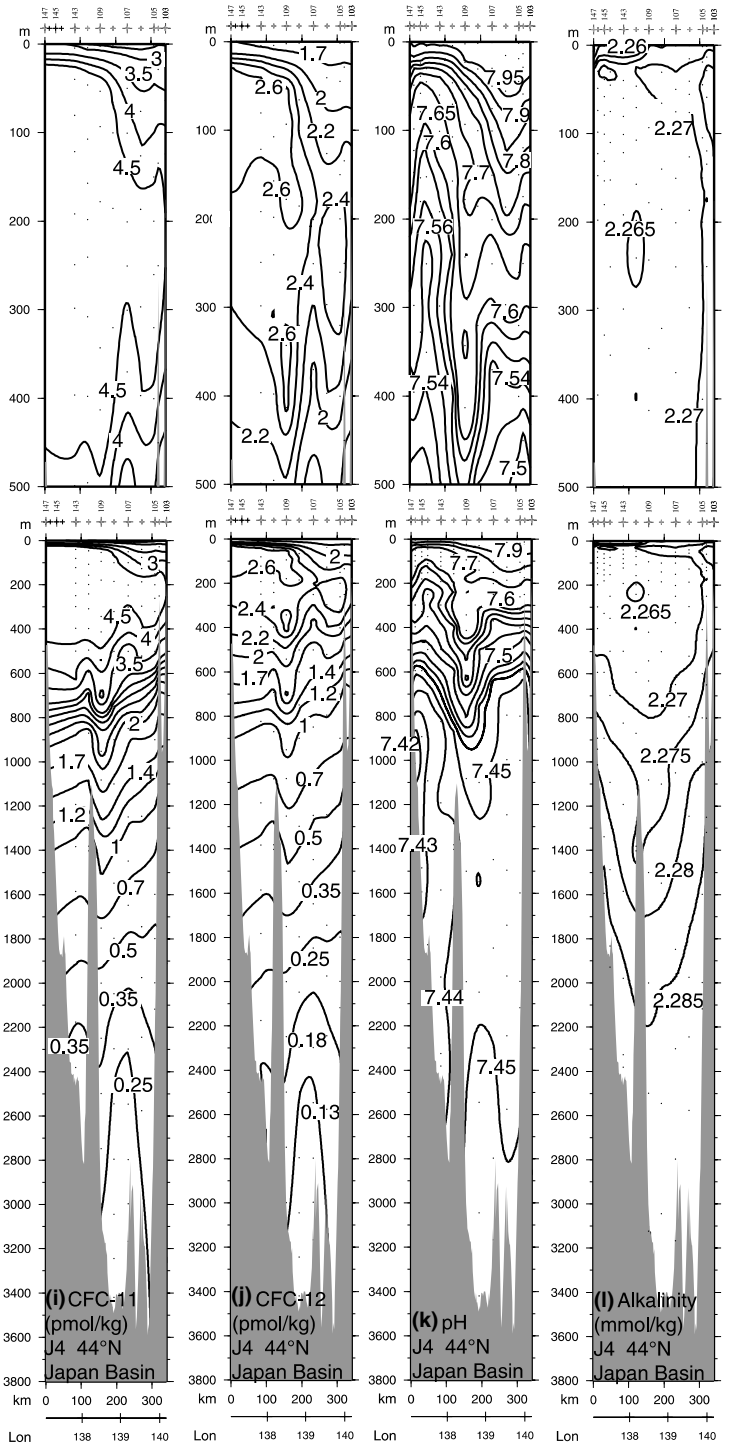

Fig. 11 (*continued*)

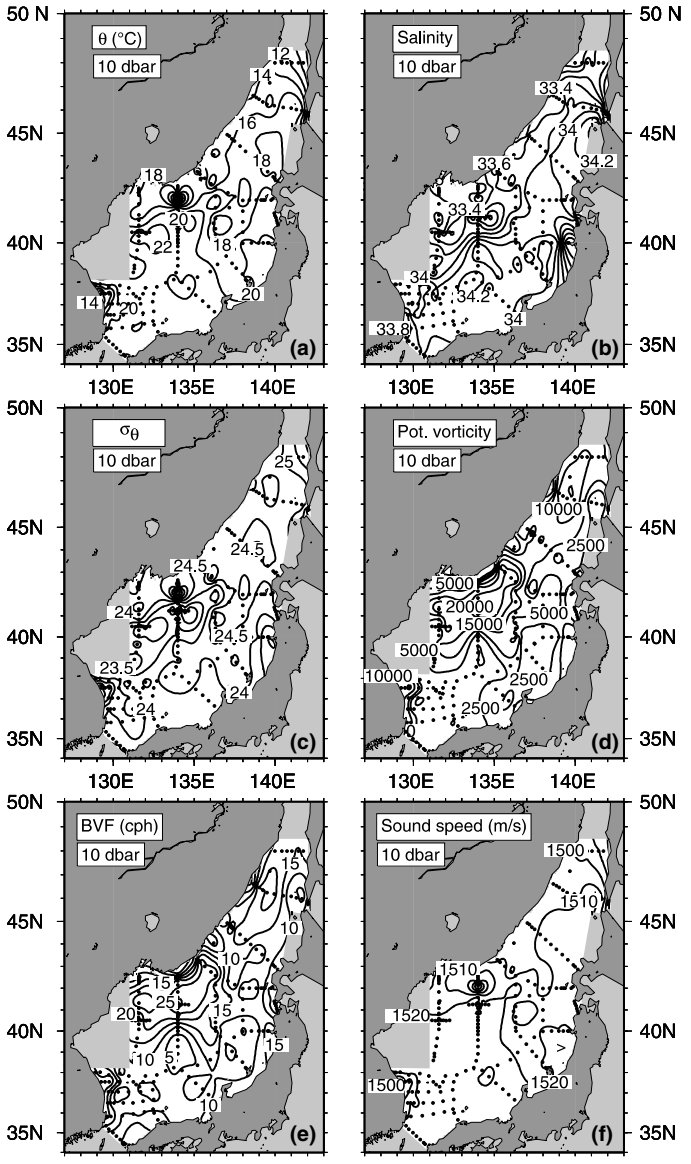

Fig. 12. Maps of: (a) potential temperature (°C), (b) salinity, (c) potential density (σ_θ), (d) isopycnal potential vorticity ($\times 10^{-14}$ cm^{-1} s^{-1}), (e) Brunt-Vaisala frequency (cph), and (f) sound speed (m/s) at 10 dbar. Color versions are in the accompanying digital atlas.

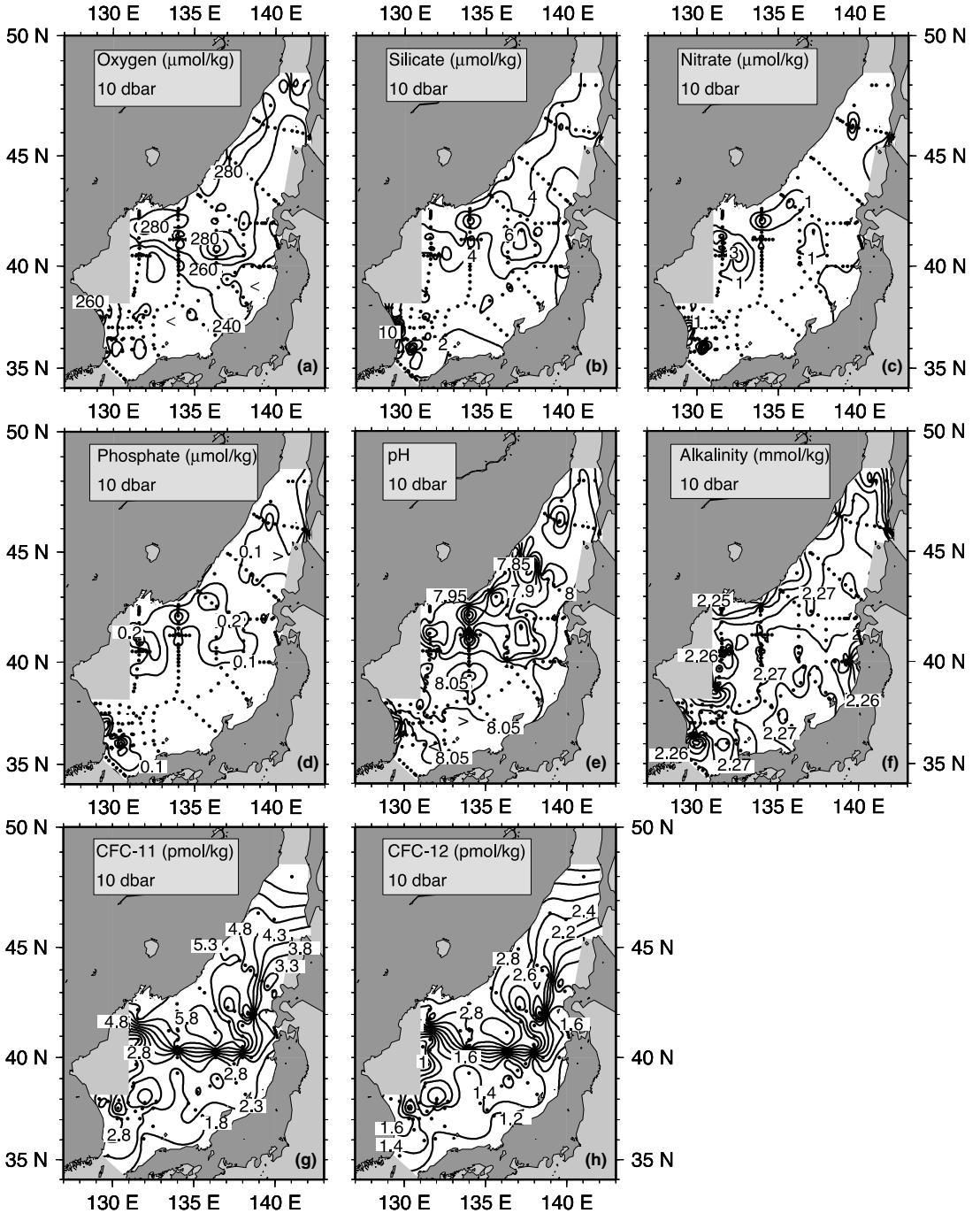

Fig. 13. (a) Oxygen (μmol/kg), (b) dissolved silica (μmol/kg), (c) nitrate (μmol/kg), (d) phosphate (μmol/kg), (e) pH, (f) alkalinity (mmol/kg), (g) CFC-11 (pmol/kg), and (h) CFC-12 (pmol/kg) at 10 dbar. Color versions are in the accompanying digital atlas.

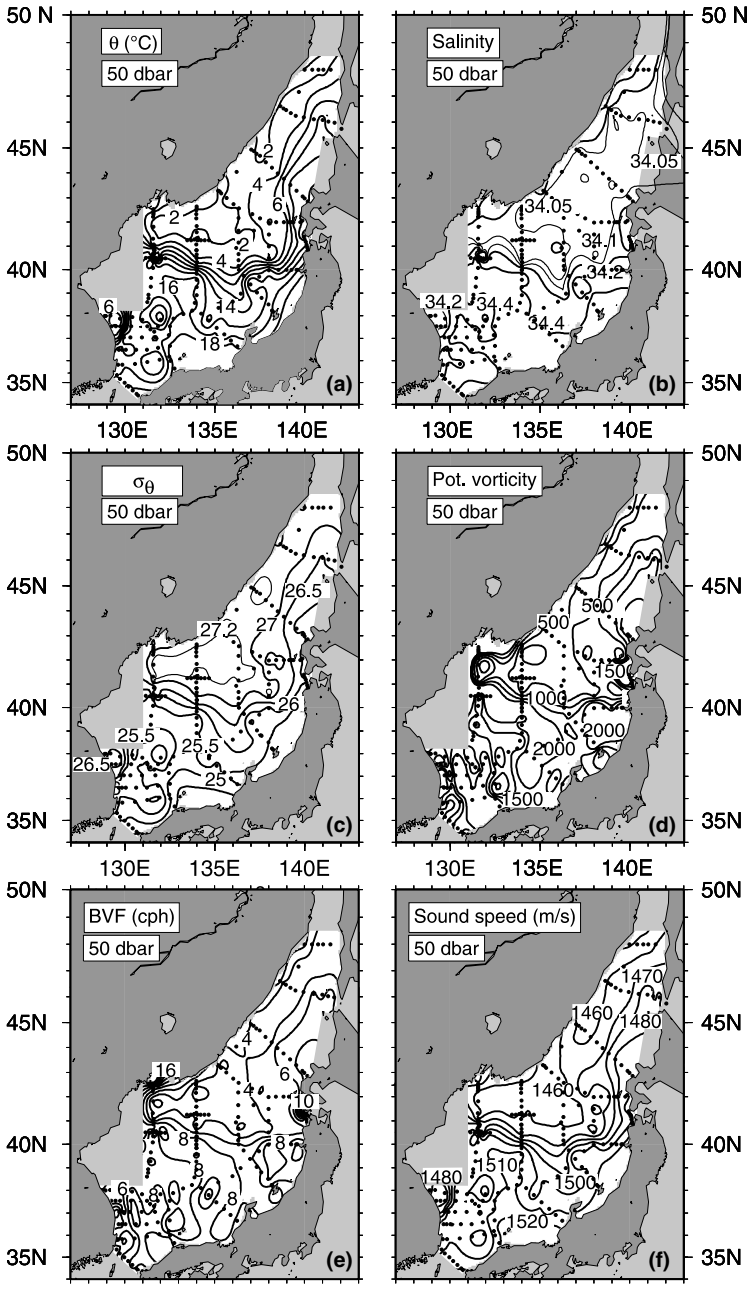

Fig. 14. Maps of: (a) potential temperature (°C), (b) salinity, (c) potential density (σ_θ), (d) isopycnal potential vorticity ($\times 10^{-14}$ cm^{-1} s^{-1}), (e) Brunt-Vaisala frequency (cph), and (f) sound speed (m/s) at 50 dbar. Colors are representative of all maps in the digital atlas.

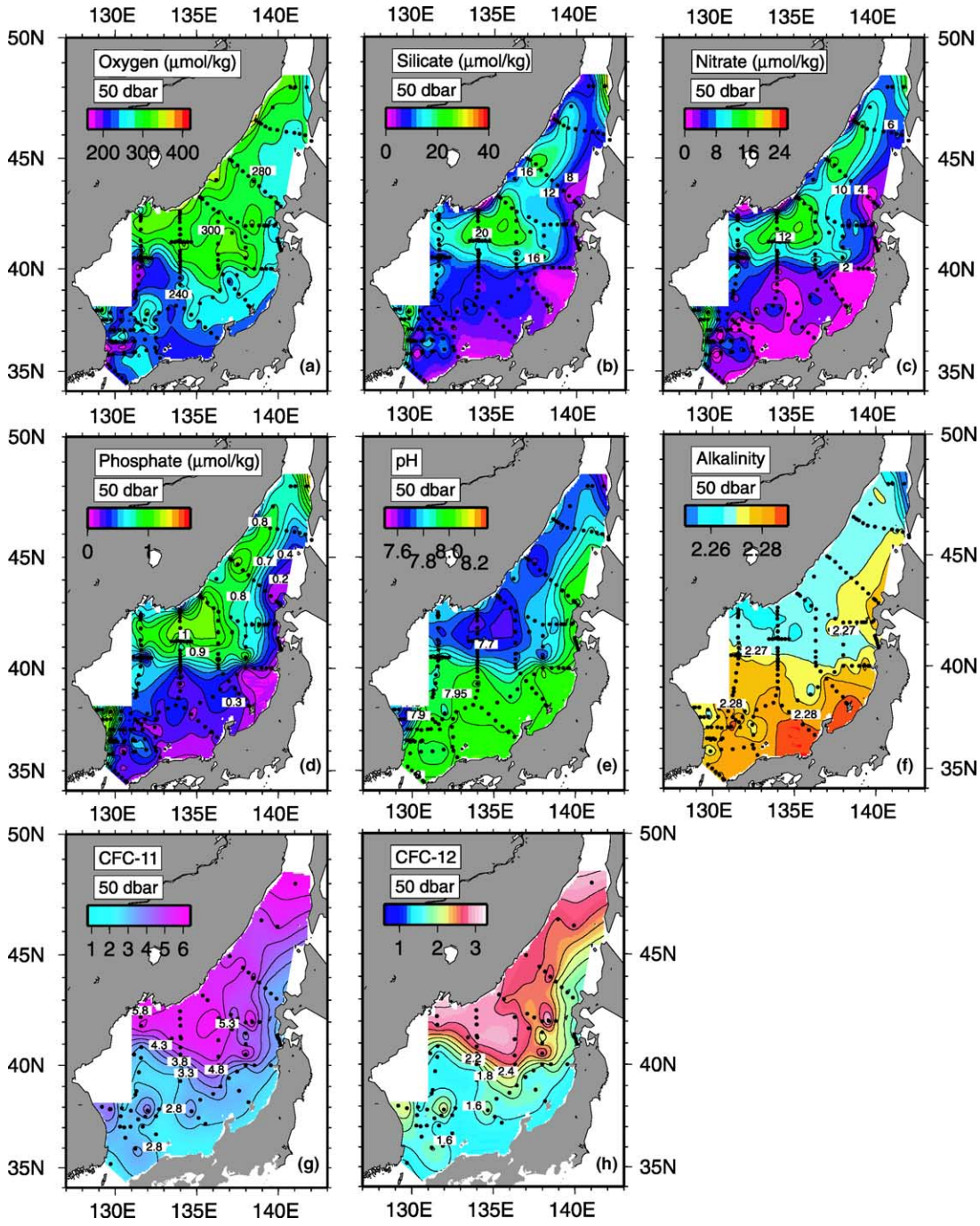

Fig. 15. (a) Oxygen (µmol/kg), (b) dissolved silica (µmol/kg), (c) nitrate (µmol/kg), (d) phosphate (µmol/kg), (e) pH, (f) alkalinity (mmol/kg), (g) CFC-11 (pmol/kg), and (h) CFC-12 (pmol/kg) at 50 dbar. Colors are representative of all maps in the digital atlas.

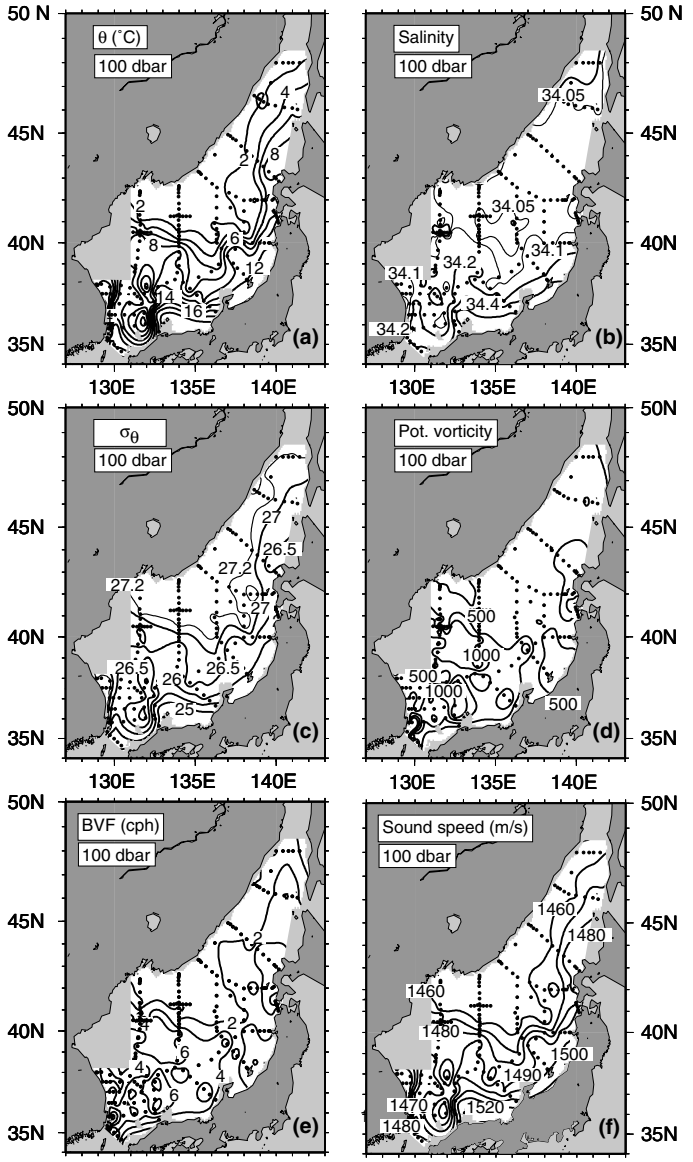

Fig. 16. Maps of: (a) potential temperature (°C), (b) salinity, (c) potential density (σ_θ), (d) isopycnal potential vorticity ($\times 10^{-14}$ cm^{-1} s^{-1}), (e) Brunt-Vaisala frequency (cph), and (f) sound speed (m/s) at 100 dbar. Color versions are in the accompanying digital atlas.

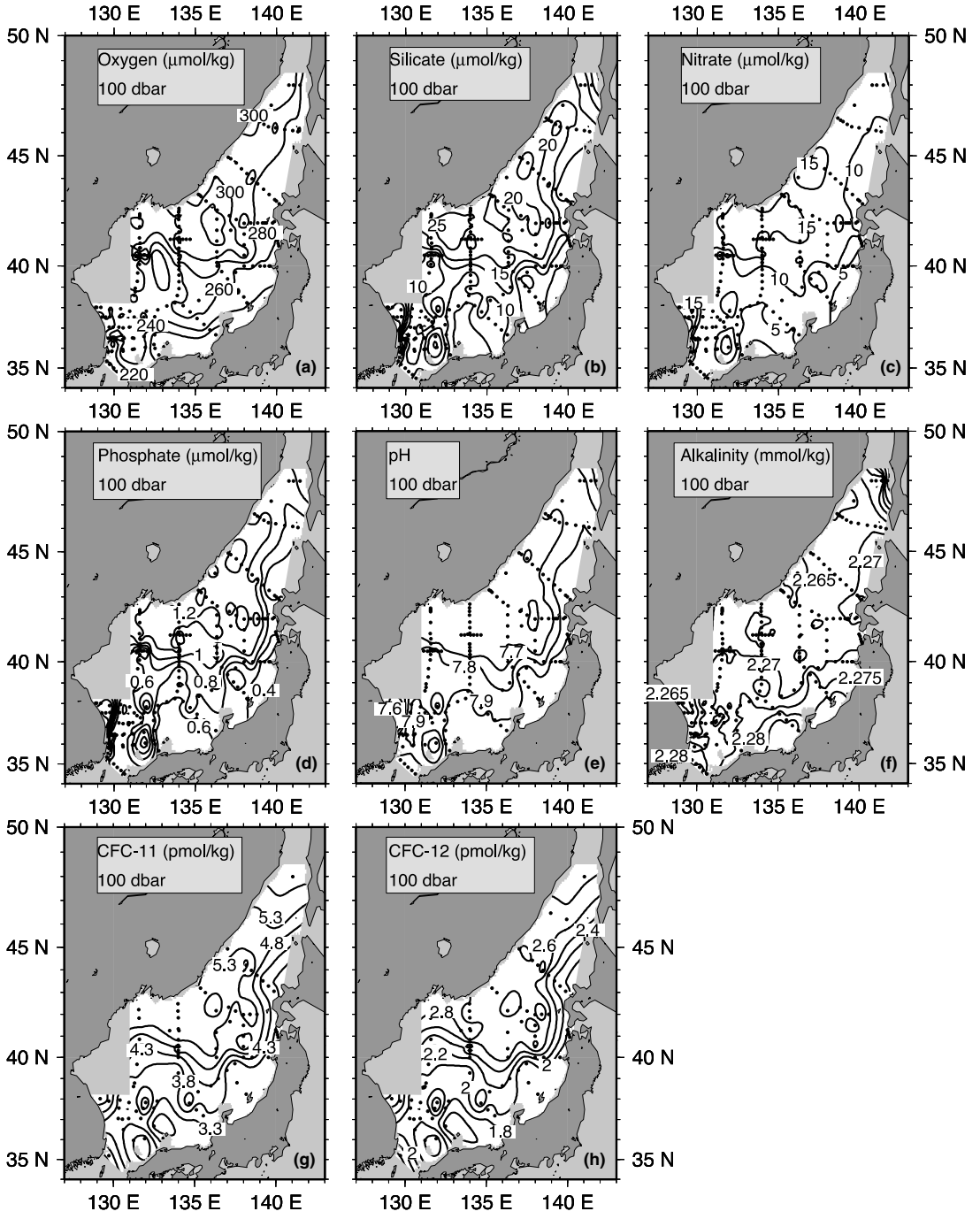

Fig. 17. (a) Oxygen (μmol/kg), (b) dissolved silica (μmol/kg), (c) nitrate (μmol/kg), (d) phosphate (μmol/kg), (e) pH, (f) alkalinity (mmol/kg), (g) CFC-11 (pmol/kg), and (h) CFC-12 (pmol/kg) at 100 dbar. Color versions are in the accompanying digital atlas.

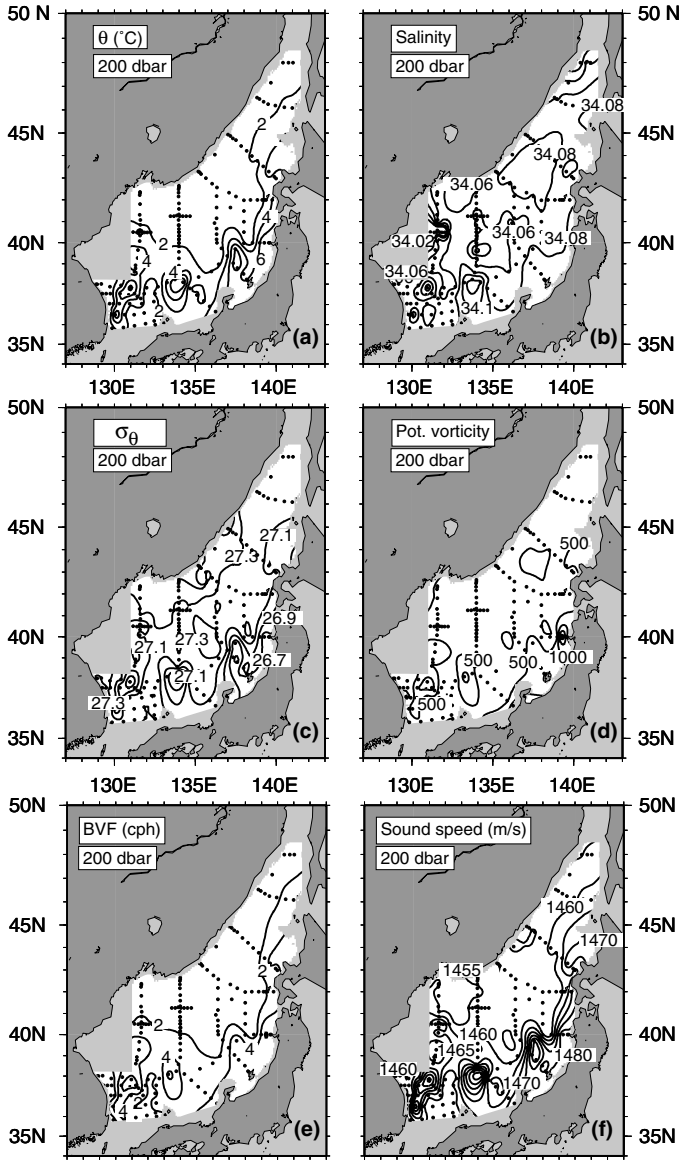

Fig. 18. Maps of: (a) potential temperature (°C), (b) salinity, (c) potential density (σ_θ), (d) isopycnal potential vorticity ($\times 10^{-14}$ cm^{-1} s^{-1}), (e) Brunt-Vaisala frequency (cph), and (f) sound speed (m/s) at 200 dbar. Colors are representative of all maps in the accompanying digital atlas.

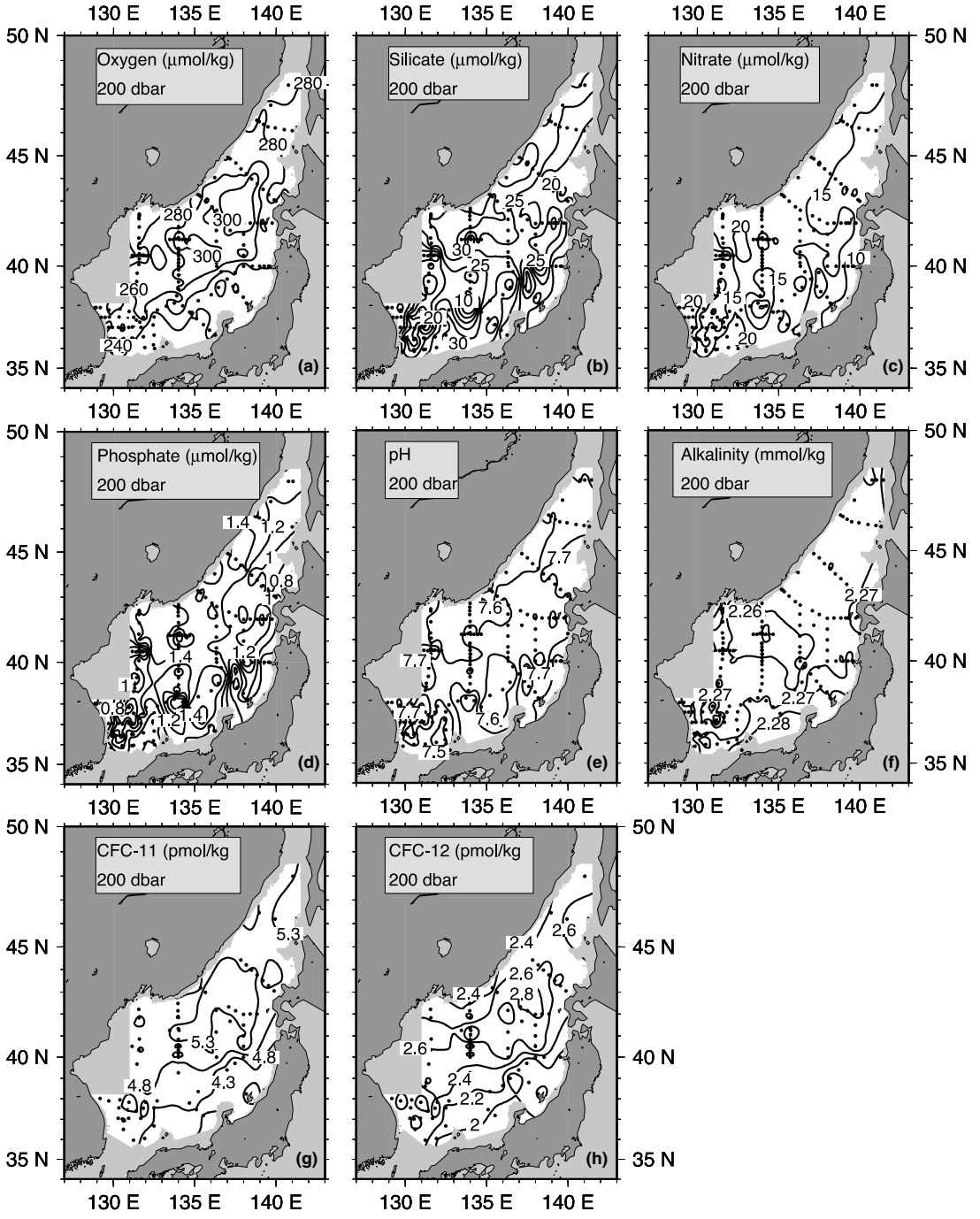

Fig. 19. (a) Oxygen (µmol/kg), (b) dissolved silica (µmol/kg), (c) nitrate (µmol/kg), (d) phosphate (µmol/kg), (e) pH, (f) alkalinity (mmol/kg), (g) CFC-11 (pmol/kg), and (h) CFC-12 (pmol/kg) at 200 dbar. Color versions are in the accompanying digital atlas.

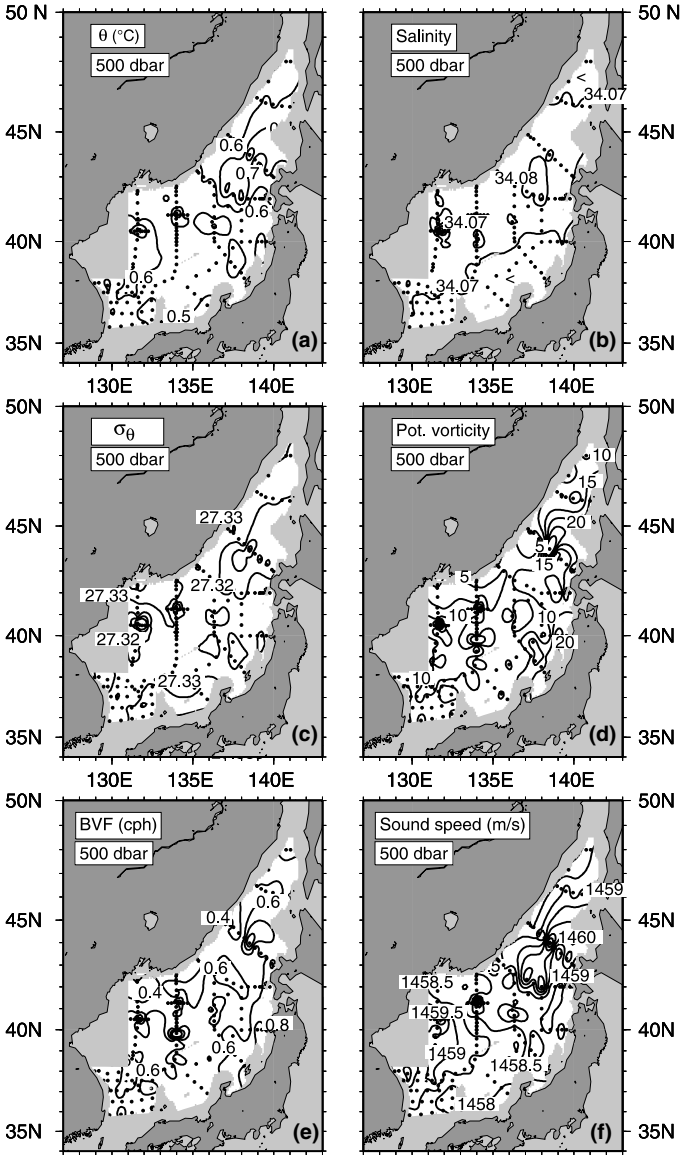

Fig. 20. Maps of: (a) potential temperature (°C), (b) salinity, (c) potential density (σ_θ), (d) isopycnal potential vorticity ($\times 10^{-14}$ cm^{-1} s^{-1}), (e) Brunt-Vaisala frequency (cph), and (f) sound speed (m/s) at 500 dbar. Color versions are in the accompanying digital atlas.

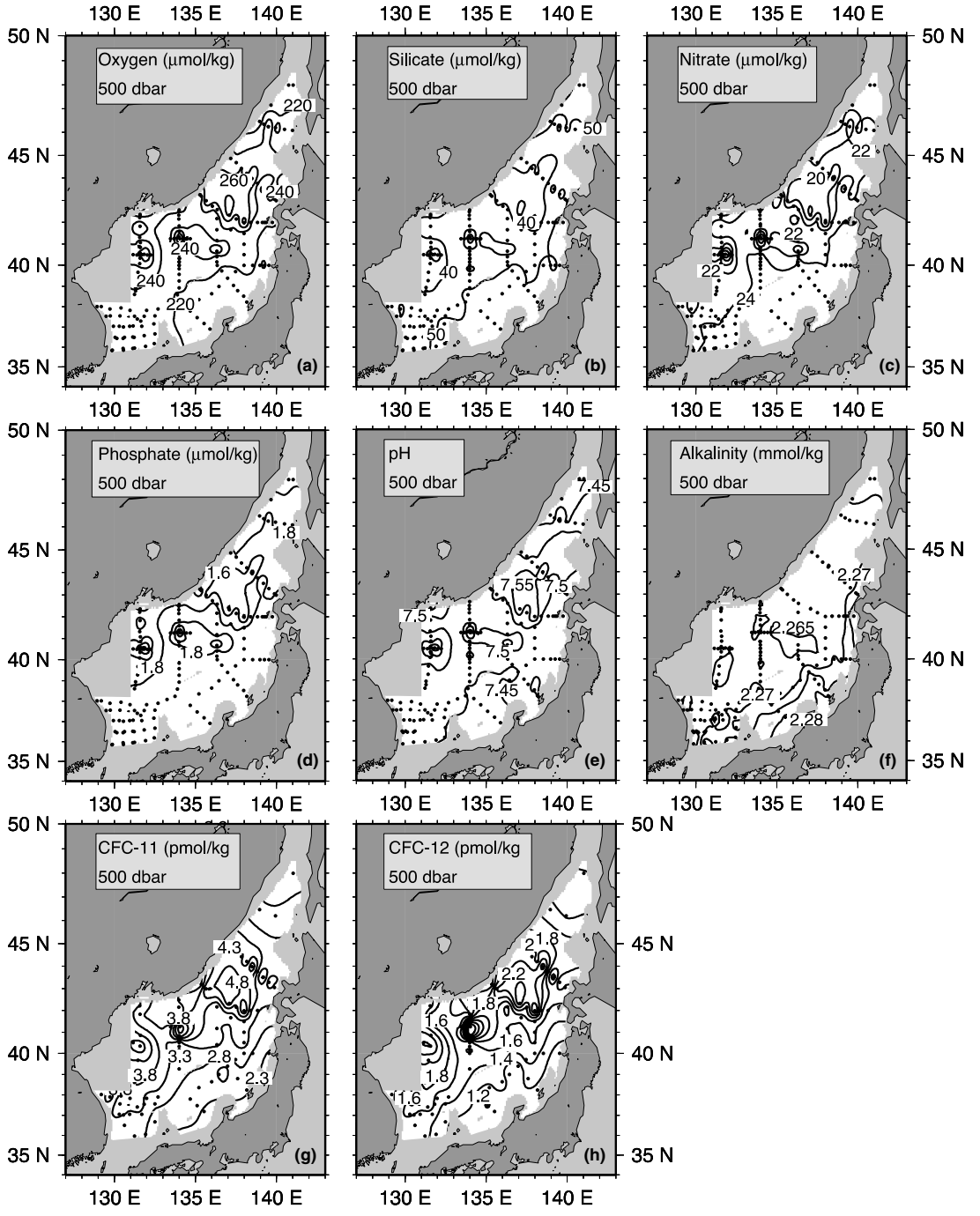

Fig. 21. (a) Oxygen (µmol/kg), (b) dissolved silica (µmol/kg), (c) nitrate (µmol/kg), (d) phosphate (µmol/kg), (e) pH, (f) alkalinity (mmol/kg), (g) CFC-11 (pmol/kg), and (h) CFC-12 (pmol/kg) at 500 dbar. Color versions are in the accompanying digital atlas.

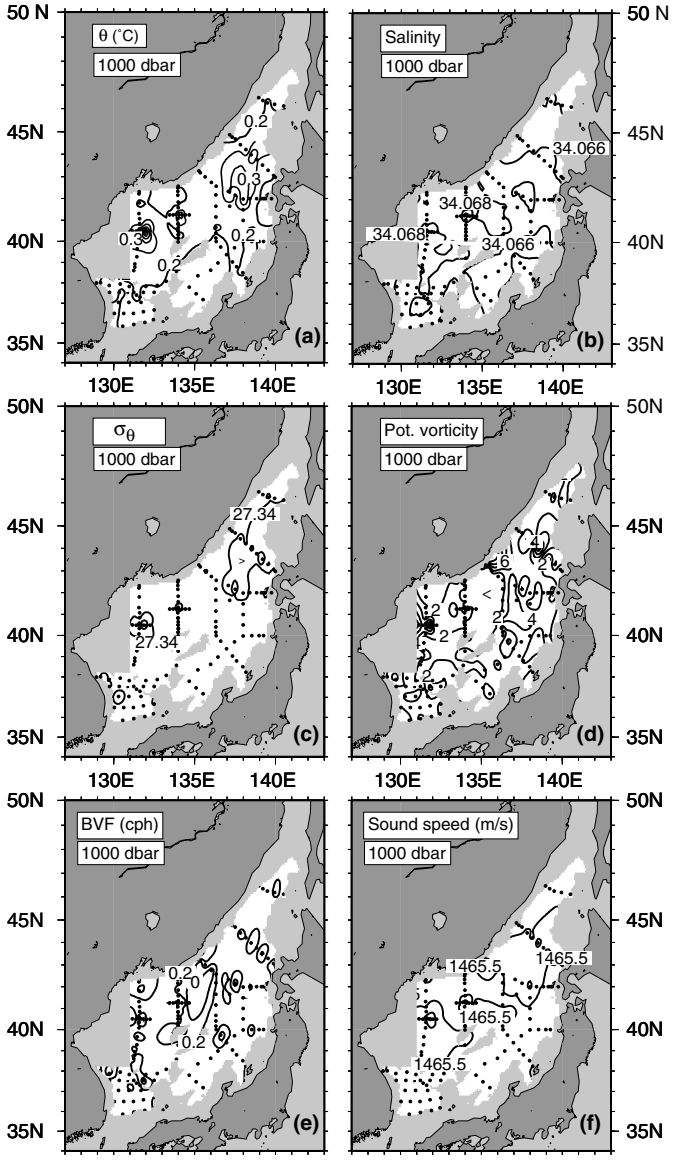

Fig. 22. Maps of: (a) potential temperature (°C), (b) salinity, (c) potential density (σ_θ), (d) isopycnal potential vorticity ($\times 10^{-14}$ cm^{-1} s^{-1}), (e) Brunt-Vaisala frequency (cph), and (f) sound speed (m/s) at 1000 dbar. Color versions are in the accompanying digital atlas.

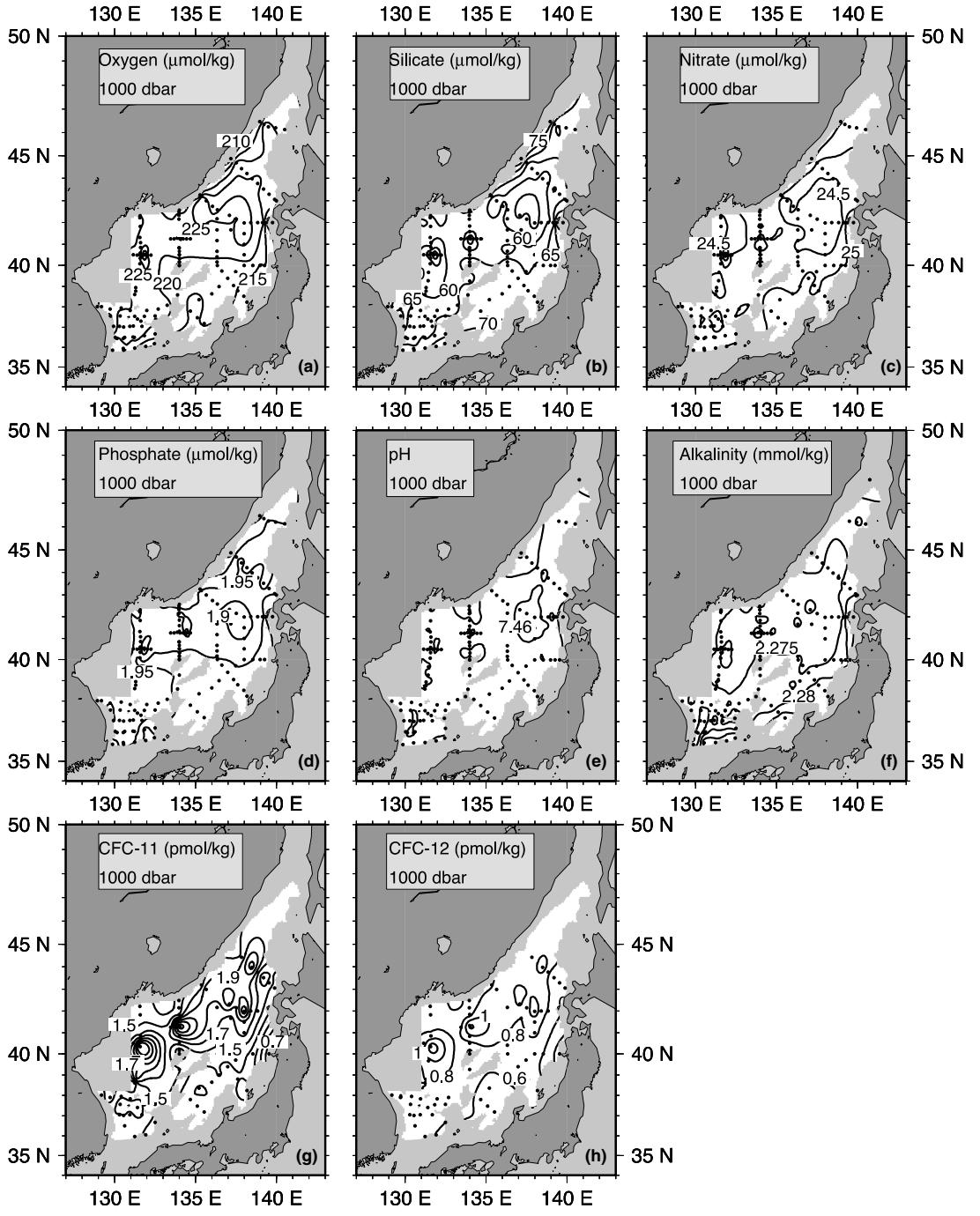

Fig. 23. (a) Oxygen (µmol/kg), (b) dissolved silica (µmol/kg), (c) nitrate (µmol/kg), (d) phosphate (µmol/kg), (e) pH, (f) alkalinity (mmol/kg), (g) CFC-11 (pmol/kg), and (h) CFC-12 (pmol/kg) at 1000 dbar. Color versions are in the accompanying digital atlas.

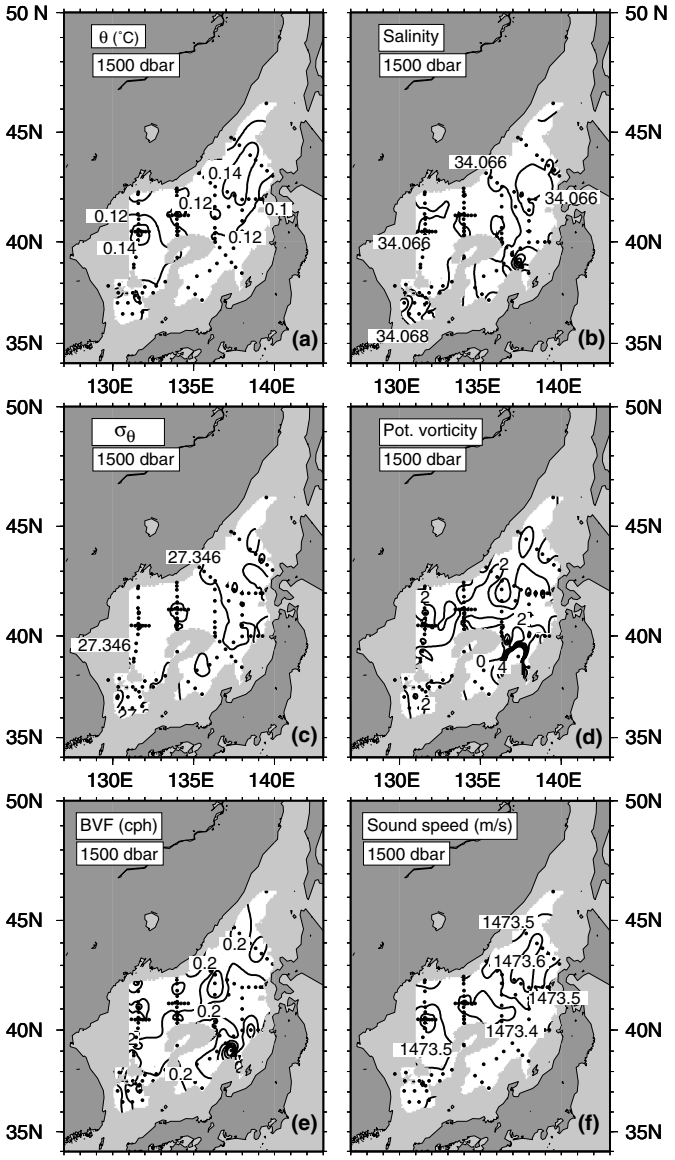

Fig. 24. Maps of: (a) potential temperature (°C), (b) salinity, (c) potential density (σ_2), (d) isopycnal potential vorticity ($\times 10^{-14}$ cm^{-1} s^{-1}), (e) Brunt-Vaisala frequency (cph), and (f) sound speed (m/s) at 1500 dbar. Color versions are in the accompanying digital atlas.

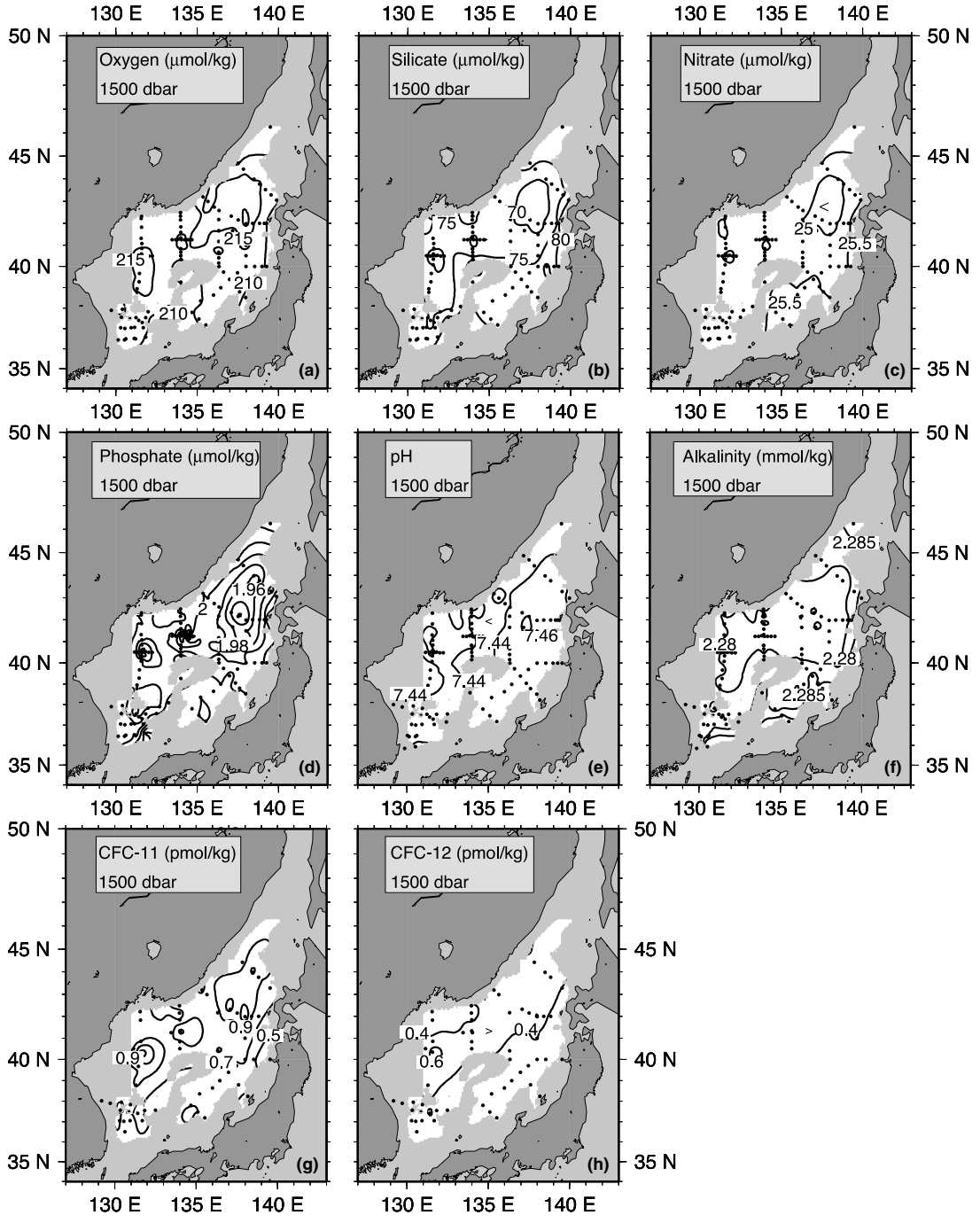

Fig. 25. (a) Oxygen (µmol/kg), (b) dissolved silica (µmol/kg), (c) nitrate (µmol/kg), (d) phosphate (µmol/kg), (e) pH, (f) alkalinity (mmol/kg), (g) CFC-11 (pmol/kg), and (h) CFC-12 (pmol/kg) at 1500 dbar. Color versions are in the accompanying digital atlas.

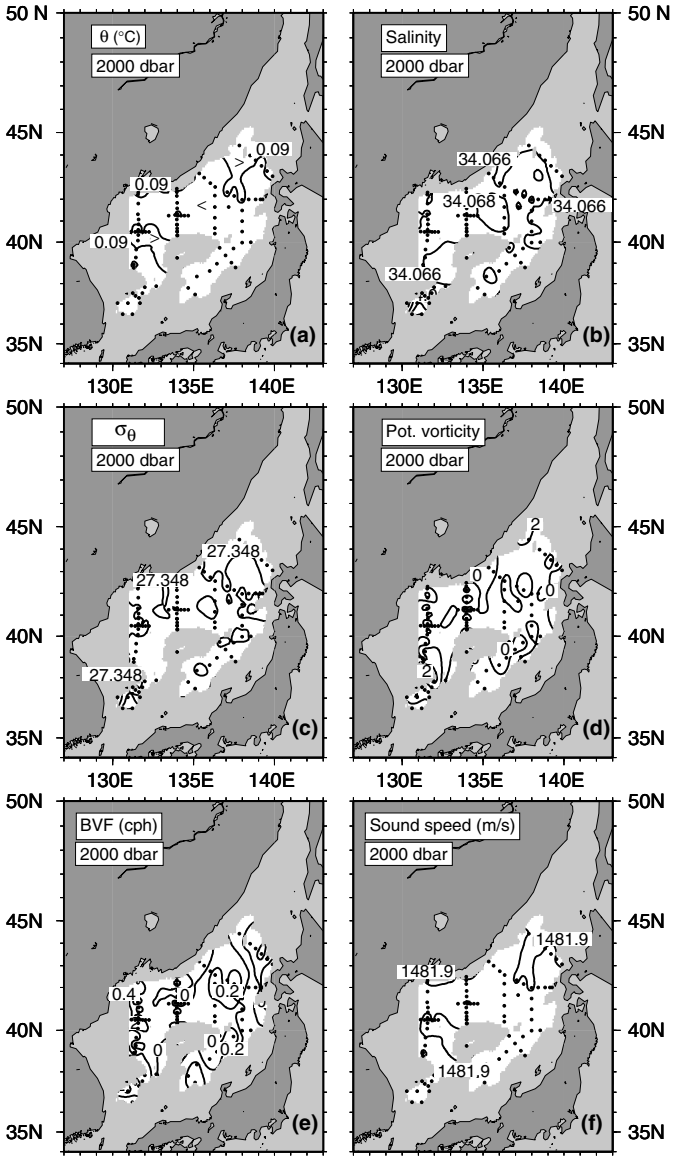

Fig. 26. Maps of: (a) potential temperature (°C), (b) salinity, (c) potential density (σ_2), (d) isopycnal potential vorticity ($\times 10^{-14}$ cm^{-1} s^{-1}), (e) Brunt-Vaisala frequency (cph), and (f) sound speed (m/s) at 2000 dbar. Color versions are in the accompanying digital atlas.

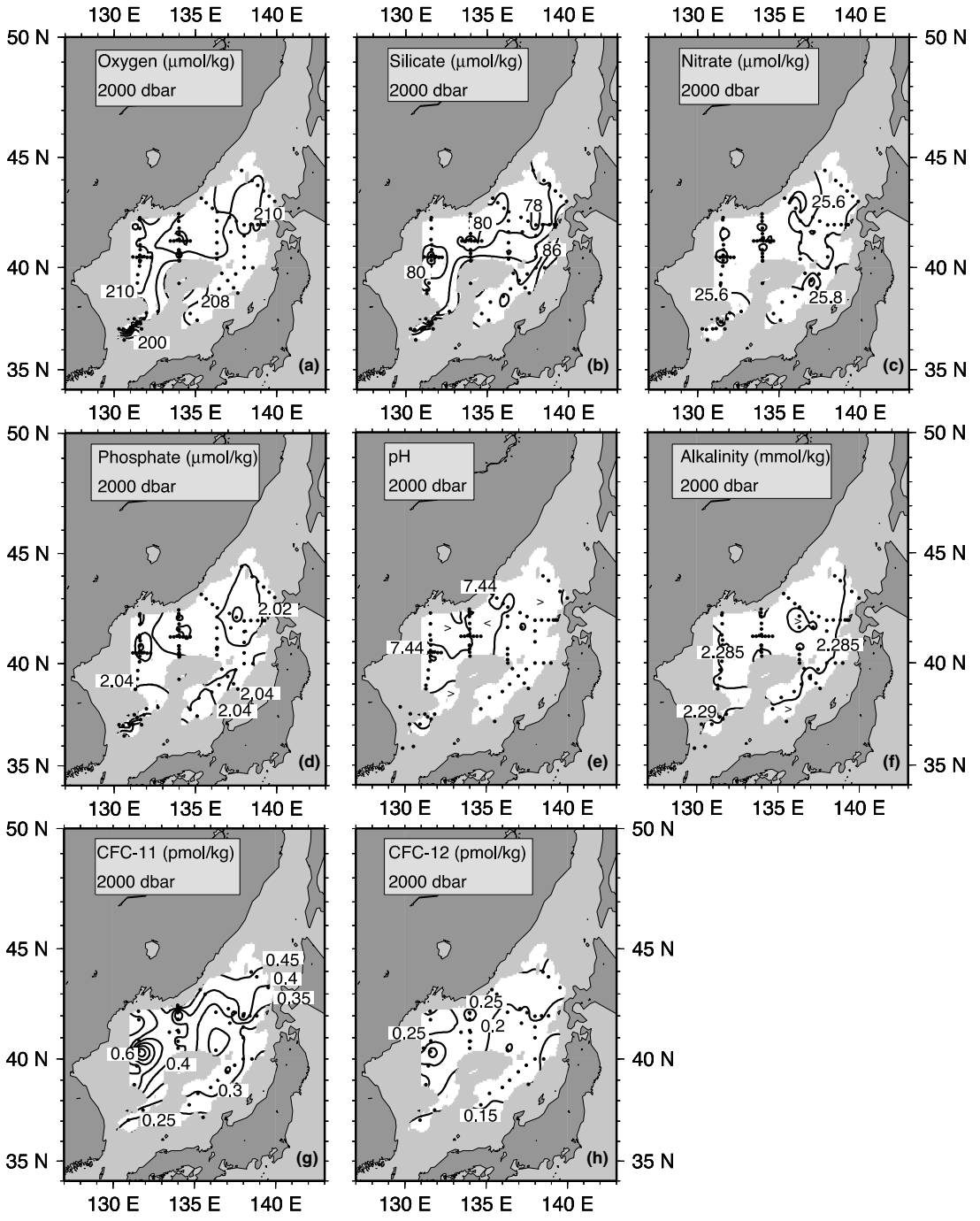

Fig. 27. (a) Oxygen (μmol/kg), (b) dissolved silica (μmol/kg), (c) nitrate (μmol/kg), (d) phosphate (μmol/kg), (e) pH, (f) alkalinity (mmol/kg), (g) CFC-11 (pmol/kg), and (h) CFC-12 (pmol/kg) at 2000 dbar. Color versions are in the accompanying digital atlas.

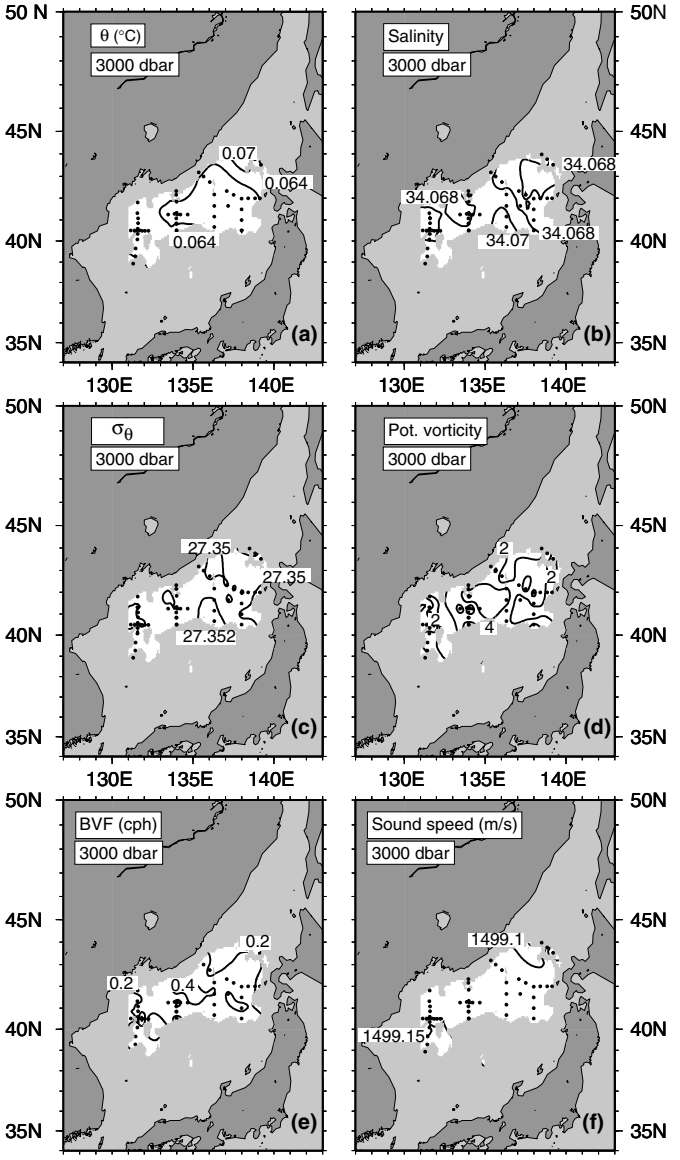

Fig. 28. Maps of: (a) potential temperature (°C), (b) salinity, (c) potential density (σ_2), (d) isopycnal potential vorticity ($\times 10^{-14}$ cm^{-1} s^{-1}), (e) Brunt-Vaisala frequency (cph), and (f) sound speed (m/s) at 3000 dbar. Color versions are in the accompanying digital atlas.

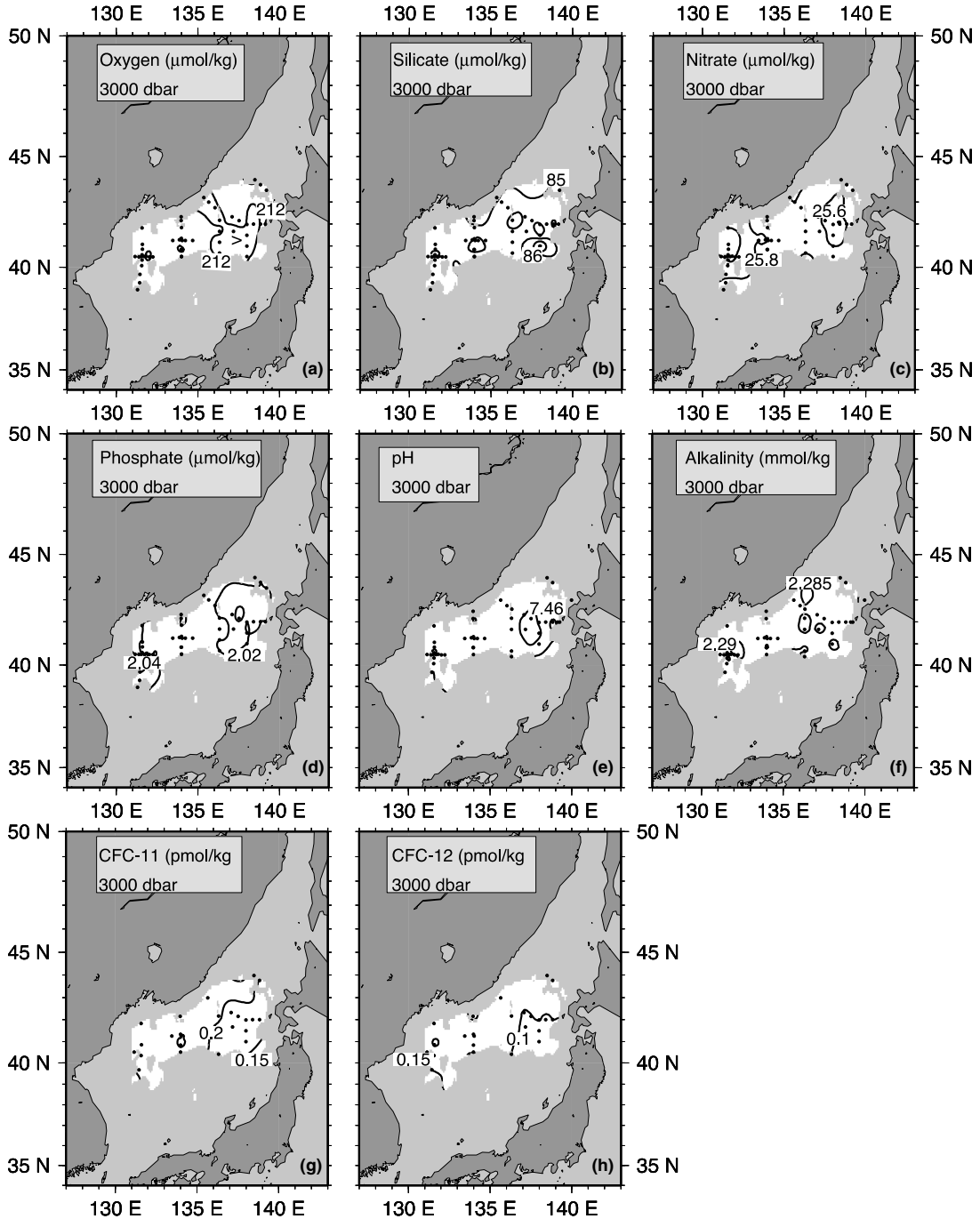

Fig. 29. (a) Oxygen (µmol/kg), (b) dissolved silica (µmol/kg), (c) nitrate (µmol/kg), (d) phosphate (µmol/kg), (e) pH, (f) alkalinity (mmol/kg), (g) CFC-11 (pmol/kg), and (h) CFC-12 (pmol/kg) at 3000 dbar. Color versions are in the accompanying digital atlas.

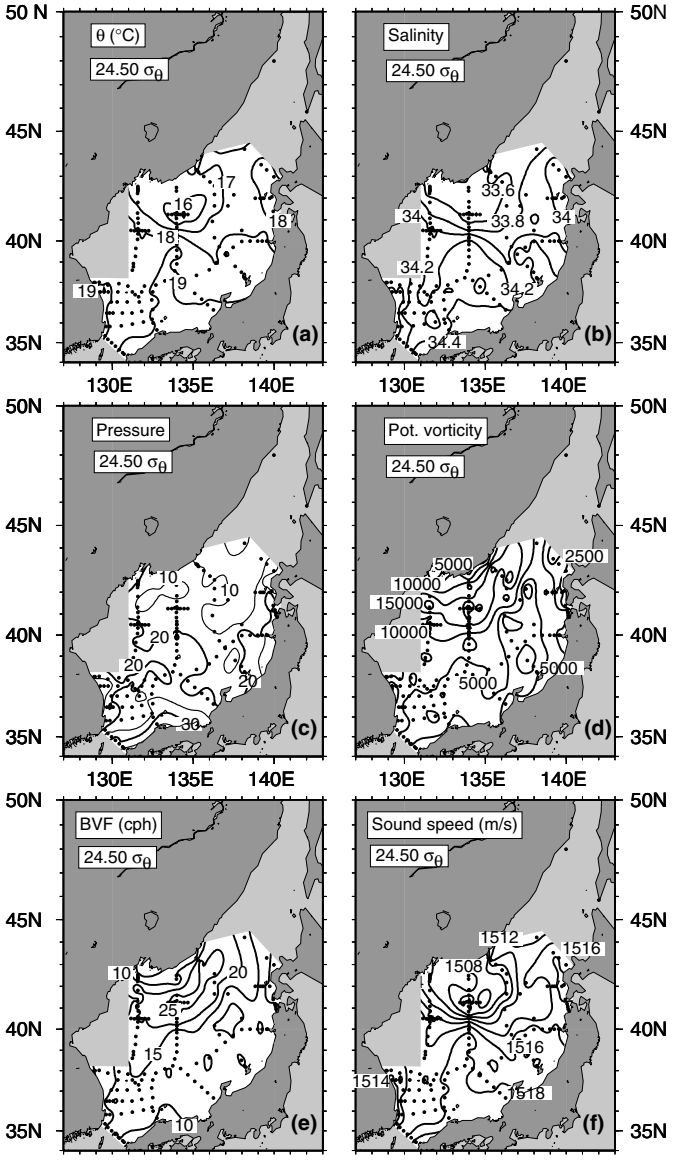

Fig. 30. Maps of: (a) potential temperature (°C), (b) salinity, (c) pressure (dbar), (d) isopycnal potential vorticity ($\times 10^{-14}$ cm^{-1} s^{-1}) at 24.50σ_θ. Color versions are in the accompanying digital atlas.

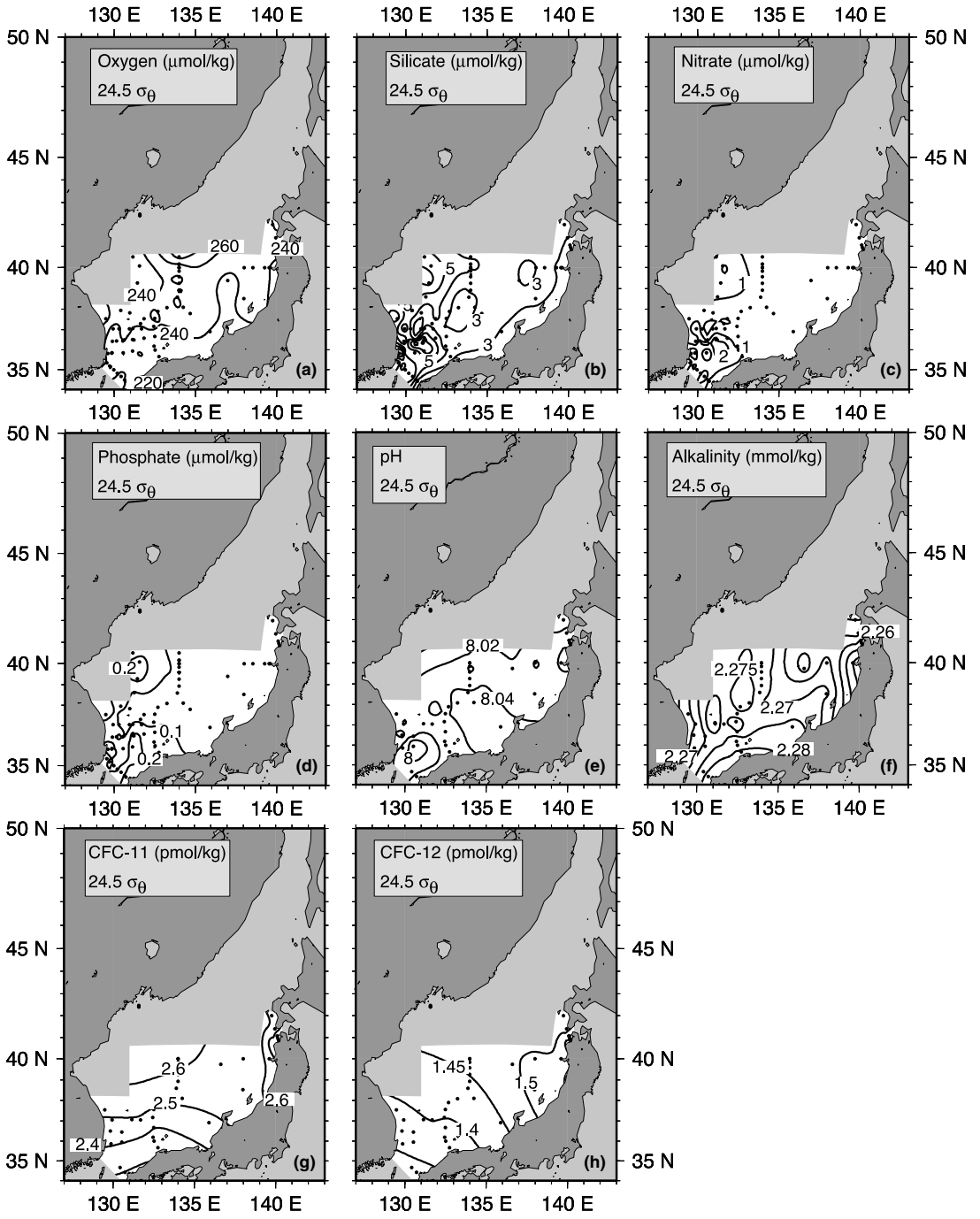

Fig. 31. (a) Oxygen (μmol/kg), (b) dissolved silica (μmol/kg), (c) nitrate (μmol/kg), (d) phosphate (μmol/kg), (e) pH, (f) alkalinity (mmol/kg), (g) CFC-11 (pmol/kg), and (h) CFC-12 (pmol/kg) at 24.50σ_θ. Color versions are in the accompanying digital atlas.

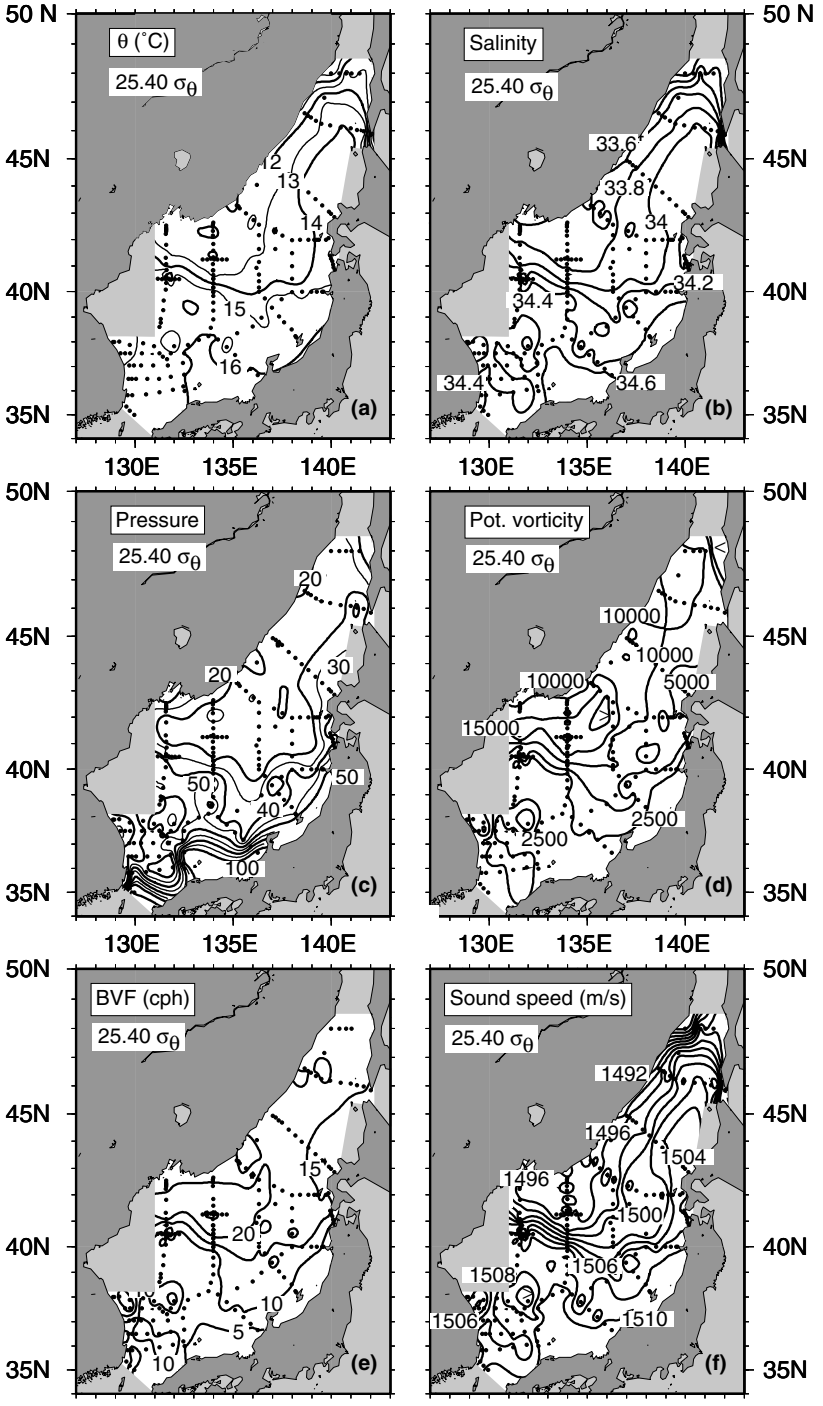

Fig. 32. Maps of: (a) potential temperature (°C), (b) salinity, (c) pressure (dbar), (d) isopycnal potential vorticity ($\times 10^{-14}$ cm^{-1} s^{-1}) at 25.40σ_θ (Tsushima water – shallow salinity maximum). Color versions are in the accompanying digital atlas.

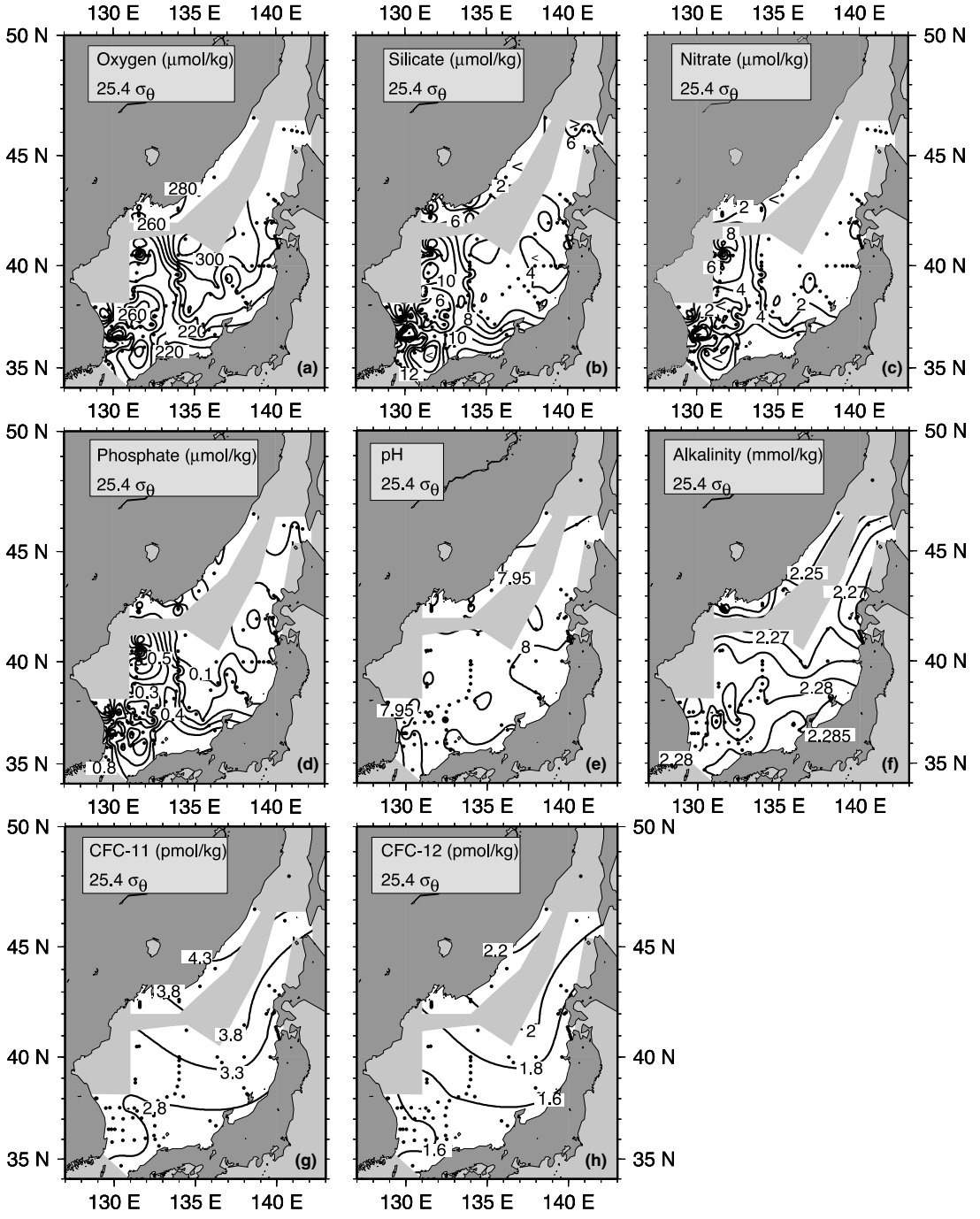

Fig. 33. (a) Oxygen (μmol/kg), (b) dissolved silica (μmol/kg), (c) nitrate (μmol/kg), (d) phosphate (μmol/kg), (e) pH, (f) alkalinity (mmol/kg), (g) CFC-11 (pmol/kg), and (h) CFC-12 (pmol/kg) at 25.40σ_θ (Tsushima water – shallow salinity maximum). Color versions are in the accompanying digital atlas.

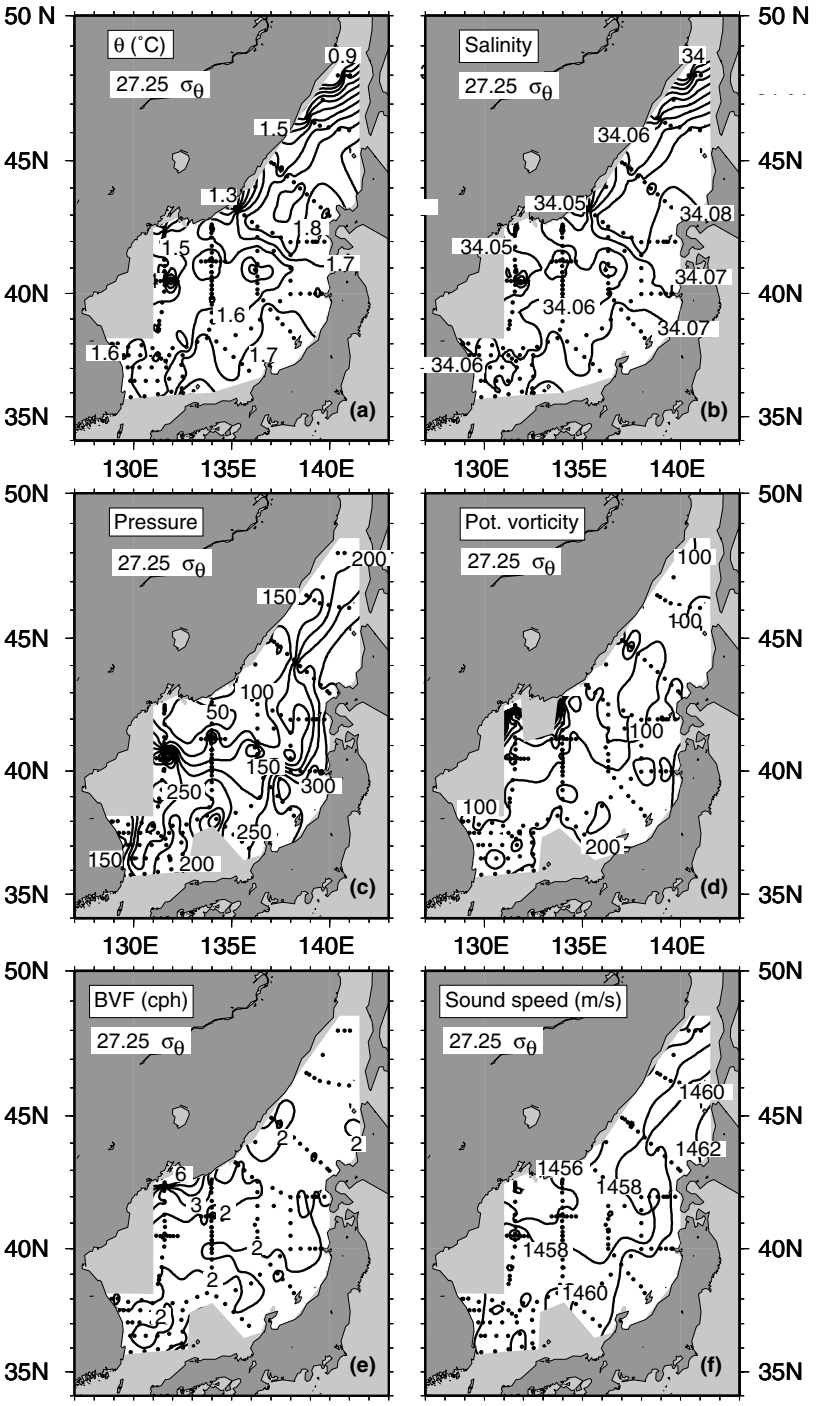

Fig. 34. Maps of: (a) potential temperature (°C), (b) salinity, (c) pressure (dbar), (d) isopycnal potential vorticity ($\times 10^{-14}$ cm^{-1} s^{-1}) at 27.25σ_θ (East Sea Intermediate Water – salinity minimum). Color versions are in the accompanying digital atlas.

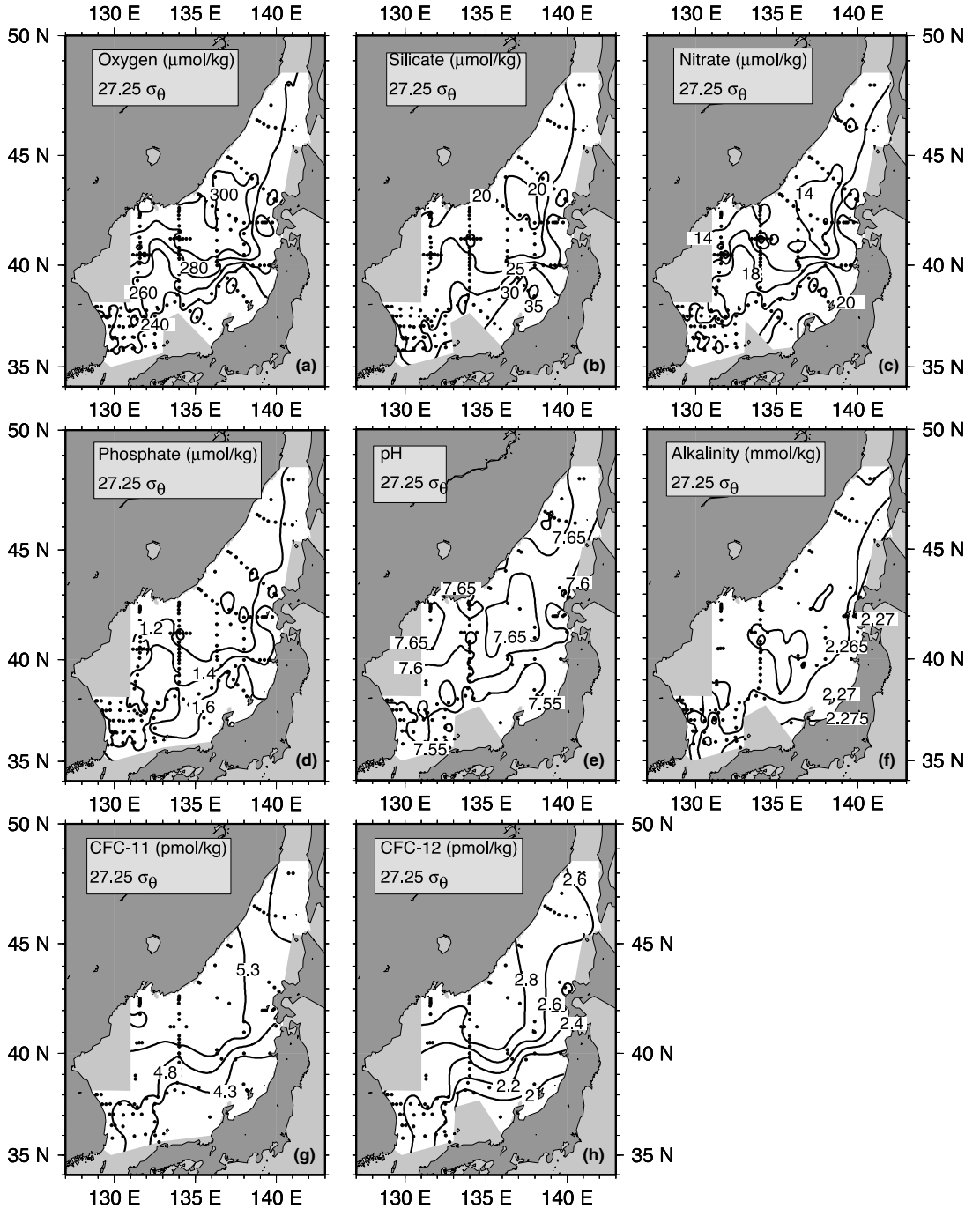

Fig. 35. (a) Oxygen (μmol/kg), (b) dissolved silica (μmol/kg), (c) nitrate (μmol/kg), (d) phosphate (μmol/kg), (e) pH, (f) alkalinity (mmol/kg), (g) CFC-11 (pmol/kg), and (h) CFC-12 (pmol/kg) at 27.25σ_θ (East Sea Intermediate Water – salinity minimum). Color versions are in the accompanying digital atlas.

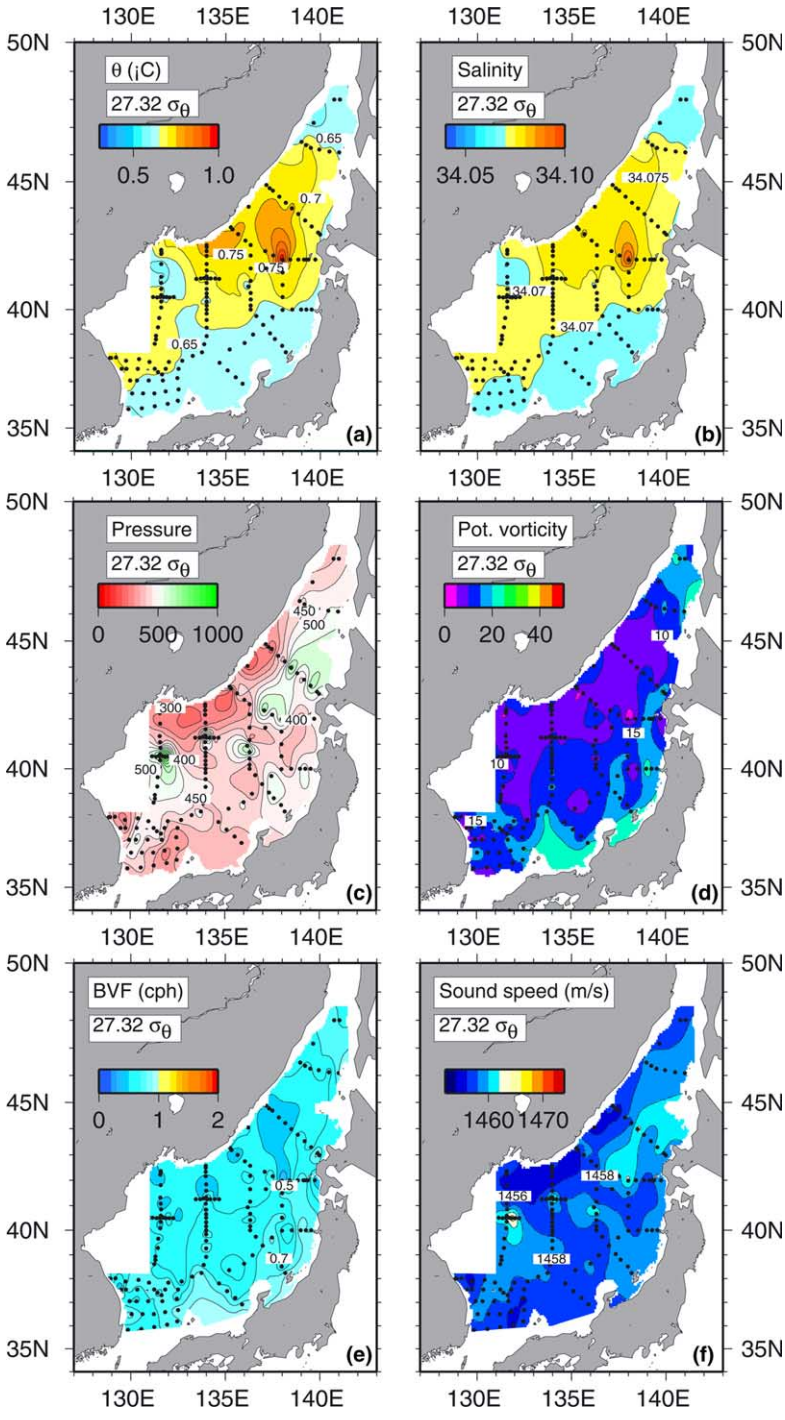

Fig. 36. Maps of: (a) potential temperature (°C), (b) salinity, (c) pressure (dbar), (d) isopycnal potential vorticity ($\times 10^{-14}$ cm^{-1} s^{-1}) at 27.32σ_θ (Upper Japan Sea Proper Water – main salinity maximum). Colors are representative of all other maps in the accompanying digital atlas.

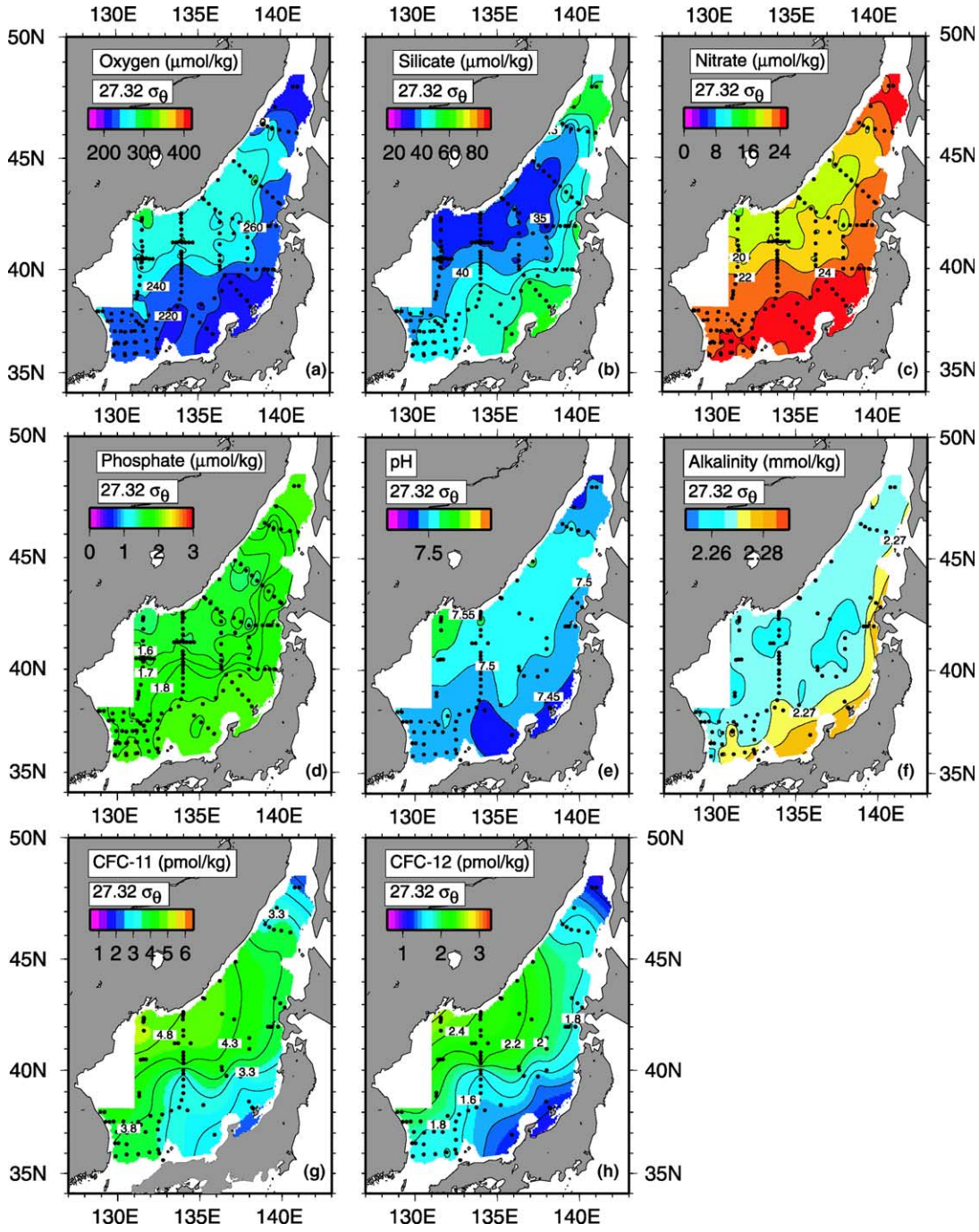

Fig. 37. (a) Oxygen (μmol/kg), (b) dissolved silica (μmol/kg), (c) nitrate (μmol/kg), (d) phosphate (μmol/kg), (e) pH, (f) alkalinity (mmol/kg), (g) CFC-11 (pmol/kg), and (h) CFC-12 (pmol/kg) at $27.32\sigma_\theta$ (Upper Japan Sea Proper Water – main salinity maximum). Colors are representative of all other maps in the accompanying digital atlas.

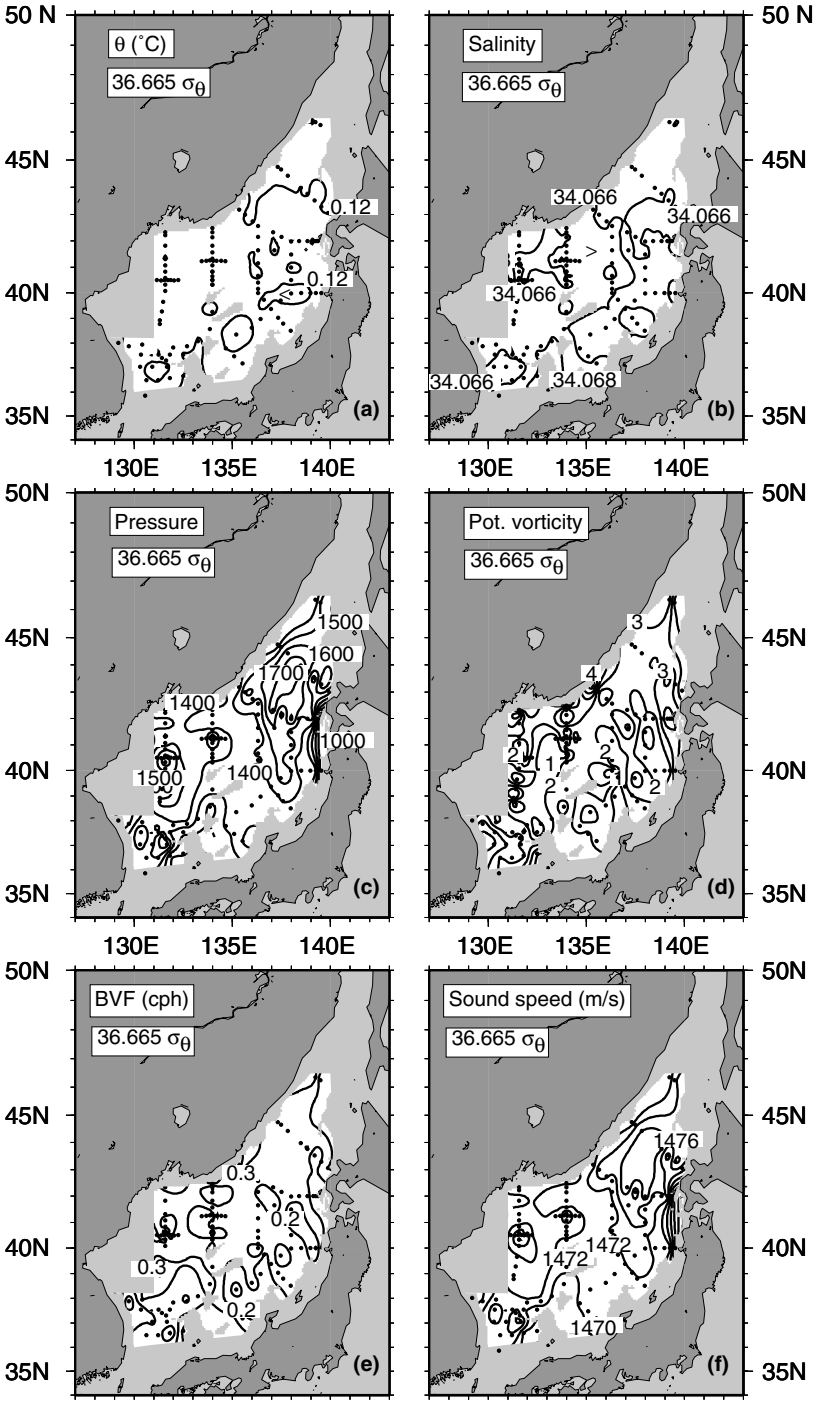

Fig. 38. Maps of: (a) potential temperature (°C), (b) salinity, (c) pressure (dbar), (d) isopycnal potential vorticity ($\times 10^{-14}$ cm^{-1} s^{-1}) at 36.665σ_2 (East Sea Deep Intermediate Water – salinity minimum). Color versions are in the accompanying digital atlas.

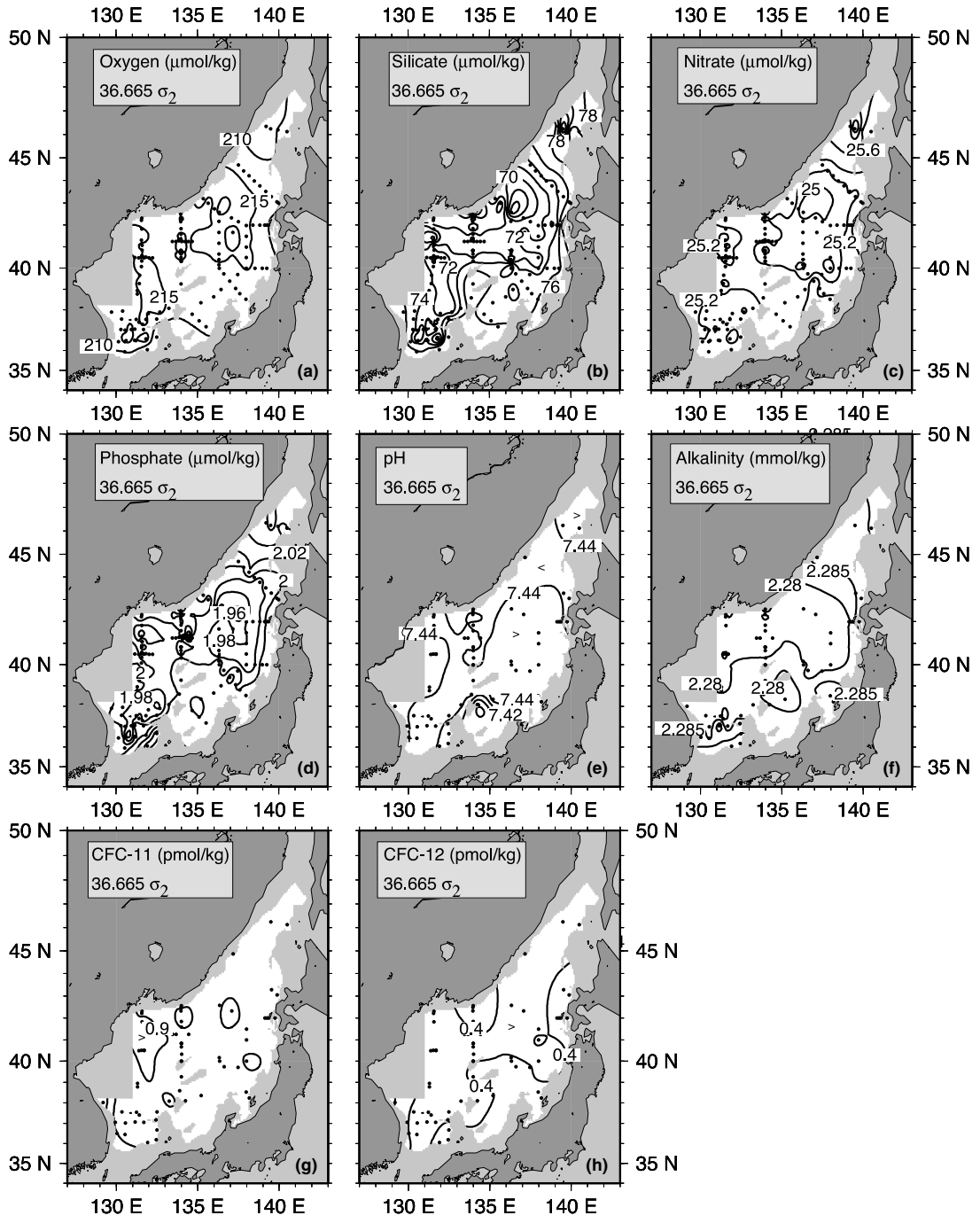

Fig. 39. (a) Oxygen (µmol/kg), (b) dissolved silica (µmol/kg), (c) nitrate (µmol/kg), (d) phosphate (µmol/kg), (e) pH, (f) alkalinity (mmol/kg), (g) CFC-11 (pmol/kg), and (h) CFC-12 (pmol/kg) at 36.665σ_2 (East Sea Deep Intermediate Water – salinity minimum). Color versions are in the accompanying digital atlas.

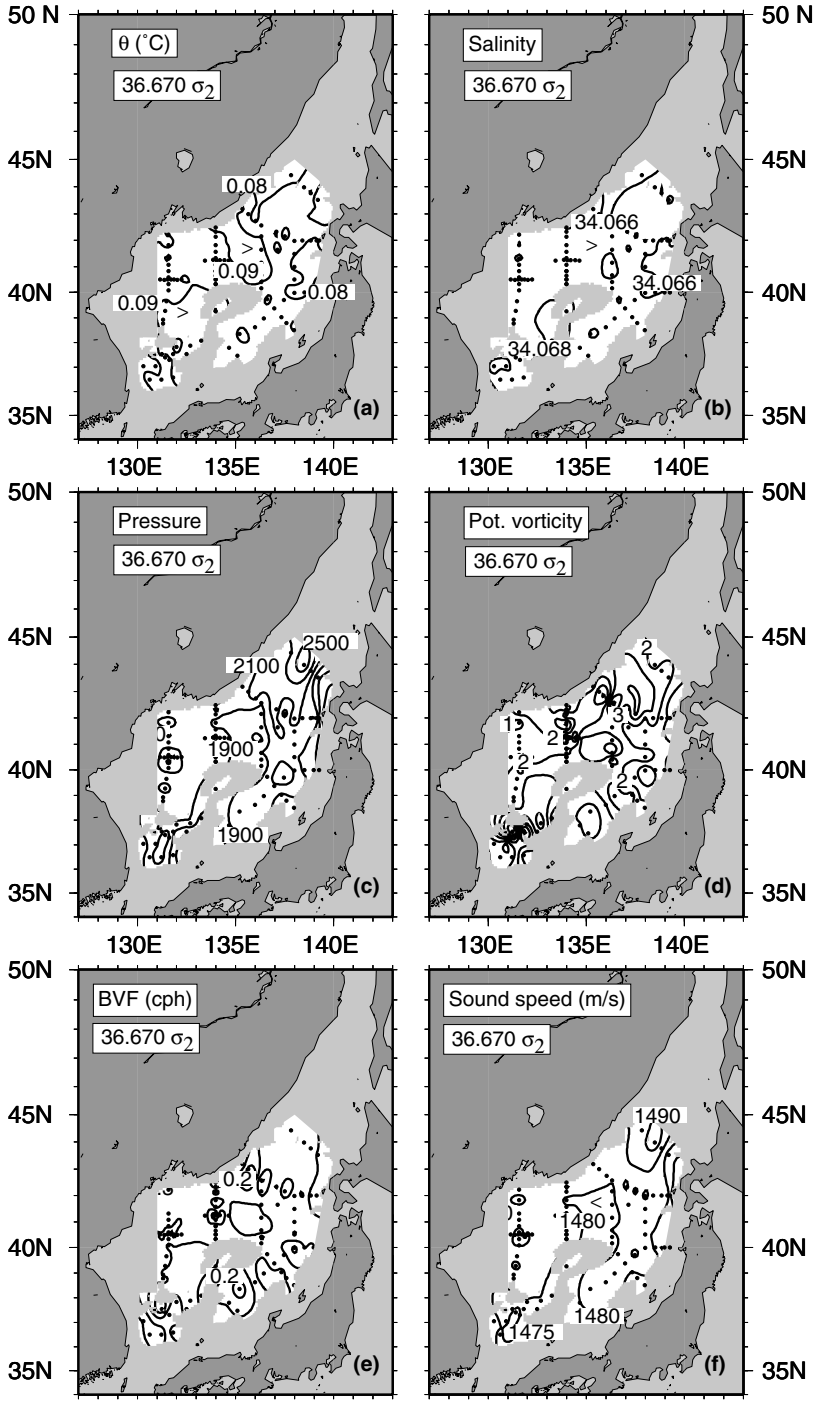

Fig. 40. Maps of: (a) potential temperature (°C), (b) salinity, (c) pressure (dbar), (d) isopycnal potential vorticity ($\times 10^{-14}$ cm^{-1} s^{-1}) at 36.670σ_2 (oxygen minimum). Color versions are in the accompanying digital atlas.

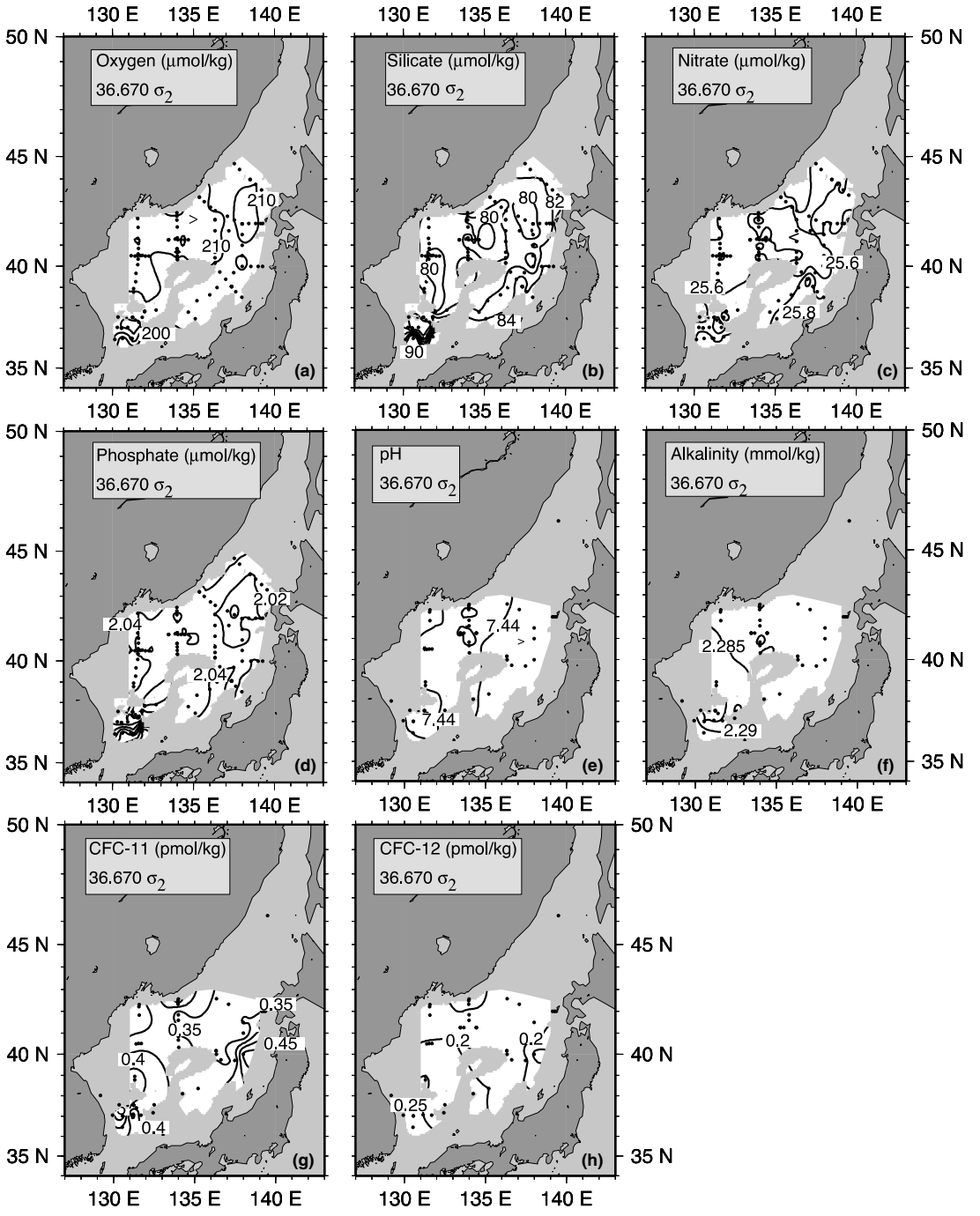

Fig. 41. (a) Oxygen (μmol/kg), (b) dissolved silica (μmol/kg), (c) nitrate (μmol/kg), (d) phosphate (μmol/kg), (e) pH, (f) alkalinity (mmol/kg), (g) CFC-11 (pmol/kg), and (h) CFC-12 (pmol/kg) at 36.670σ_2 (oxygen minimum). Color versions are in the accompanying digital atlas.